

FILTRATION EFFICIENCY MEASUREMENTS FOR
PLEATED FILTERS

By

FAKHRODDIN M. JADBABAEI

Bachelor of Science in Mechanical Engineering

Tehran University

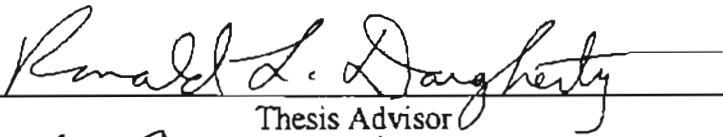
Tehran, Iran

1988

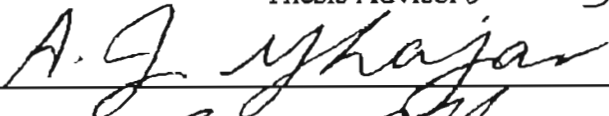
Submitted to the faculty of the
Graduate College of the
Oklahoma State University
in partial fulfillment of
the requirements for
the Degree of
MASTER OF SCIENCE
July, 1997

FILTRATION EFFICIENCY MEASUREMENTS FOR
PLEATED FILTERS

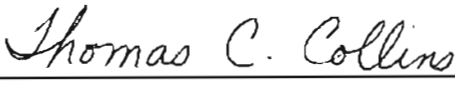
Thesis Approved:



Thesis Advisor







Dean of the Graduate College

ACKNOWLEDGMENTS

I would like to thank my advisor Dr. R. L. Dougherty for giving me the opportunity to be part of the OSU research team and for guiding me throughout my graduate studies. My sincere thanks to the committee members, Dr. A. J. Ghajar and Dr. F. Chambers, for their guidance and support. I would like to express my appreciation to my colleague, Sachin Anand who made this teamwork happen. Also, thanks to my other colleagues Balu Natarajan, Jeffery Williams, S. H. Yao, Wayne Gimlin and A. Al-Sarkhi for their continuous help and support.

I would like to thank James Davis and MAE North Lab personnel for their efforts that have been great help to this work.

My special thanks to my wife, Sheila, for her moral support and to my parents who have been guiding me throughout my life.

Finally, I extend my gratitude to Dayco-Purolator, a division of Mark IV Industries, and the Oklahoma Center for the Advancement of Science and Technology (OCAST) for financially supporting this study.

TABLE OF CONTENTS

Chapter	Page
I. INTRODUCTION	1
1.1 Objectives	2
II. LITERATURE REVIEW	4
2.1 Single Fiber Efficiency Theory	4
2.2 Mechanisms of Particle Collection	6
2.2.1 Diffusion	6
2.2.2 Inertial Impaction	7
2.2.3 Interception	8
2.2.4 Other Collection Mechanisms	9
2.3 Classical Filtration Theories	10
2.4 Experimental Studies for Flat Filter Media	11
2.4.1 Flat Filter Media Measurements with Aerosol Particles	11
2.4.2 Flat Filter Measurements with Dust Particles	14
2.5 Pleated Filters	16
2.6 Standard Testing Methods	22
2.6.1 SAE J1669	22
2.6.2 ASTM F1215-89	23
2.6.3 SAE J726 Code	24
2.7 The OSU Research	24
2.7.1 Theoretical Models	24
2.7.2 Experimental Studies	29
2.8 The Present Study	36
III. LDV FUNDAMENTALS	38
3.1 The Doppler Shift	38
3.3 The Optical Beating or Heterodyning	39
3.3 Differential Doppler Beating	41
3.4 Interference and Interpretation of Interference Fringes	42
3.5 Signal Processing	44
3.6 The Doppler Signal Analyzer	45

IV.	THE EXPERIMENTAL SETUP	47
	4.1 Description of the System Components	47
	4.1.1 Flow System	47
	4.1.2 The LDV System	54
	4.1.3 The Traverse	58
	4.2 The Experimental Setup Description	58
	4.3 Measurement Procedure.....	61
V.	EFFICIENCY AND NUMBER DENSITY CALCULATIONS	63
	5.1 Calculation of Efficiencies Using Number Density.....	64
	5.2 Local Efficiency Calculation and the Swept Volume Technique	64
	5.3 SVT for One-Dimensional Flow with Different Velocities	66
	5.4 SVT for One-Dimensional Flow with Gaussian Velocity Profile	69
	5.5 SVT in Recirculation Zones.....	73
	5.6 SVT for Flow with Different Velocities in Different Directions.....	76
VI.	CONSISTENCY MEASUREMENTS	83
	6.1 Factors Affecting Measured Data	84
	6.1.1 The Power of the Laser Beams	85
	6.1.2 DSA Parameters	86
	6.1.2.1 High Voltage	86
	6.1.2.2 Threshold	86
	6.1.2.3 Velocity Range	87
	6.1.2.4 Coincidence	87
	6.1.2.5 Other Parameters	88
	6.1.3 Polarization Angle of the Beams	88
	6.1.4 Flow Rate and Particle Seeding Rate	89
	6.1.5 Possible Leaks	90
	6.2 Consistency Measurements	91
	6.2.1 Consistency Measurements on Air Flow with Water Droplets	91
	6.2.2 Consistency Measurements in Particle Flow	93
	6.2.3 Zero Efficiency Measurements at the Center of the Housing	95
	6.2.4 Zero Efficiency Measurements at All Grid Points.....	96
VII.	RESULTS AND DISCUSSION	98
	7.1 Summary of the Tests in the Small Angle Diffuser Housing	98
	7.2 Results of Measurements in the Small Angle Diffuser Housing	100

7.3	Three Point Measurements	112
7.4	SAE Housing Measurements	114
7.5	Comparison of Results with Previous Studies	118
7.5.1	Comparison with Theoretical Models	118
7.5.1.1	The Single Fiber Efficiency	118
7.5.1.2	Comparison of Results with Duran's Model	121
7.5.2	Comparison with Experimental Data	122
7.6	The Stokes Number Analysis	124
VIII.	CONCLUSIONS	128
8.1	Summary	128
8.2	Recommendations for Future Work	130
	REFERENCES	132
	APPENDICES	137
APPENDIX A	THE DSA PARAMETERS	138
APPENDIX B	TEST RESULTS: SMALL ANGLE DIFFUSER HOUSING	141
APPENDIX C	TEST RESULTS: SAE HOUSING	163
APPENDIX D	TSI FLOWMETER CALIBRATION PLOTS	166
APPENDIX E	AN EXAMPLE OF THE STOKES NUMBER CALCULATION	168
APPENDIX F	LIST OF EQUIPMENT	169
APPENDIX G	COMPARISON OF EFFICIENCY CALCULATION METHODS	171
APPENDIX H	COMPARISON OF THE AVERAGE EFFICIENCIES	174

LIST OF TABLES

Table		Page
4.1	A13192 Pleated Filter Dimensions [Duran, 1995].	54
7.1	Summary of the Small Angle Diffuser Housing Tests.	99
7.2	Summary of the Three Point Measurements.	113
C.1	Summary of the SAE Housing Tests.	163

LIST OF FIGURES

Figure		Page
2.1	Definition of the Single Fiber Efficiency [Lee, 1977].	5
2.2	Three Main Mechanisms of Particle Collection [Lee, 1977].	8
2.3	Schematic Diagram of the Collection Efficiencies of Different Particle Capture Mechanisms [Liu et al., 1985].	9
2.4	Comparison of Theoretical and Experimental Filter Efficiency as a Function of Particle Size, Dacron Filter, $D_f = 11.3$ Microns, $\alpha = 0.0493$, $U=0.0396$ m/s [Yeh, 1972].	12
2.5	Comparison of Experimental Efficiency Measurements with the Theory of Harrop and Stenhouse [1969] in the Inertial Impaction Regime [Lee, 1977].	13
2.6	SAE Dust Size Distribution [Gidley, 1993].	14
2.7	Filter Performance Versus Dust Loading [Jaroszczyk, 1987].	15
2.8	Fractional Efficiency Requirement for Cabin Air Filter [Person and Cashin, 1994].	16
2.9	Conflicting Design Requirements for Cabin Air Filter [Person and Cashin, 1994].	17
2.10	Dependence of Initial Efficiency on Flow Rate [Ptak et al., 1994].	17
2.11	Fractional Efficiency at Various Dust Loading [Reinhart and Weisert, 1983].	18
2.12	Isometric Representation of Efficiency, Particle Size and Dust Loading [Reinhart and Weisert, 1983].	18

2.13	Variation of Pressure Drop with Pleat Count for Rectangular and Triangular Pleats, HEPA Filter [Chen et al., 1994].	20
2.14	Pressure Drop Versus Pleat Count [Chen et al., 1994].	21
2.15	Typical Initial Fractional Efficiencies in Inlet System of Combustion Turbines [Gidley, 1993].	21
2.16	Elemental Efficiencies for A13192 Filter [Sabnis, 1993].	25
2.17	Elemental Efficiencies for A13192 Filter, Small Angle Diffuser Housing [Newman, 1994].	26
2.18	Elemental Efficiencies for A13192 Filter, SAE J726 Housing [Newman, 1994].	26
2.19	Comparison of Single Fiber Efficiency Calculated by Sabnis' Model with Classical Models [Duran, 1995].	27
2.20	Velocity Distribution Upstream of a Dirty Filter Loaded to 127 mm of Water [Liu, 1995].	28
2.21	Overall Efficiency Versus Flow Rate [Natarajan, 1995].	29
2.22	Overall Filter Efficiencies [Anand, 1997].	30
2.23	Local Efficiency for Flat Filter [Anand, 1997].	31
2.24	Axial Velocities Upstream of the A13192 Pleated Filter (204 m ³ /hr, SAE Housing, 0.966 Micron Particle Diameter) [Liang, 1994].	31
2.25	Axial Velocities Upstream of the A13192 Pleated Filter (204 m ³ /hr, Small Angle Diffuser Housing, 0.966 Micron Particle Diameter) [Natarajan, 1995].	32
2.26	Elemental Efficiencies Over A13192 Filter (Small Angle Diffuser Housing, Duran's Model with Packing Density of 0.49) [Natarajan, 1995].	33
2.27	Elemental Efficiencies Over A13192 Filter (Small Angle Diffuser Housing, Duran's Model with Packing Density of 0.345) [Natarajan, 1995].	34
2.28	Measured Local Efficiencies Over A13192 Filter [Natarajan, 1995].	35

3.1	Illustration of the Doppler Frequency Shift Experienced by a Moving Observer [Drain, 1980].	39
3.2	The Heterodyning of Two Frequencies [Drain, 1980]. The Addition of Signals (a) and (b) Yields Wave Form (c) Which Is Rectified to Form the Beat Signal (d).	40
3.3	Arrangement of Illuminating Beams in the Differential Doppler Technique [Drain, 1980].	41
3.4	Fringe Pattern Produced by Crossing Beams in the Differential Doppler Technique [Drain, 1980].	42
3.5	Types of Signals from Particles Crossing a Region of Intersection of Laser Beams [Drain, 1980].	43
3.6	PMT Output Signal from Photodetector, Before High-Pass Filter [Durst and Whitelaw, 1976].	45
3.7	PMT Output Signal from Photodetector, After High-Pass Filter [Durst and Whitelaw, 1976].	46
4.1	Dimensions of the Small Angle Diffuser Housing.	50
4.2	Dimensions of the SAE Housing.	51
4.3	The Bypass System.	53
4.4	Arrangement of the A13192 Pleats.	54
4.5	The A13192 Pleated Filter.	55
4.6	Schematic Diagram of the Fiber Drive.	56
4.7	Laser Beams Emitted from Transceiver.	57
4.8	The Experimental Setup.	59
4.9	Top View of the Test Filter Positioning.	60
4.10	Grid Locations (Not to Scale).	60
5.1	The Swept Volume Technique, (a) at $T = 0$, (b) at $T = T_0$.	65
5.2	SVT for One-Dimensional Flow with Two Velocities.	67

5.3	Example of Number Density Calculation for Two Streams.	68
5.4	Ideal Gaussian Velocity Histogram.	71
5.5	Typical Non-Symmetric Velocity Histogram.	72
5.6	Symmetric and Non-Symmetric Parts of the Velocity Histogram of Fig. 5.5, (a) Symmetric Part, (b) Non-Symmetric Part.	73
5.7	One-Dimensional Flow Streams, a) Moving in the Same Direction, b) Moving in the Opposite Direction.	74
5.8	Calculation of Number Density for One-Dimensional Flow with Opposite Streams, a) Total Velocity Histogram, b) Negative Velocity Histogram, c) Positive Velocity Histogram.	75
5.9	Two Flow Streams in Different Directions.	76
5.10	Typical Example of Measurement of One Particle Velocity, a) Axial Velocity, b) Transverse Velocity.	77
5.11	Velocity Streams for the Example of Four Flows in Different Directions.	79
5.12	Velocity Histograms for the Example of Four Flows in Four Different Directions Velocity, a) Axial Velocity, b) Transverse Velocity.	80
6.1	Consistency Measurements in Open Air Flow with Water Droplets, Valid Samples/Run = 20000, Validity = 93%, Laser Power = 0.8 W.	92
6.2	Summary of the Consistency Measurements for Flow with Water Droplets (30 Runs per Test).	92
6.3	Consistency Measurements for Flow inside the Housing with PSL Particles, Valid Samples/Run = 1000, Validity = 92%, Laser Power = 0.8 W.	94
6.4	Summary of the Consistency Measurements for Flow with Particles inside the Housing (30 Runs per Test).	94
6.5	Zero Efficiency Measurements at One Location inside the Housing with Flow Rate = 103.7 m ³ /hr, Valid Samples/Run = 1000, Validity = 92%, Laser Power = 0.8 W, 3/19/96.	97
7.1	Upstream Velocity Profiles for Test F15, Flow Rate = 5.68 m ³ /hr.	101

7.2	Downstream Velocity Profiles for Test F15, Flow Rate = 5.68 m ³ /hr.	101
7.3	Upstream Number Density Plot for Test F15, Flow Rate = 5.68 m ³ /hr.	102
7.4	Downstream Number Density Plot for Test F15, Flow Rate = 5.68 m ³ /hr.	103
7.5	Efficiency Plot for Test F15, Flow Rate = 5.68 m ³ /hr.	103
7.6	Upstream Velocity for Test F5, Flow Rate = 187.7 m ³ /hr.	104
7.7	Downstream Velocity for Test F5, Flow Rate = 187.7 m ³ /hr.	105
7.8	Upstream Number Density Plot for Test F5, Flow Rate = 187.7 m ³ /hr.	105
7.9	Downstream Number Density Plot for Test F5, Flow Rate = 187.7 m ³ /hr.	108
7.10	Efficiency for Test F5, Flow Rate = 187.7 m ³ /hr.	109
7.11	Upstream Velocity for Test F8, Flow Rate = 313.75 m ³ /hr.	109
7.12	Downstream Velocity for Test F8, Flow Rate = 313.75 m ³ /hr.	110
7.13	Upstream Number Density Plot for Test F8, Flow Rate = 313.75 m ³ /hr.	110
7.14	Downstream Number Density Plot for Test F8, Flow Rate = 313.75 m ³ /hr.	111
7.15	Efficiency for Test F8, Flow Rate = 313.75 m ³ /hr.	111
7.16	Comparison of the Filter Efficiencies.	114
7.17	Upstream Velocity for Flow Rate = 187.7 m ³ /hr, SAE Housing.	115
7.18	Downstream Velocity for Flow Rate = 187.7 m ³ /hr, SAE Housing.	116
7.19	Upstream Number Density Plot for Flow Rate = 187.7 m ³ /hr, SAE Housing.	116
7.20	Downstream Number Density for Flow Rate = 187.7 m ³ /hr, SAE Housing.	117
7.21	Efficiency for Flow Rate = 187.7 m ³ /hr, SAE Housing.	117

7.22	Pleated Filter Modeling with Different Thicknesses, a) Filter paper Thickness, b) Pleat Height Thickness.	120
7.23	Comparison of Single Fiber Efficiencies.	120
7.24	Comparison of Efficiencies with Duran's Model.	122
7.25	Comparison of Present Measurements with Natarajan Measurements.	123
7.26	Efficiency Versus Initial Pressure Drop for Flat and Pleated Filters.	127
B.1	Local Efficiency, Upstream and Downstream Number Densities and Velocity Profiles, A13192 Pleated Filter, Diffuser Housing, 0.966 Micron PSL Particles, 5.68 m ³ /hr Air Flow, Test # F15, 7/1/96.	142
B.2	Local Efficiency, Upstream and Downstream Number Densities and Velocity Profiles, A13192 Pleated Filter, Diffuser Housing, 0.966 Micron PSL Particles, 5.68 m ³ /hr Air Flow, Test # F16, 7/2/96.	143
B.3	Local Efficiency, Upstream and Downstream Number Densities and Velocity Profiles, A13192 Pleated Filter, Diffuser Housing, 0.966 Micron PSL Particles, 29.5 m ³ /hr Air Flow, Test # F11, 6/24/96.	144
B.4	Local Efficiency, Upstream and Downstream Number Densities and Velocity Profiles, A13192 Pleated Filter, Diffuser Housing, 0.966 Micron PSL Particles, 29.5 m ³ /hr Air Flow, Test # F12, 6/25/96.	145
B.5	Local Efficiency, Upstream and Downstream Number Densities and Velocity Profiles, A13192 Pleated Filter, Diffuser Housing, 0.966 Micron PSL Particles, 53.3 m ³ /hr Air Flow, Test # F23, 7/16/96.	146
B.6	Local Efficiency, Upstream and Downstream Number Densities and Velocity Profiles, A13192 Pleated Filter, Diffuser Housing, 0.966 Micron PSL Particles, 53.3 m ³ /hr Air Flow, Test # F22, 7/15/96.	147
B.7	Local Efficiency, Upstream and Downstream Number Densities and Velocity Profiles, A13192 Pleated Filter, Diffuser Housing, 0.966 Micron PSL Particles, 53.3 m ³ /hr Air Flow, Test # F24, 7/17/96.	148
B.8	Local Efficiency, Upstream and Downstream Number Densities and Velocity Profiles, A13192 Pleated Filter, Diffuser Housing, 0.966 Micron PSL Particles, 77.1 m ³ /hr Air Flow, Test # F9, 6/19/96.	149

B.9	Local Efficiency, Upstream and Downstream Number Densities and Velocity Profiles, A13192 Pleated Filter, Diffuser Housing, 0.966 Micron PSL Particles, 77.1 m ³ /hr Air Flow, Test # F10, 6/20/96.	150
B.10	Local Efficiency, Upstream and Downstream Number Densities and Velocity Profiles, A13192 Pleated Filter, Diffuser Housing, 0.966 Micron PSL Particles, 103.7 m ³ /hr Air Flow, Test # F20, 7/5/96.	151
B.11	Local Efficiency, Upstream and Downstream Number Densities and Velocity Profiles, A13192 Pleated Filter, Diffuser Housing, 0.966 Micron PSL Particles, 103.7 m ³ /hr Air Flow, Test # F19, 7/5/96.	152
B.12	Local Efficiency, Upstream and Downstream Number Densities and Velocity Profiles, A13192 Pleated Filter, Diffuser Housing, 0.966 Micron PSL Particles, 145.7 m ³ /hr Air Flow, Test # F1, 5/8/96.	153
B.13	Local Efficiency, Upstream and Downstream Number Densities and Velocity Profiles, A13192 Pleated Filter, Diffuser Housing, 0.966 Micron PSL Particles, 145.7 m ³ /hr Air Flow, Test # F4, 5/14/96.	154
B.14	Local Efficiency, Upstream and Downstream Number Densities and Velocity Profiles, A13192 Pleated Filter, Diffuser Housing, 0.966 Micron PSL Particles, 145.7 m ³ /hr Air Flow, Test # F2, 5/13/96.	155
B.15	Local Efficiency, Upstream and Downstream Number Densities and Velocity Profiles, A13192 Pleated Filter, Diffuser Housing, 0.966 Micron PSL Particles, 187.7 m ³ /hr Air Flow, Test # F18, 7/4/96.	156
B.16	Local Efficiency, Upstream and Downstream Number Densities and Velocity Profiles, A13192 Pleated Filter, Diffuser Housing, 0.966 Micron PSL Particles, 187.7 m ³ /hr Air Flow, Test # F21, 7/8/96.	157
B.17	Local Efficiency, Upstream and Downstream Number Densities and Velocity Profiles, A13192 Pleated Filter, Diffuser Housing, 0.966 Micron PSL Particles, 187.7 m ³ /hr Air Flow, Test # F5, 5/21/96.	158
B.18	Local Efficiency, Upstream and Downstream Number Densities and Velocity Profiles, A13192 Pleated Filter, Diffuser Housing, 0.966 Micron PSL Particles, 313.8 m ³ /hr Air Flow, Test # F7, 6/7/96.	159
B.19	Local Efficiency, Upstream and Downstream Number Densities and Velocity Profiles, A13192 Pleated Filter, Diffuser Housing, 0.966 Micron PSL Particles, 313.8 m ³ /hr Air Flow, Test # F8, 6/18/96.	160

B.20	Local Efficiency, Upstream and Downstream Number Densities and Velocity Profiles, A13192 Pleated Filter, Diffuser Housing, 0.966 Micron PSL Particles, 481.8 m ³ /hr Air Flow, Test # F14, 6/28/96.	161
B.21	Local Efficiency, Upstream and Downstream Number Densities and Velocity Profiles, A13192 Pleated Filter, Diffuser Housing, 0.966 Micron PSL Particles, 481.8 m ³ /hr Air Flow, Test # F17, 7/3/96.	162
C.1	Local Efficiency, Upstream and Downstream Number Densities and Velocity Profiles, SAE Housing, A13192 Pleated Filter, 0.966 Micron PSL Particles, 61.2 m ³ /hr Air Flow, Test # SAE3, 9/3/96.	164
C.2	Local Efficiency, Upstream and Downstream Number Densities and Velocity Profiles, SAE Housing, A13192 Pleated Filter, 0.966 Micron PSL Particles, 313.8 m ³ /hr Air Flow, Test # SAE4, 9/4/96.	165
D.1	Calibration Plot for TSI Flow Meter for Flow Rates Less Than 50 Scfm (85.5 Sm ³ /hr) [Anand, 1997].	166
D.2	Calibration Plot for TSI Flow Meter for Flow Rates More Than 50 Scfm (85.5 Sm ³ /hr).	167
G.1	The Swept Volume Technique.	172
H.1	Comparison of the Average Efficiencies.	175

NOMENCLATURE

A_1	cross-sectional area of the flow upstream the filter (m^2)
A_2	cross-sectional area of the flow downstream the filter (m^2)
A_P	projected cross-sectional area of the probe volume (m^2)
A_{PF}	area of the pleated filter (m^2)
A_{FF}	area of the unfolded pleated filter (m^2)
C	packing density
C_m	Cunningham slip correction factor
C_w	wave speed (m/s)
D_i	particle diffusivity (seconds)
D_f	diameter of fiber (m)
D_p	diameter of particle (m)
e	velocity increment (m/s)
E	overall collision efficiency for a filter
f	wave frequency (Hz)
H_p	pleat height (m)
K	hydrodynamic factor of Kuwabara flow

L	filter thickness (m)
m_1	local mass flux upstream the filter ($\text{kg}/\text{m}^2\text{-s}$)
m_2	local mass flux upstream the filter ($\text{kg}/\text{m}^2\text{-s}$)
M_1	mass of particles seeded upstream of the filter (kg)
M_2	mass of particles collected downstream of the filter (kg)
M_C	mass of particles collected by the filter (kg)
N	particle count
N_i	particle count for stream i
N_T	total particle count
n	particle number density (m^{-3})
n_i	particle number density for stream i (m^{-3})
n_{ns}	particle number density for non-symmetric velocity histogram (m^{-3})
n_s	particle number density for symmetric velocity histogram (m^{-3})
n_T	total number density (m^{-3})
P	pressure (Pa)
Pe	Peclet number ($= U \frac{D_i}{D_p}$)
Q	flow rate (m^3/hr)
$Q_{\text{flow nozzle}}$	volumetric flow rate measured by ASME flow nozzle (Scfm)
Q_{TSI}	volumetric flow rate measured by TSI flow meter (Scfm)
R, R_F	fiber radius (m)
R_p	particle radius (m)

Re	Reynolds number ($= \frac{\rho_a U D_p}{\mu_o}$)
s'_1, s'_2	number densities with error (m^{-3})
S	spacing of fringes (m)
St	Stokes number ($= \frac{C_m D_p^2 \rho_p U}{18 \mu_a D_f}$)
T	time (seconds)
T_{FF}	filter paper thickness (m)
T_0	run time (seconds)
U	velocity (m/s)
U_o	velocity of the flow approaching (and outside of the pleats of) the filter (m/s)
U_a	velocity of the particles inside the filter (m/s)
V	particle velocity (m/s)
V_i	velocity of particle for stream i (m/s)
V_{FF}	volume of the flat filter (m^3)
V_P	peak velocity (m/s)
V_{PF}	volume of the pleated filter (m^3)
Y	flow stream layer thickness (m)
α	filter solidity or packing density (= volume of fibers/total volume of filter)
β	angle of particle path measured from normal to the plane of two

intersecting beams

θ_1	angle of particle path measured from beam A
θ_2	angle of particle path measured from beam A'
θ'_1	angle of particle path measured from detector
η	local efficiency
η_D	collection efficiency due to diffusion
η_{DR}	collection efficiency due to interaction of interception and diffusion
η_I	collection efficiency due to inertial impaction
η_R	collection efficiency due to interception
η_s	single fiber efficiency
λ	wavelength of light (m)
μ_a	dynamic viscosity of air (Pa-s)
ρ_a	density of air (kg/m^3)
ρ_p	density of seeding particles (kg/m^3)
ν	Doppler frequency shift (Hz)

CHAPTER I

INTRODUCTION

The history of air induction filters for automobiles goes back to the early twentieth century when a ring filter was made out of many interlocking layers of metal fibers which provided a filtration efficiency of about 70 to 85 percent [Rodman, 1992].

The first pleated filter media was then developed by the British Air Ministry shortly after World War One. Later in 1951, Fram developed the pleated paper air filter with a dust removal efficiency of 98 percent [Rodman, 1992]. In the late 1960s, Japanese automobile manufacturing companies introduced ring air filters made out of pleated composite nonwoven materials. Such media provided a better dust removal efficiency (up to 99%) and increased the dust holding capacity [Rodman, 1992].

In 1978 Fram introduced a pleated non-woven air filter having a 150% increase in dust holding capacity and 99% dust removal efficiency with less than 60 percent of the number of pleats compared to standard pleated filter elements available at that time [Rodman, 1992]. From Fram's modification up to the present time, after nearly two decades, several modifications have been made by manufacturers in order to reduce the

filter size and cost and increase the filtration efficiency as well as filter dust holding capacity.

This study presents measurements of local efficiency for a pleated filter media exposed to different flow conditions. Laser Doppler Velocimetry (LDV) is used to measure the particle counts and velocities above and below the filter.

1.1 Objectives

The present research is a continuation of previous OSU research on local efficiency measurements of pleated and flat filter media. As a continuation of that previous work, more emphasis has been placed on reliability and repeatability of the measurements. For this reason, the variation of the different parameters of the measurement system has been analyzed in order to evaluate the effect of each on the measured data. As a result, certain conditions were dictated so that under those conditions, using the optimum values of the system parameters, the data would be reliable with minimum achievable error. Repeatability of the data was also verified.

Consistency measurements were made at a specific location in a uniform flow without any filtration in order to achieve the above mentioned goals. These measurements were also made at two different locations in the uniform flow in order to verify the behavior of different parameters of the system. Local efficiencies were calculated for uniform flows without filtration (zero efficiency) so that the local efficiencies and the local behavior of the flow could be studied.

The main measurements were made on the A13192 pleated filter manufactured by Purolator Products, Inc (now Dayco-Purolator, a Division of Mark IV Industries). The

filter was tested in a small angle diffuser housing as well as the standard SAE J726 housing, both constructed from plexiglass. Spherical latex polystyrene (PSL) particles of 0.966 micron diameter were used as seeding particles. The particles were seeded into the flow by a TSI six jet atomizer (see Appendix F for equipment list). A heater was used to evaporate any water droplets coming out of the atomizer so that only dry PSL particles were fed into the flow. Measurements of particle counts and velocities were made upstream and downstream of the filter using an LDV system.

The number densities (or particle concentrations) were calculated based on a technique called “Swept Volume Technique”, and efficiencies were calculated using the number densities upstream and downstream of the filter. The calculated data was compared with previous tests performed by Natarajan [1995]. They were also compared with flat filter media (Anand [1997], Williams [1995]).

The following Chapter of this thesis presents some of the theoretical models for calculating filtration efficiencies and the literature survey. LDV fundamentals are discussed in Chapter three. The next Chapter (Chapter four) describes the experimental setup and system components. The basic assumptions, validity range and different models of the Swept Volume Technique (SVT), used for number density and local efficiency calculations, are described in Chapter five. Consistency measurements and optimum setting of the system parameters are discussed in Chapter six and discussion of results are presented in Chapter seven. Conclusions and future recommendations are presented in Chapter eight. Other useful information such as the definition of LDV system parameters and examples of Stokes number calculation are presented in the appendices.

CHAPTER II

LITERATURE REVIEW

Several studies have been made on different aspects of the air filtration theory in the past. The basic concepts of the air filtration by fibrous filters and previous theoretical and experimental studies of air filtration are discussed in this chapter.

2.1 Single Fiber Efficiency Theory

The classical theory of the air filtration by fibrous filters is based on the motion of the particles in a flow stream approaching a single cylindrical fiber. As air flows around a fiber, the trajectories of the particles may deviate from the streamlines due to different mechanisms. As a result, particles may be collected by the fiber and become deposited on it. The major mechanisms causing particle deposition are diffusion, inertial impaction and interception. In addition, electrostatic forces and gravitational settling may contribute to the particle collection. Single fiber efficiency is defined as the ratio of the number of particles collected by a fiber (due to all collection mechanisms) to the number which would be collected if the streamlines were not diverted [Lee, 1977]. If a fiber of radius R_f removes all particles contained in a layer of thickness Y , as shown in Fig. 2.1, the single

fiber efficiency is then defined as Y/R_f [Lee, 1977]. Based on its definition, the single fiber efficiency is independent of the filter thickness. Therefore, the single fiber efficiencies of two different filters with different thicknesses could be compared while the total efficiencies of these filters might not be comparable.

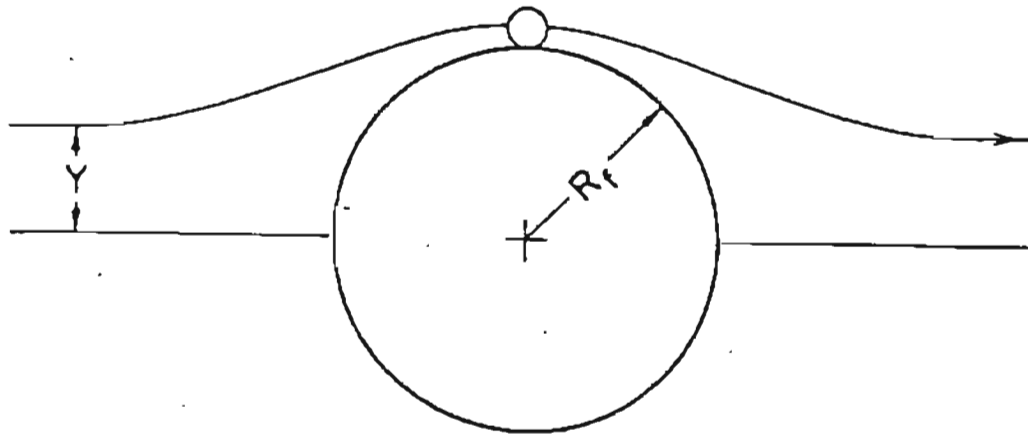


Figure 2.1 Definition of the Single Fiber Efficiency [Lee, 1977].

The single fiber efficiency theory is based on the uniform distribution of cylindrical fibers having uniform diameters throughout the filter media. Such assumptions might not be accurate for industrial air filters which have non-uniform distributions of the fibers. Also, the diameters of the fibers might not be the same. Non-homogeneity of the fibers usually results in a reduced efficiency [Lee, 1977]. Another disadvantage of the single fiber theory is that the calculated theoretical efficiency can not be determined by experiment since it is difficult to measure the efficiency of a single fiber. Yeh [1972] has

correlated the total efficiency with the single fiber efficiency for a flat filter. Assuming a flat filter with thickness L and fiber volume fraction α (the ratio of the volume of the fibers divided by the total fiber volume in a unit surface area of the filter), he calculated the air velocity between the fibers (inside the filter paper) as:

$$U_{\alpha} = \frac{U_0}{1-\alpha} \quad (2-1)$$

where U_0 is the undisturbed velocity upstream the filter. Using the air velocity inside the filter and integrating the particle concentration rate over the filter thickness, he calculated the efficiency of the unit surface area of the filter as:

$$E = 1 - \exp\left(-\frac{2\eta_s \alpha L}{\pi(1-\alpha)R_f}\right) \quad (2-2)$$

where E is the filter efficiency, α is the volume fraction of the filter, L is filter thickness, R_f is the fiber radius and η_s is the single fiber efficiency.

2.2 Mechanisms of Particle Collection

There are a number of known mechanisms which cause the collection of a particle by the filter fibers. The importance of their effect depends on the particle and fiber diameters as well as the Stokes number. These mechanisms are described below.

2.2.1 Diffusion

The Brownian motion of the particles will cause their trajectory to deviate from the streamlines of the flow. Particles may diffuse away from the streamline to the fibers and be collected. Figure 2.2a presents the path of a particle affected by Brownian motion and

collected by the fiber. Since Brownian motion increases with decreasing particle size, the diffusive deposition of the particles increases when the particle size is reduced.

2.2.2 Inertial Impaction

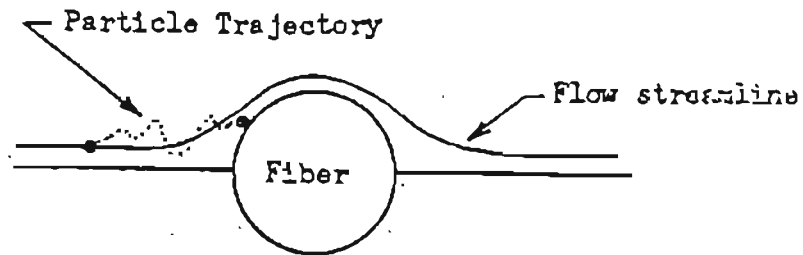
Assuming a cylindrical fiber, the streamlines of the air passing around a fiber are curved. Particles with a finite mass moving with the flow might not follow the streamlines because of their inertia. If the particle mass is sufficiently large and the fiber radius is large enough (as compared to the particle diameter), the particle may deviate from the streamline and collide with the fiber (Fig. 2.2c). Unlike diffusion, the probability of the collision of a particle with the fiber increases with increasing the particle mass. The mechanism of the inertial impaction can be studied by the dimensionless Stokes number. Stokes number is defined as [Brown, 1993]:

$$St = \frac{C_m D_p^2 \rho_p U}{18 \mu_a D_f} \quad (2-3)$$

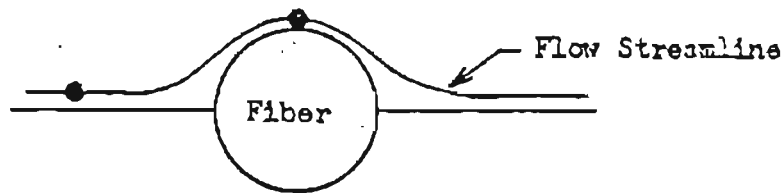
Where ρ_p is the particle density, D_p and D_f are particle and fiber diameters respectively. U is the air stream velocity, μ_a is the air viscosity and C_m is the Cunningham slip correction factor which is unity for particles of one micron diameter and larger. For particles smaller than one micron, the slip correction factor is less than one. The correction factor is used in order to consider possible sliding of the fluid flow stream on the particles which may result in lower particle velocities than the flow stream. In other words, the velocity of the small sized particles (less than one micron) flowing in a fluid flow with velocity U , is calculated as $C_m U$. Liu and Lee [1982] have used a different correlation for the Stokes number calculation. He used a factor of 9 instead of 18 in Eq. (2-3). Therefore his calculated Stokes number values are twice those calculated by Eq. (2-3).

2.2.3 Interception

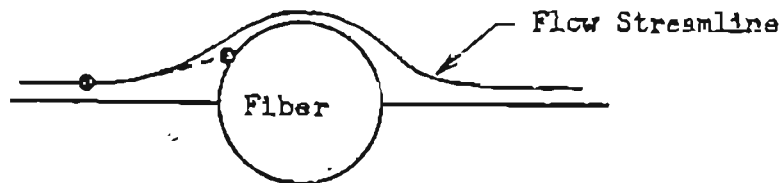
If a particle follows the fluid streamlines and does not deviate by diffusion and inertial impaction, it might be collected by interception. The particle will be collected by a fiber if the streamline brings the particle center closer than one particle radius away from the fiber surface (Fig. 2.2b). Interception is independent of the flow velocity. The ratio of the particle diameter to the fiber diameter is an index which quantifies the importance of the collection by interception as compared with other collection mechanisms (diffusion and inertial impaction).



(a) Brownian Diffusion.



(b) Direct Interception



(c) Inertial Impaction

Figure 2.2 Three Main Mechanisms of Particle Collection [Lee, 1977].

2.2.4 Other Collection Mechanisms

In addition to the above mentioned mechanisms, gravitational and electrostatic forces might also contribute to the collection of the particles by the fiber. If the particles and fibers are electrically charged, the attraction forces might result in the collection of the particles. Large size particles (particles having diameters of a few microns or larger) may deviate from the streamlines due to gravitational forces. Molecular forces and rotational motion of a particle in shear flow near the fiber surface are other mechanisms which may enhance particle collection. However, the main mechanisms of the particle collection are diffusion, inertial impaction and interception. Several studies have been made in these areas and there are models and correlations which can describe the effect of each of these mechanisms. Liu et al. [1985] have shown the importance of different collection efficiency mechanisms for different particle sizes (Fig. 3.3).

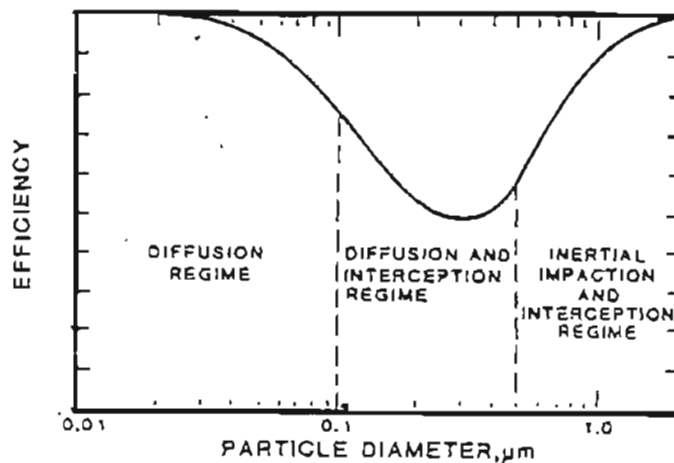


Figure 2.3 Schematic Diagram of the Collection Efficiencies of Different Particle Capture Mechanisms [Liu et al., 1985].

2.3 Classical Filtration Theories

As stated earlier, several theoretical and experimental studies were made on the subject of air filtration by fibrous filters. Theoretical studies are mainly based on the models which calculate collection efficiencies of the different major particle capturing mechanisms (diffusion, inertial impaction and interception). Davies [1973] calculated the effect of the interception for a filter with a volume fraction of α and assumed that both the inertial impaction and diffusion mechanisms are affected to the same extent by the neighboring fibers as the interception. He derived the single fiber efficiency as:

$$\eta = (0.16 + 10.9\alpha - 17\alpha^2)[R + (0.5 + R)(St + Pe) - 0.1052R(St + Pe)^2] \quad (2-4)$$

In the above equation, α is the volume fraction, R is the fiber radius, St is the Stokes number and Pe is the Peclet number.

Hoppel [1959] and Kuwabara [1959] modeled a filter as equal sized cylinders placed in a staggered pattern transverse to the flow. The boundary of the system is a hexagon around the staggered cylinders. Deriving the Navier Stokes equations for such a system, Kuwabara came up with a correlation representing stream function as well as the radial and tangential velocities in terms of system parameters such as face velocity, volume fraction and particle and fiber diameters.

Harrop and Stenhouse [1969] used the Hoppel flow field and computed the particle trajectories numerically by computer. The calculation covered only inertial impaction for finite particle sizes, and the result was presented in a graphical form.

Stechkina et al. [1969] calculated the filtration efficiency using the Kuwabara flow field. They expressed the total single fiber efficiency as a summation of single fiber efficiencies due to inertial impaction, η_i , interception, η_R , diffusion, η_D and interaction of diffusion and interception, η_{DR} , in other words:

$$\eta = \eta_i + \eta_R + \eta_D + \eta_{DR} \quad (2-5)$$

He then calculated the terms on the right hand side as :

$$\eta_i = \frac{1}{2K^2} [(29.6 - 28\alpha^{0.62})R^2 - 27.5R^{2.8}] St \quad (2-6)$$

$$\eta_R = \frac{1}{2K} [(2(1+R) \ln(1+R) - (1+R) + (1+R)^{-1})] \quad (2-7)$$

$$\eta_D = 2.7 Pe^{-2/3} \quad (2-8)$$

$$\eta_{DR} = 1.24 K^{-1/2} Pe^{-1/2} R^{2/3} \quad (2-9)$$

where $K = -\frac{1}{2} \ln(\alpha) - \frac{1}{2} + \alpha - \frac{\alpha^2}{4}$, Pe is the Peclet number, and St is the Stokes number.

2.4 Experimental Studies for Flat Filter Media

A number of experimental studies on air filtration by flat filter media are found in the literature. These studies can be categorized based on particle sizes.

2.4.1 Flat Filter Media Measurements with Aerosol Particles

As defined in ASTM F-1215 [1989], aerosols are particles with diameters less than one micron. Aerosol particle counts are usually measured by optical counting systems.

Among different optical counting systems, the Laser Doppler technique is a common system which is widely used for measurements of aerosol particles.

Yeh [1972] and Lee [1977] have studied filtration of submicron aerosols by fibrous filters. They used a condensation aerosol generator to seed the particles into the flow. DOP particles (Triphenyl Phosphate Dioctyl Phthalate) were used and Dacron filters with different packing densities were selected as test filters. They performed the filtration experiments and compared the data with the results of the classical theories. A typical efficiency plot presented by Yeh is shown in Fig. 2.4. Lee used Eq. (2-2) in order to obtain the single fiber efficiency. He compared his results with the theory of Harrop [1969] in the inertial impaction regime (Fig. 2.5). The Stokes number used by Lee is twice the value calculated by Eq. (2-3).

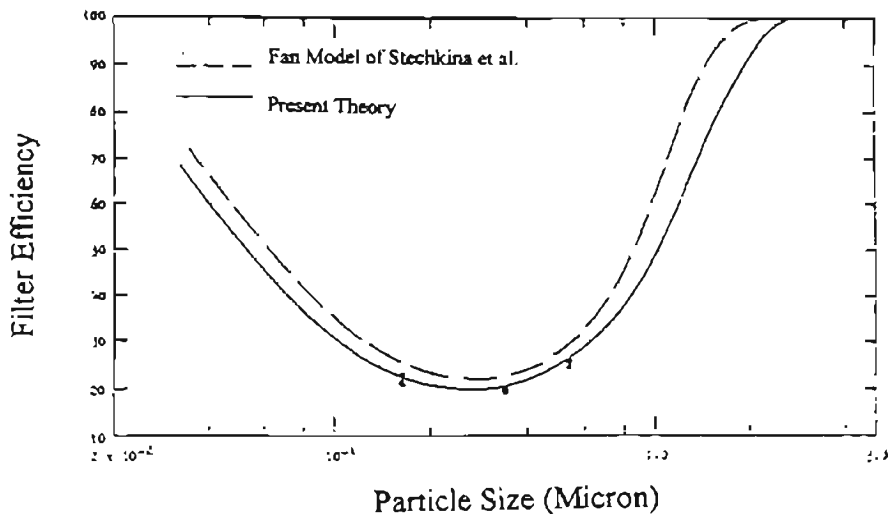


Figure 2.4 Comparison of Theoretical and Experimental Filter Efficiency as a Function of Particle Size, Dacron Filter, $D_f = 11.3$ Microns, $\alpha = 0.0493$, $U = 0.0396$ m/s [Yeh, 1972].

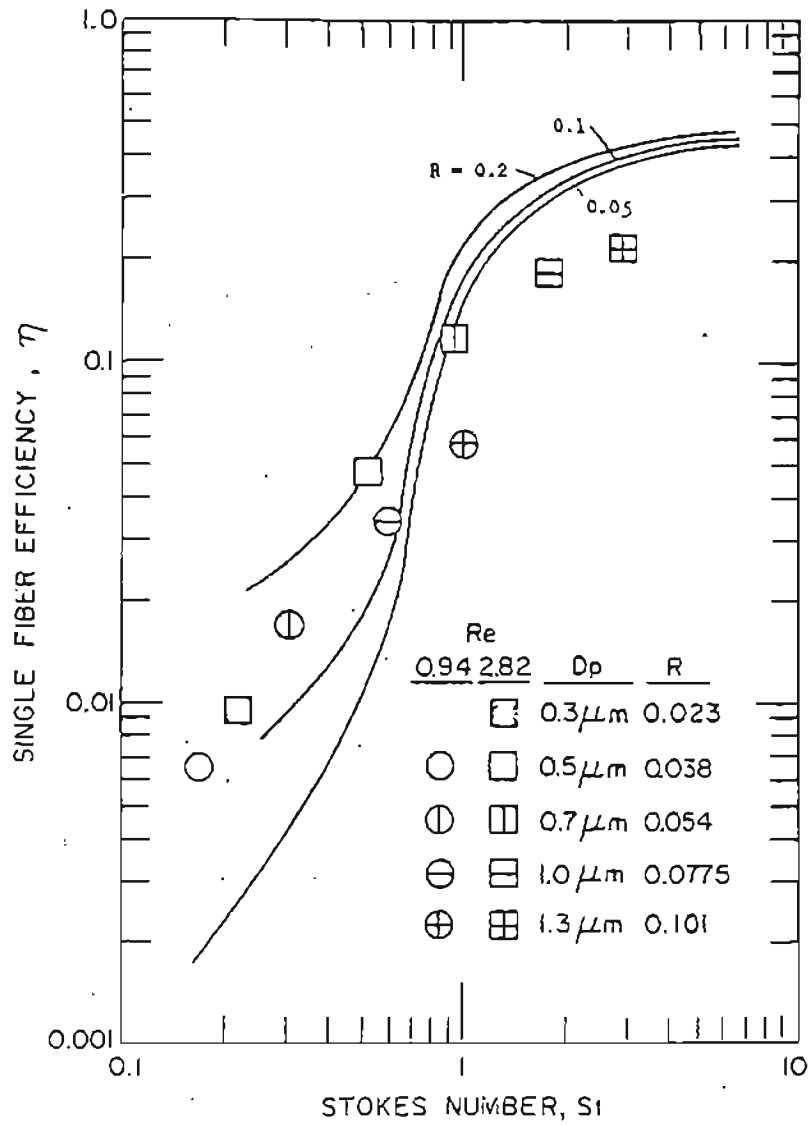


Figure 2.5 Comparison of Experimental Efficiency Measurements with the Theory of Harrop and Stenhouse [1969] in the Inertial Impaction Regime [Lee, 1977].

2.4.2 Flat Filter Measurements with Dust Particles

Other than aerosols, dust particles are often used for filter efficiency measurements. The Society of Automotive Engineers (SAE) has defined two categories of dust particles, the fine dust (SAF) and the coarse dust (SAC). The SAF dust, according to its definition, contains a mixture of different size dust particles, most of them ranging from 0.5 to 80 microns. The SAC dust contains a mixture of dust particles with most of the particles having sizes between 0.5 to 100 micron. The size distribution of SAF and SAC are shown in Fig. 2.6 [Gidley, 1993].

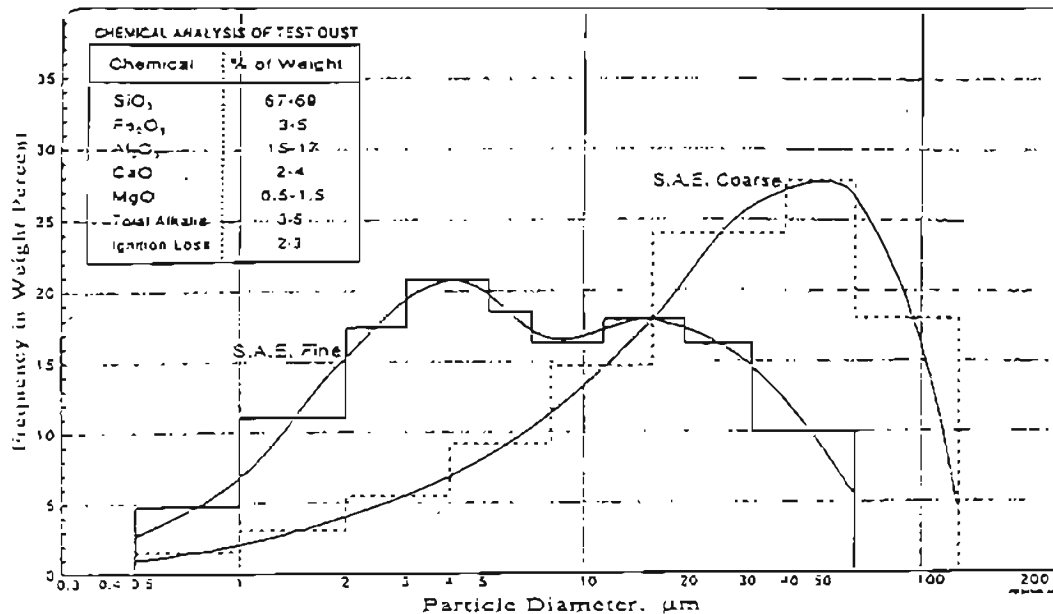


Figure 2.6 SAE Dust Size Distribution [Gidley, 1993].

Jaroszcyk [1987] has conducted measurements on different filters made of polyacrylonitrile fibers with an average diameter of 27 microns and different packing densities ranging from 0.0188 to 0.0612. A typical plot of his measurements is shown in Fig. 2.7. As can be seen from the figure, the efficiencies are in the range of 95 to 99.5 percent. This implies the fact that efficiency measurements for dust particles give higher efficiencies than values obtained from aerosol particles with smaller sizes. Filter efficiency changes with time when dust particles are used. Since the dust particles are collected by the filter, less area is available for the flow to pass the filter. As a result, the pressure drop across the filter increases. This is true until the time when the weight of the collected dust is less than filter dust holding capacity. Efficiency will then drop a little because of the breakage of the dust cake constructed on the filter. The phenomenon is known as re-entrainment.

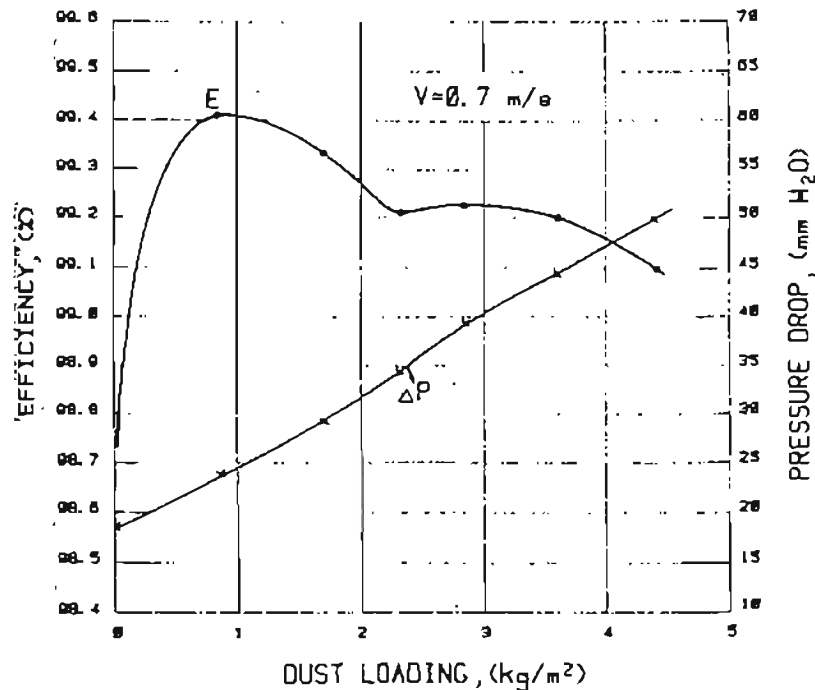


Figure 2.7 Filter Performance Versus Dust Loading [Jaroszcyk, 1987].

It is difficult to conduct dust measurements by measuring particle counts with optical particle counting systems. The high efficiency will cause a low number of samples downstream of the filter. Increasing the particle seeding rate will increase the filter loading so that it reaches the filter dust holding capacity sooner.

2.5 Pleated Filters

Person and Cashin [1994] have studied recent developments in pleated cabin air filters. They have highlighted the fractional efficiency requirement for pleated filters (Fig. 2.8). Also, they have discussed the conflicting design requirements of the cabin air filters (Fig. 2.9). According to their analysis, filter size and life, pressure drop across the filter and filter efficiency are items which should be optimized for the best design. The design goal is to have a filter with low pressure drop, high efficiency, long life and adaptable to any geometry.

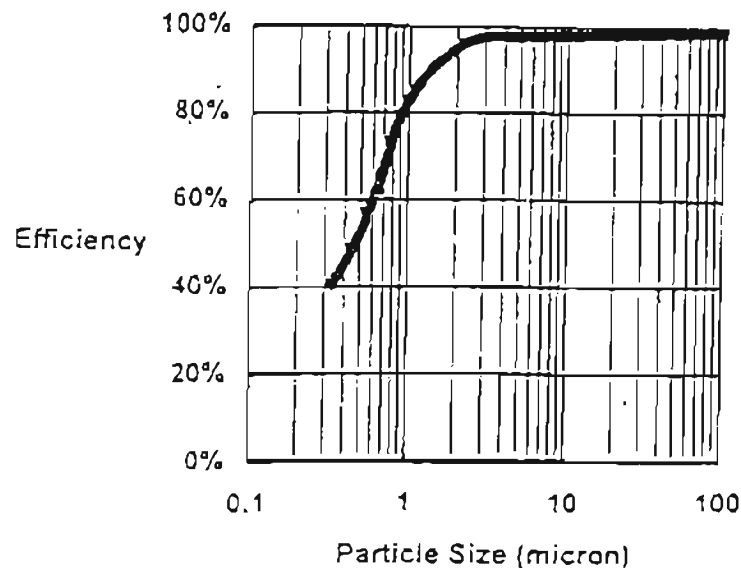


Figure 2.8 Fractional Efficiency Requirement for Cabin Air Filter
[Person and Cashin, 1994].

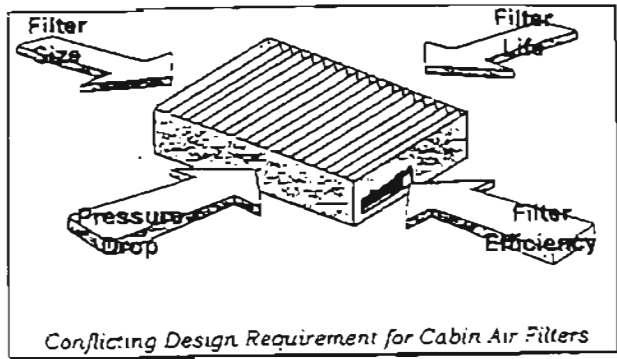


Figure 2.9 Conflicting Design Requirement for Cabin Air Filter

[Person and Cashin, 1994].

Ptak et al. [1994] evaluated the effects of the flow rate on the initial efficiency of two different car interior filters (Fig. 2.10).

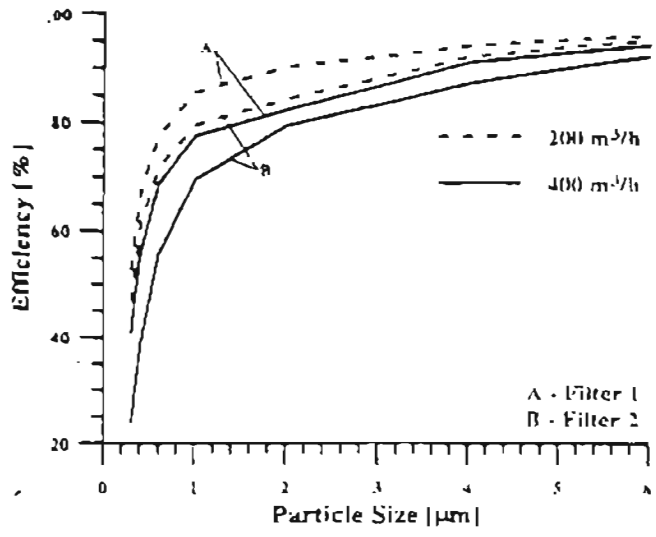


Figure 2.10 Dependence of Initial Efficiency on Flow Rate [Ptak et al., 1994].

Reinhart and Weisert [1983] have studied engine air cleaner efficiencies. They used SAE fine dust and loaded two similar filters. Measurements were made by an optical particle counting system. Their measurements show a rapid increase of the filtration efficiency, especially for particles greater than 3 microns, after loading the filter by 0.0242 grams per unit area. Figure 2.11 shows the fractional efficiencies at various dust loading. Figure 2.12 is an isometric representation of the efficiency versus dust loading and particle size.

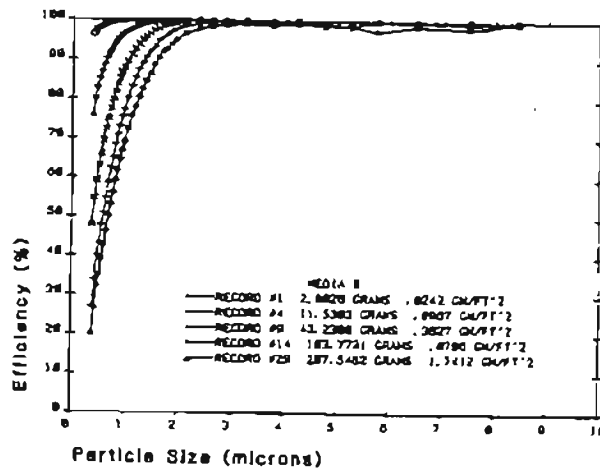


Figure 2.11 Fractional Efficiency at Various Dust Loading [Reinhart and Weisert, 1983].

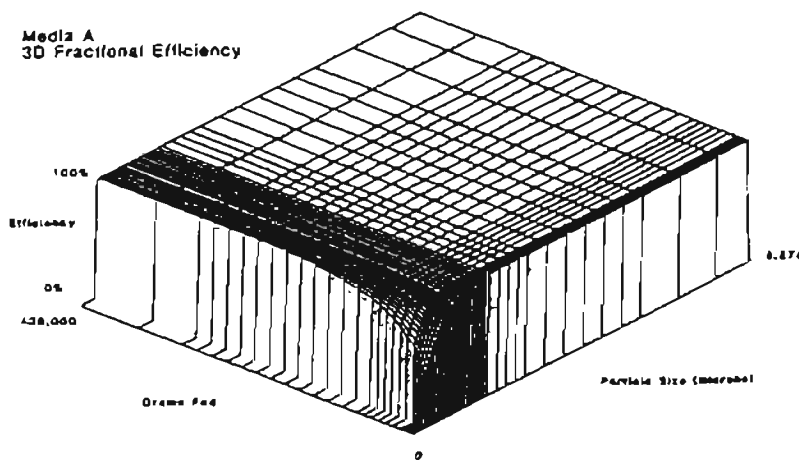


Figure 2.12 Isometric Representation of Efficiency, Particle Size and Dust Loading [Reinhart and Weisert, 1983].

Chen et al. [1994] have modeled a pleated filter based on the geometry of the pleat. They studied two different kinds of pleats, rectangular and triangular, and modeled a pleated filter with a steady laminar air flow. They used the finite element method for solving the governing equations.

Based on their model, there is an optimum pleat count per unit length which gives the minimum pressure drop across the filter. The regime for pleat counts lower than that value is called filter medium dominated domain; and for higher values, it is called the viscosity dominated domain. Figure 2.13 shows the pressure drop across the pleated filter with different pleat counts per unit length of the filter. These measurements were conducted using HEPA filter media and 95% DOP filter media with a flow velocity of 100 feet per minute (0.51 m/s).

According to their results for the triangular pleat shape, the viscosity effect is reduced due to the wide entrance and gradual shape change of the pleats. Consequently, the number of pleat counts which corresponds to the lowest pressure drop across the filter is higher for triangular pleats as compared to rectangular pleats.

Chen et al. mentioned that the pressure drop across the pleated filter is lower than that of the flat media for the same flow rate. They also stated that the air velocity inside the pleats is higher than the approaching velocity because of the converging shape of the pleats. Also in the viscous domain, since the viscosity is dominant, there is a velocity profile at each pleat cross-section, with lower velocity close to the filter paper and higher velocity at the center of the pleat at each cross-section. The velocity profile at different cross-sections between the pleats will be different. Chen et al. gave stated the variation,

but they did not calculate the profile. They also measured the pressure drop across filters with different pleat counts at different flow rates (Fig. 2.14).

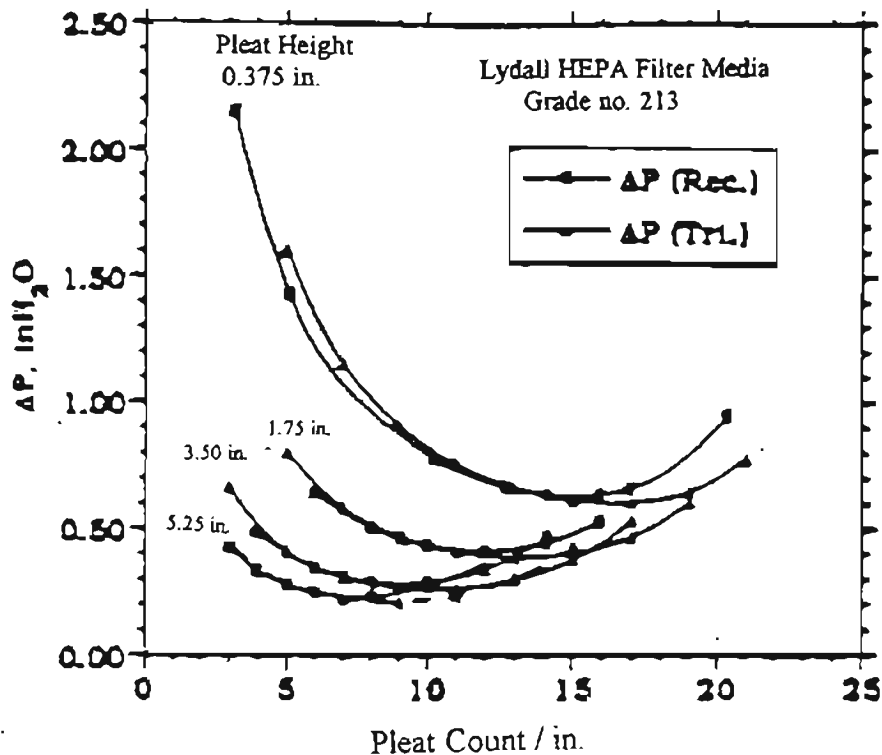


Figure 2.13 Variation of Pressure Drop with Pleat Count for Rectangular and Triangular Pleats, HEPA Filter [Chen et al., 1994].

Gidley [1993] has studied the initial efficiency of different pleated filters used in the inlet system of combustion turbines. He has measured the fractional efficiency of different filters (Fig. 2.15). He used a 24"x 24" (0.61m x 0.61m) filter. The filter was tested with an air flow of 2000 cfm (3418 m³/hr) or velocity of 500 fpm (2.545 m/s).

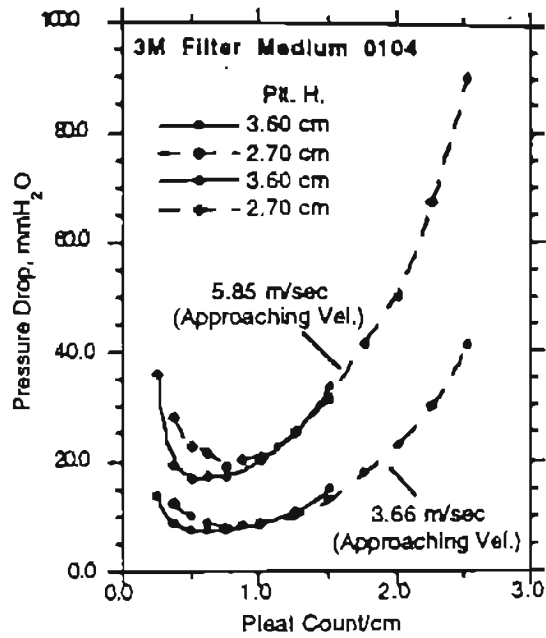


Figure 2.14 Pressure Drop Versus Pleat Count [Chen et al., 1994].

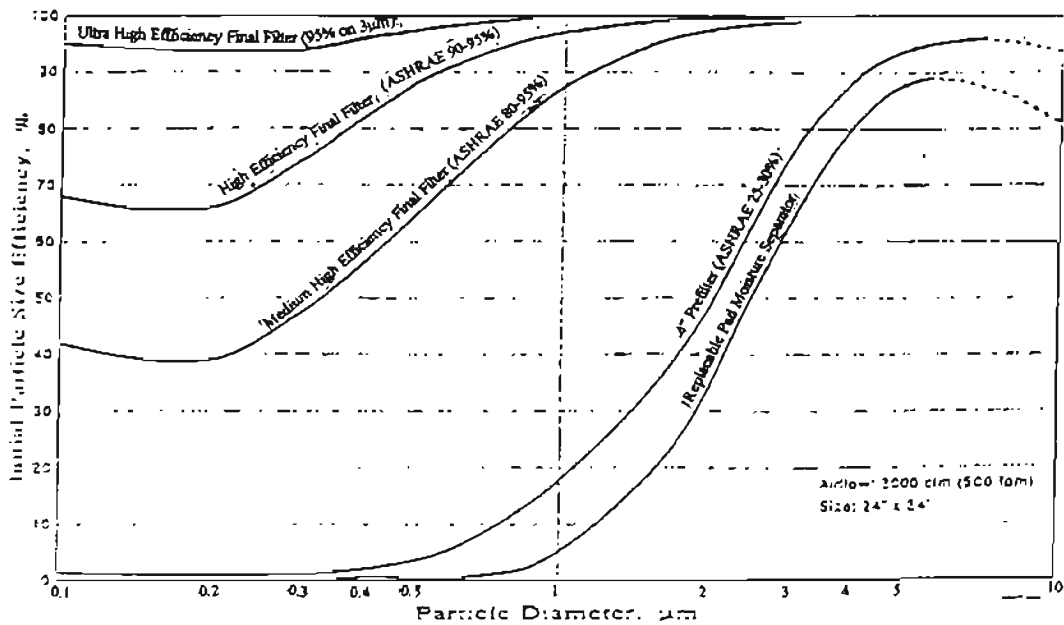


Figure 2.15 Typical Initial Fractional Efficiencies in Inlet System of Combustion Turbines [Gidley, 1993].

2.6 Standard Testing Methods

There are a few standards for testing of the industrial filters. SAE J1669, ASTM F1215-89, and SAE J726 are typical standard codes for these tests. Each of them is applicable under specific conditions. These procedures are described briefly in this section.

2.6.1 SAE J1669

This test code has been established to cover the dry cabin particulate air filters used in automotive powered ventilation system. The test procedure is used for the measurement of overall efficiencies, fractional efficiencies and incremental efficiencies. An aerosol generator or dust feeding system is recommended as a particle seeding system. According to SAE J1669, fractional efficiency could be calculated based on number densities for particles with the same size. The variation of air flow velocity shall be no more than 10% of the mean velocity. Tests should be also conducted using the air entering the system with a temperature of $20^{\circ}\text{C} \pm 5^{\circ}\text{C}$ and a relative humidity of $65\% \pm 15\%$. Two particle counting methods are recommended by SAE J1669 for counting particles upstream and downstream the filter.

- Sequential Counting System:

Using this method, the upstream particles should be counted; then the downstream samples should be counted. For stable aerosol generators, a single upstream-downstream counting system is sufficient. An aerosol source is considered to be stable if the counts vary by less than 2% from one sample period to the next. For other aerosol sources, the

upstream-downstream cycle should be repeated twice more for a total of three upstream and three downstream samples.

- Simultaneous counting system

The particles for both upstream and downstream measurements should be counted and recorded simultaneously.

The tests made in accordance with SAE 1669 should demonstrate that, by identical tests performed on three separate days of no less than three days apart, the filter efficiencies measured are in agreement within $\pm 5\%$ of each other. Other restrictions are also applied for SAE J1669 testing such as limited variation of relative humidity and calibration of measuring instrumentation.

2.6.2 ASTM F1215-89

This is a standard test procedure for determining the initial efficiency of a flat sheet filter medium in air flow with latex spherical particles. The standard was published by the American Society of Testing and Materials (ASTM) in 1989.

The test method covers techniques for measuring the initial particle size efficiency of a flat sheet filter media with monodisperse aerosols. It utilizes a light scattering particle counting system using particles ranging from 0.5 to 5 microns and air flow test velocities of 0.01 m/s to 0.025 m/s with efficiencies less than 99.9 percent.

The aerosol generator must be capable of generating sphere count concentrations of 10^7 to 10^8 particles per cubic meter. The filter medium testing should be conducted in a relative humidity of 30 to 50 percent. The system should measure average efficiency of $0\% \pm 1\%$ when the filter element is not placed.

2.6.3 SAE J726 Code

The SAE J726 is a standard practice of pressure drop and dust collection capacity measurements for panel air filters. The efficiency is calculated on a mass basis. The weight of total dust fed to the system as well as dust collected by the filter is measured in order to calculate the efficiency. The air flow rate should remain within $\pm 2\%$ of the actual value. The entering air temperature should be at $24^{\circ}\text{C} \pm 8^{\circ}\text{C}$. The humidity should remain within the range of $50\% \pm 15\%$.

2.7 The OSU Research

As mentioned earlier, the present research is a continuation of previous theoretical and experimental studies. Experimental measurements and theoretical modeling were made on the A13192 filter (previously AF3192) manufactured by Dayco-Purolator, a division of Mark IV Industries (previously Purolator Inc.), and on flat sheet filter paper which is used for the manufacture of this filter.

2.7.1 Theoretical Models

Sabnis [1993] studied effects of non-uniform air flow through A13192 (previously AF3192) filters on the filter efficiency. He conducted measurements in the SAE J726 test housing and modeled the flow. He predicted the local filter efficiency based on an average fiber radius of 19 microns, a filter thickness of 700 microns and a packing density of 0.23. He calculated elemental efficiencies by his model for different particle sizes. A typical plot of his calculation is shown in Fig. 2.10. According to his model, the filtration efficiency will be lower than 4 % for one micron diameter particles and a flow

rate of $197.7 \text{ m}^3/\text{hr}$. The most dominant collection mechanism, according to his model, is inertial impaction.

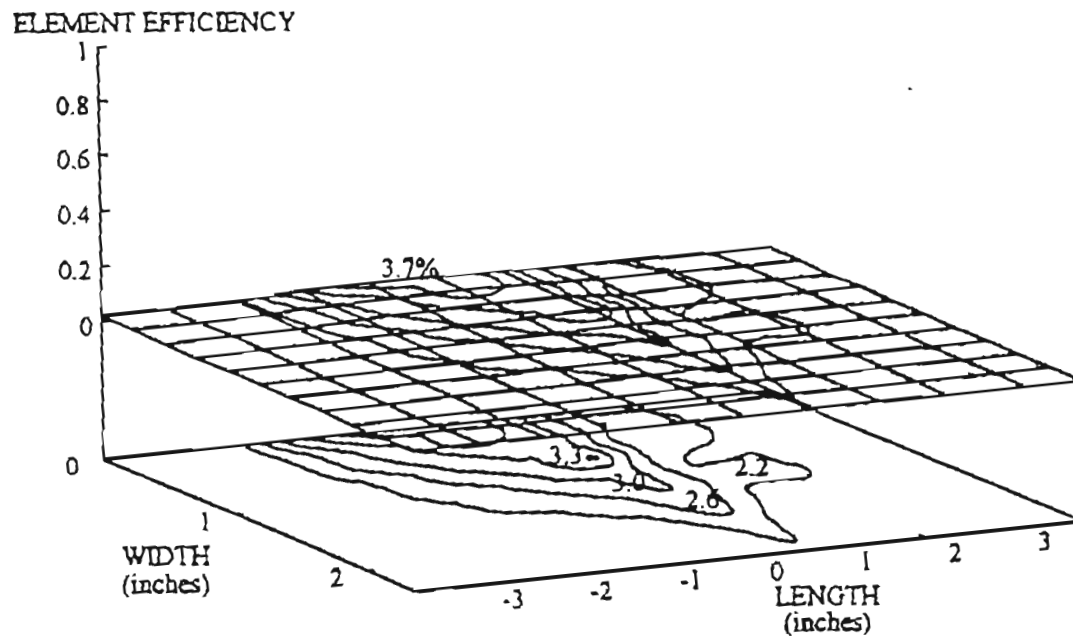


Figure 2.16 Elemental Efficiencies for A13192 Filter [Sabnis, 1993].

Newman [1994] modeled the A13192 pleated filter based on the following assumptions:

1. No re-entrainment of the particles.
2. Diffusive filtration is not dominant.
3. Uniform particle concentration over the filter.
4. Uniform fiber diameter and packing density throughout the filter.
5. Uniform air velocity over the filter.

Using a flow rate of $212 \text{ m}^3/\text{hr}$, he calculated an efficiency of the flow with one micron particles in the small angle diffuser and SAE J726 test housings (Figs. 2.17 and 2.18).

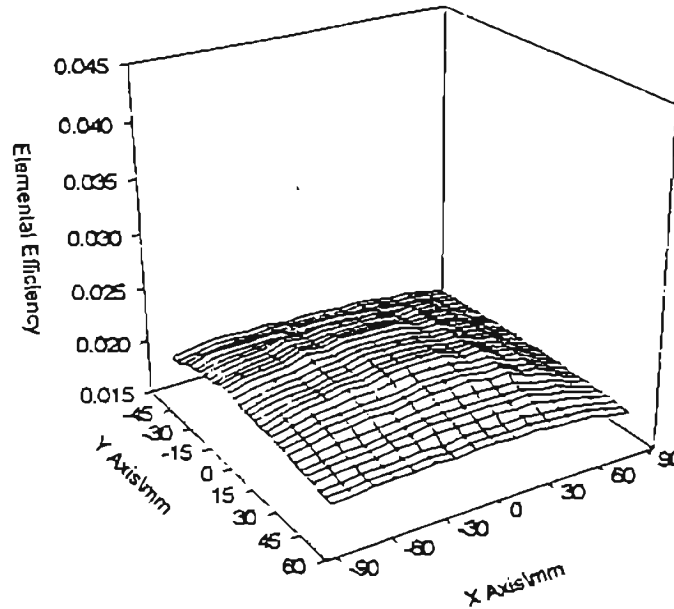


Figure 2.17 Elemental Efficiencies for A13192 Filter, Small Angle Diffuser Housing [Newman, 1994].

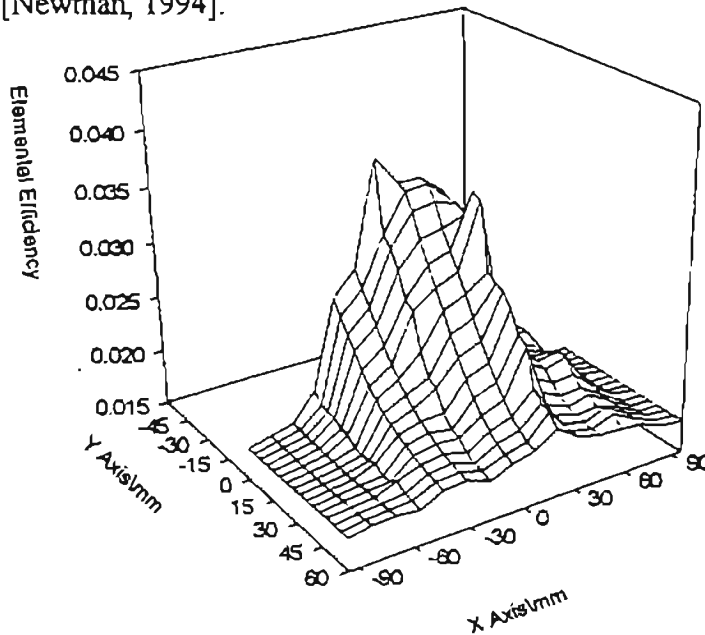


Figure 2.18 Elemental Efficiencies for A13192 Filter, SAE J726 Housing [Newman, 1994].

Both Newman's and Sabnis' calculated efficiencies for one micron particles are much less than experimental results (Anand [1997], Williams [1996], Natarajan [1995]). However, the single fiber efficiency calculated by Sabnis' model conforms with the theoretical models for Stokes numbers greater than 0.1 (Fig. 2.19).

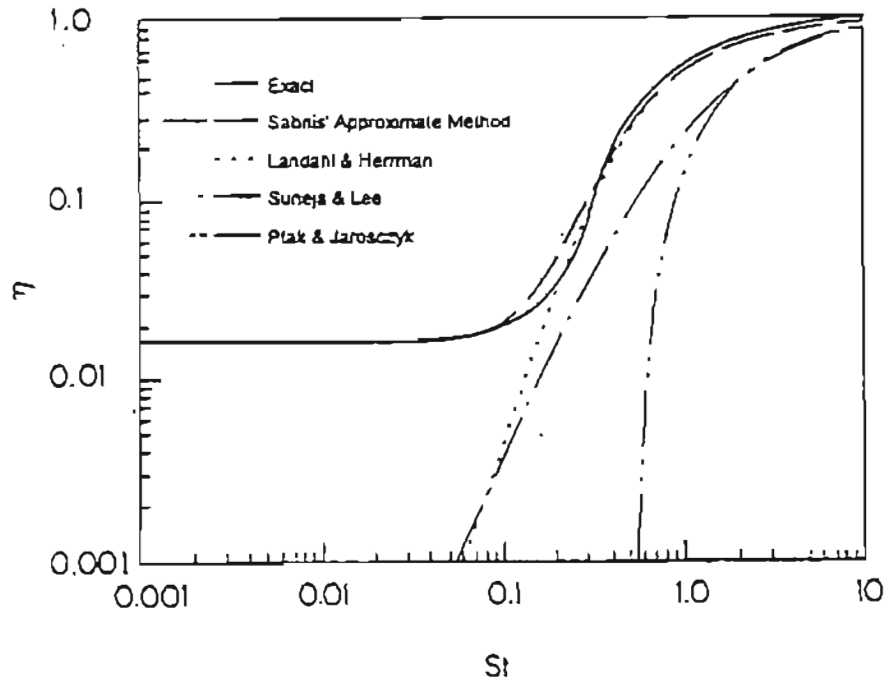


Figure 2.19 Comparison of Single Fiber Efficiency Calculated by Sabnis' Model with Classical Models [Duran, 1995].

Liu [1995] studied and modeled velocity profiles upstream and downstream of the loaded filters. He loaded the A13192 filter with SAE fine dust to reach desired pressure

drops across the filter (for the design flow rate of $212 \text{ m}^3/\text{hr}$). Figure 2.20 is a typical plot of his measurements. He compared his measurements with his CFD model for velocity calculations.

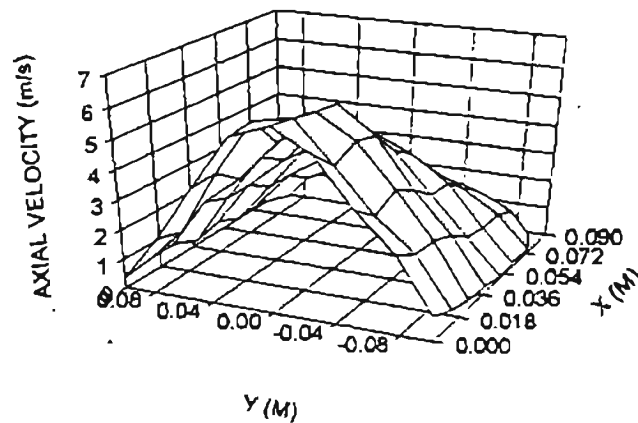


Figure 2.20 Velocity Distribution Upstream of a Dirty Filter Loaded to 127 mm of Water [Liu, 1995].

Duran [1995] modeled the A13192 filter elemental efficiencies with SAE coarse dust particles. Unlike Sabnis, he assumed an average fiber diameter of 51.78 microns and a packing density of 0.345. His model was based on implementation of three models: interception model by Liu and Lee [1982], inertial impaction model by Landhal and Heirmann [1949] and the adhesion model by Ptak and Jaroszczyk [1990]. His calculated efficiencies for one micron particles was similar to Newman's and Sabnis' calculated values.

2.7.2 Experimental Studies

Experimental measurements were made on flat filter media by Anand [1997] and Williams [1996]. Natarajan [1995] conducted measurements on A13192 pleated filters. He stated that he had problems regarding the repeatability of the measured data, variation of the power of the laser beams and other factors affecting the number density calculations. His plot of overall efficiencies measured for different flow rates in a small angle diffuser housing with 0.966 micron PSL particles is shown in Fig. 3.21.

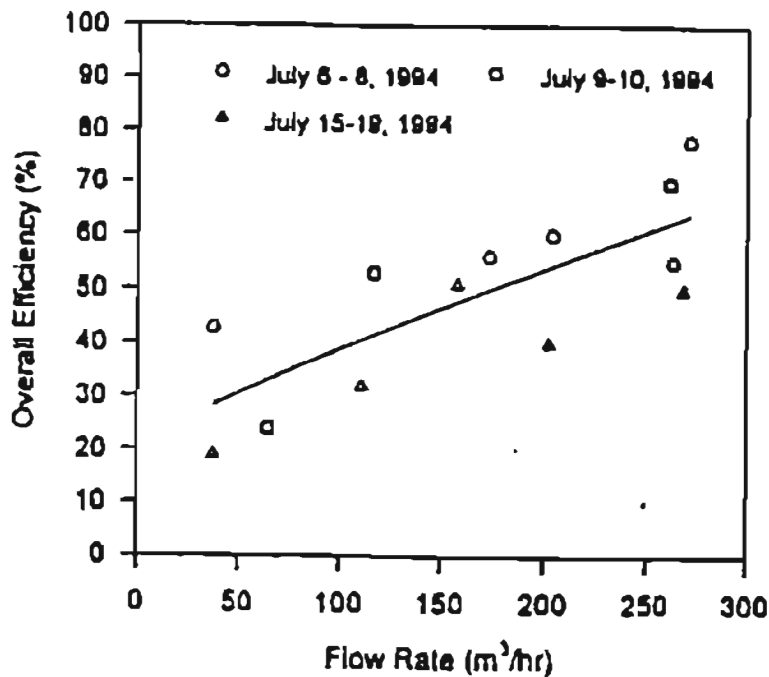


Figure 2.21 Overall Efficiency Versus Flow Rate [Natarajan, 1995].

Anand [1997] improved the measurement system and verified the repeatability of his measurements by repeating the identical tests. He measured the flat media efficiencies and compared his results with data from Lee [1977] (Fig. 2.22). He also showed that in

the central region of the filter, the local efficiencies are within $\pm 10\%$ of the overall average efficiency. Figure 2.23 shows a typical plot of the local efficiency measurements on the flat filter media conducted by Anand. He defined the X axis and Y axis as the directions of the shorter and longer sides of the A13192 filter, respectively.

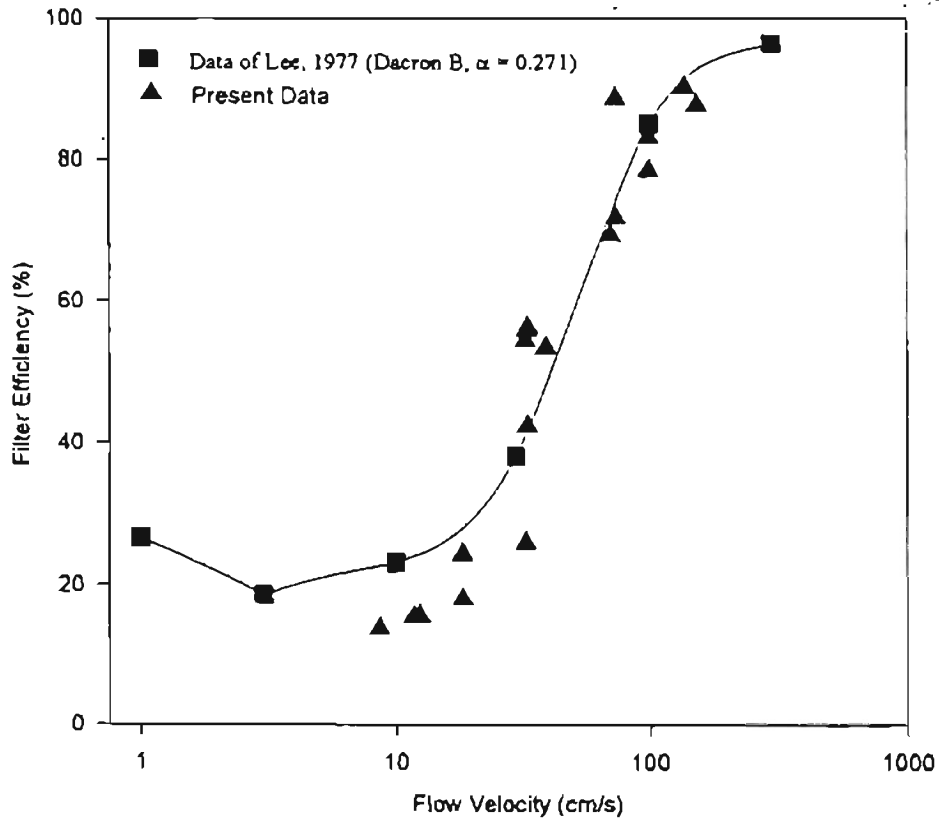


Figure 2.22 Overall Filter Efficiencies [Anand, 1997].

Liang [1994] has measured the axial upstream velocity in the SAE J726 housing over a pleated filter (Fig 2.24). He defined the X and Y axes as the directions of the longer and shorter sides of the filter, respectively.

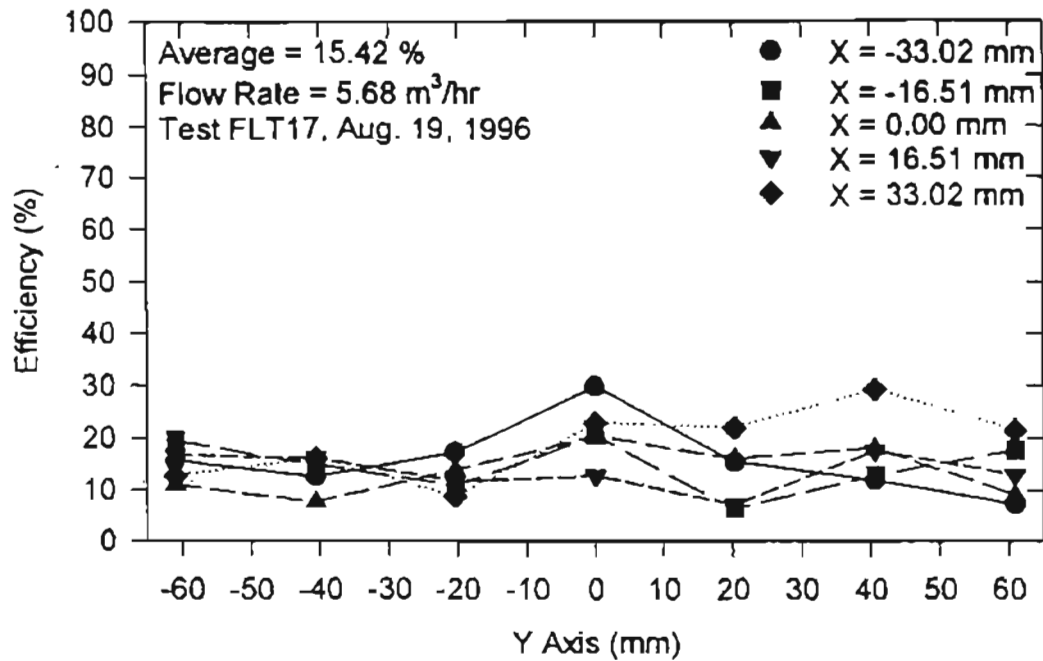


Figure 2.23 Local Efficiency for Flat Filter [Anand, 1997]

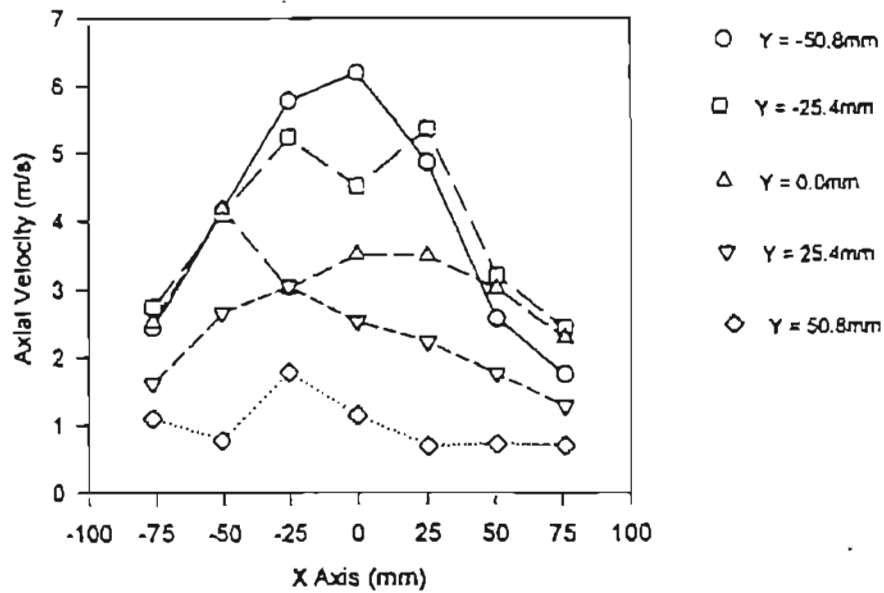


Figure 2.24 Axial Velocities Upstream of the A13192 Pleated Filter (204 m³/hr, SAE Housing, 0.966 Micron Particle Diameter) [Liang, 1994].

Similar measurements were conducted by Natarajan [1995] in a different test housing, the small angle diffuser housing (Fig. 2.25). As can be seen, the velocities are more uniform in the small angle diffuser housing as compared to the SAE J726 housing.

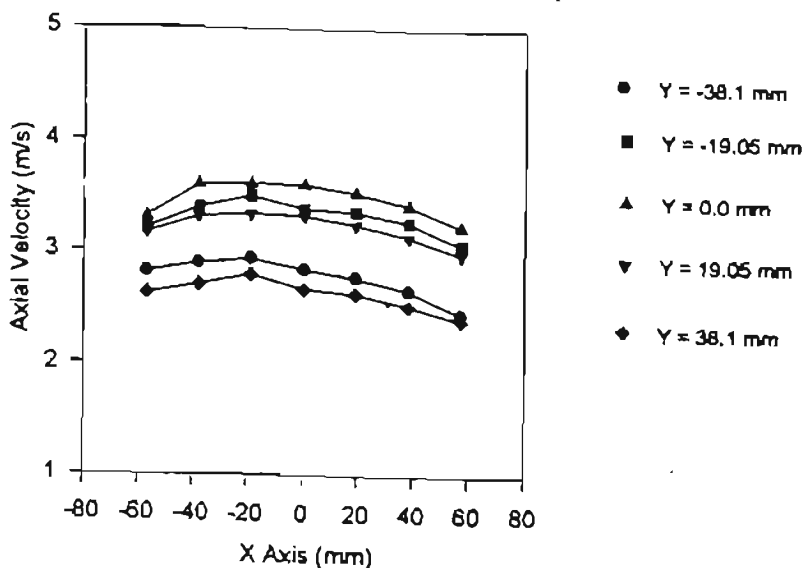


Figure 2.25 Axial Velocities Upstream of the A13192 Pleated Filter (204 m³/hr, Small Angle Diffuser Housing, 0.966 Micron Particle Diameter) [Natarajan, 1995].

Natarajan also used Duran's model for efficiency calculation to compare his results. He calculated the local efficiencies for a flow rate of 204 m³/hr using 0.966

particles in the small angle diffuser housing. He picked an arbitrary value of 0.49 for the packing density as well as a value of 0.345 which was recommended by Duran [1995]. He calculated local efficiencies for an A13192 filter using Duran's model and the velocity distribution shown in Fig. 2.25. He used an average fiber diameter of 51.78 microns which was suggested by Duran. His efficiency calculations are shown in Figs. 2.26 and 2.27.

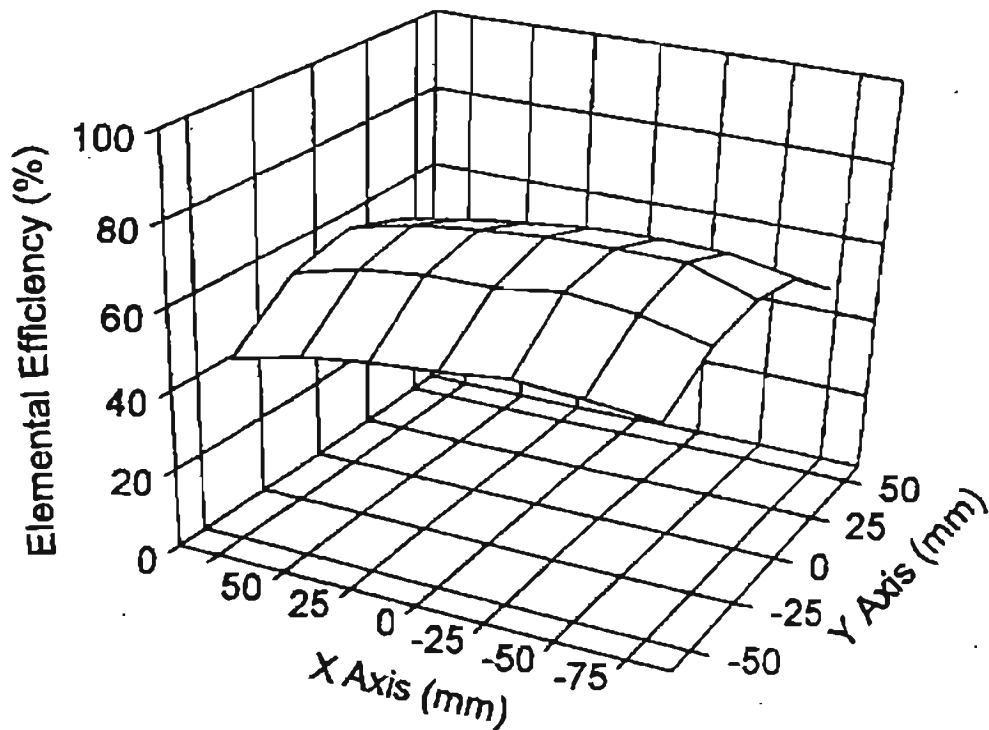


Figure 2.26 Elemental Efficiencies Over A13192 Filter (Small Angle Diffuser Housing, Duran's Model with Packing Density of 0.49) [Natarajan, 1995].

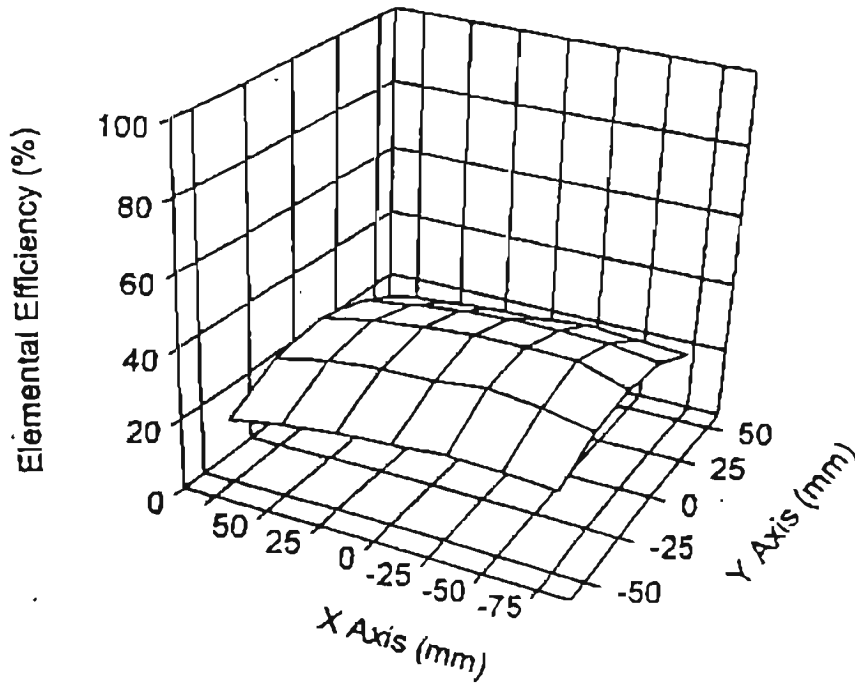


Figure 2.27 Elemental Efficiencies Over A13192 Filter (Small Angle Diffuser Housing, Duran's Model with Packing Density of 0.345) [Natarajan, 1995].

He also calculated the local efficiencies based on his downstream and upstream number density measurements over the filter and the actual measurements on the A13192 pleated filter. Results of his measurements are shown in Fig. 2.28.

Comparing Figs. 2.26, 2.27 and 2.28, it can be seen that most of the calculated local efficiencies (using the experimental data, Fig. 2.28) lay between the other two plots

(Figs. 2.26 and 2.27) which are calculated using Duran's model with different packing densities (0.49 and 0.345).

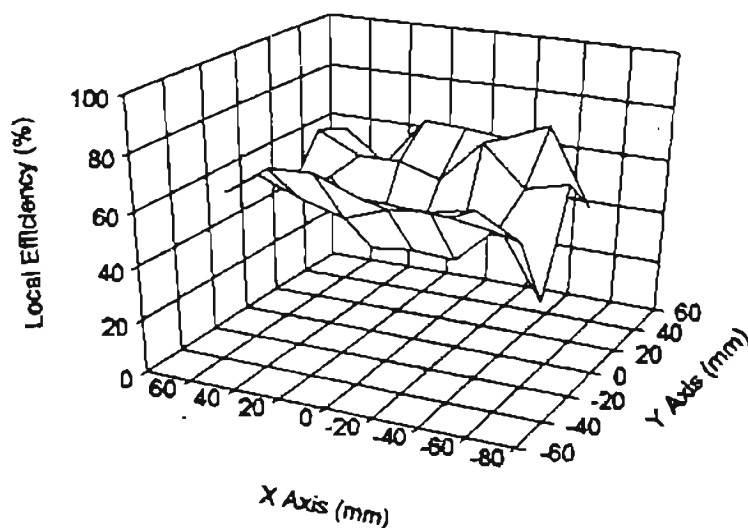


Figure 2.28 Measured Local Efficiencies Over A13192 Filter [Natarajan, 1995].

Natarajan used the actual flow velocity of the air inside the small angle diffuser housing to calculate the Stokes number for different flow rates. The total filtration area of the pleated filter is 19.3 times the duct cross-sectional area. Therefore, the velocity calculated based on the flow rate divided by the total filtration area (area of the unfolded filter) will give Stokes numbers about 5% of the values calculated by Natarajan for similar tests.

Anand [1997] studied the Stokes numbers calculated based on both of the above mentioned velocities. He concluded that neither of these velocities will give the correct Stokes number. He stated that the proper velocity for Stokes number calculation is about 4 times of the velocity calculated by unfolded filter area which is about 20% of the duct velocity. Further discussion regarding the Stokes number analysis for the pleated filter is presented in Chapter seven.

2.8 The Present Study

Using modifications of testing procedures introduced by Anand [1997] (constant ambient temperature, laser power and optimized DSA parameters), the current measurements were made in order to calculate the local efficiency of pleated filters using the A13192 filter and 0.966 PSL particles. These measurements are compared with measurements made by previous researchers of the OSU team as well as the theoretical and experimental literature. The main objectives of the current measurements are:

- Local filter efficiency measurements on pleated filters using optimum system parameters suggested by Anand [1997].
- Comparison of the overall filter efficiencies with flat media.
- Evaluation of single fiber efficiencies and comparison with theoretical studies.
- Stokes number analysis and research for a proper velocity for Stokes number calculation.

The current measurements were conducted in order to establish the above mentioned objectives. In addition to these goals, the following findings are the outcome of the present research:

- Verification of the reliability of the results by repeating the tests.
- Measurements of the filter efficiencies at flow rates lower than 50 m³/hr using the new bypass system.
- Modification of the number of density calculations, the Swept Volume Technique and analysis of the accuracy of the calculations.
- Comparison of non-uniformity of the local efficiencies with the overall testing system errors.
- Investigation of the possible correlation between the efficiencies of the flat and pleated filter media.

Also, with the help of the present measurements, conceptual models for calculation of the Stokes number are described.

CHAPTER III

LDV FUNDAMENTALS

Laser Doppler Velocimetry (LDV) has been widely used for particle velocity and count measurements in a fluid flow. The technique of using the Doppler shift of laser light for velocity determination was first demonstrated by Yeh and Cummins [1964]. A brief review of basic concepts of LDV is presented in this chapter.

3.1 The Doppler Shift

The change in the frequency of wave motion (electromagnetic or other type) because of relative movement of an object with respect to a wave producing source is known as the Doppler frequency shift.

Consider a wave generated from a stationary source *S*. A moving observer *P* with velocity *V* (with respect to stationary source *S*) will intercept more waves per unit time than if the observer had remained stationary (Fig. 3.1). Knowing that the distance traveled by *P* in direction *S* is $V\cos(\theta)$, the increase in wave frequency apparent to the moving observer (*P*) will be:

$$\Delta\nu = \frac{V \cos(\theta)}{\lambda} \quad (3-1)$$

Where ν is the wave frequency emitted by S or measured by a stationary observer. Using the wave speed, the fractional change in frequency will be:

$$\frac{\Delta\nu}{\nu} = \frac{V \cos(\theta)}{C_w} \quad (3-2)$$

where C_w is the wave speed. Now, if by some mechanism the frequency change is detected, the moving observer's velocity could be calculated. Indeed this is the basic concept of the LDV system.

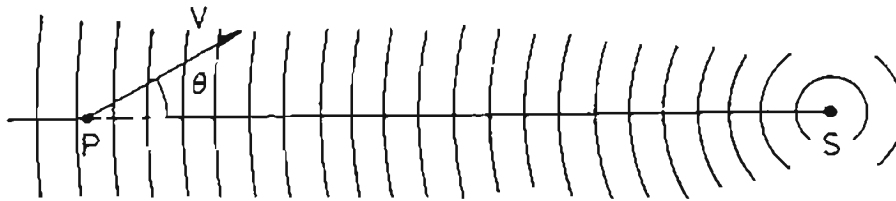


Figure 3.1 Illustration of the Doppler Frequency Shift Experienced by a Moving Observer [Drain, 1980].

3.2 The Optical Beating or Heterodyning

If two sinusoidal signals with a relatively small difference in frequency are added together (Figs. 3.2 a and b), the resultant wave will be a wave with a frequency of $f_1 - f_2$ due to the alternating constructive and destructive interference (or “beating”) of the two signals (Fig. 3.2c). When this signal is detected, it yields an output signal in the form of Fig. 3.2d.

Exactly the same principle may be applied in optics. The beating will be observed by illuminating an optical detector simultaneously by two light beams with different frequencies.

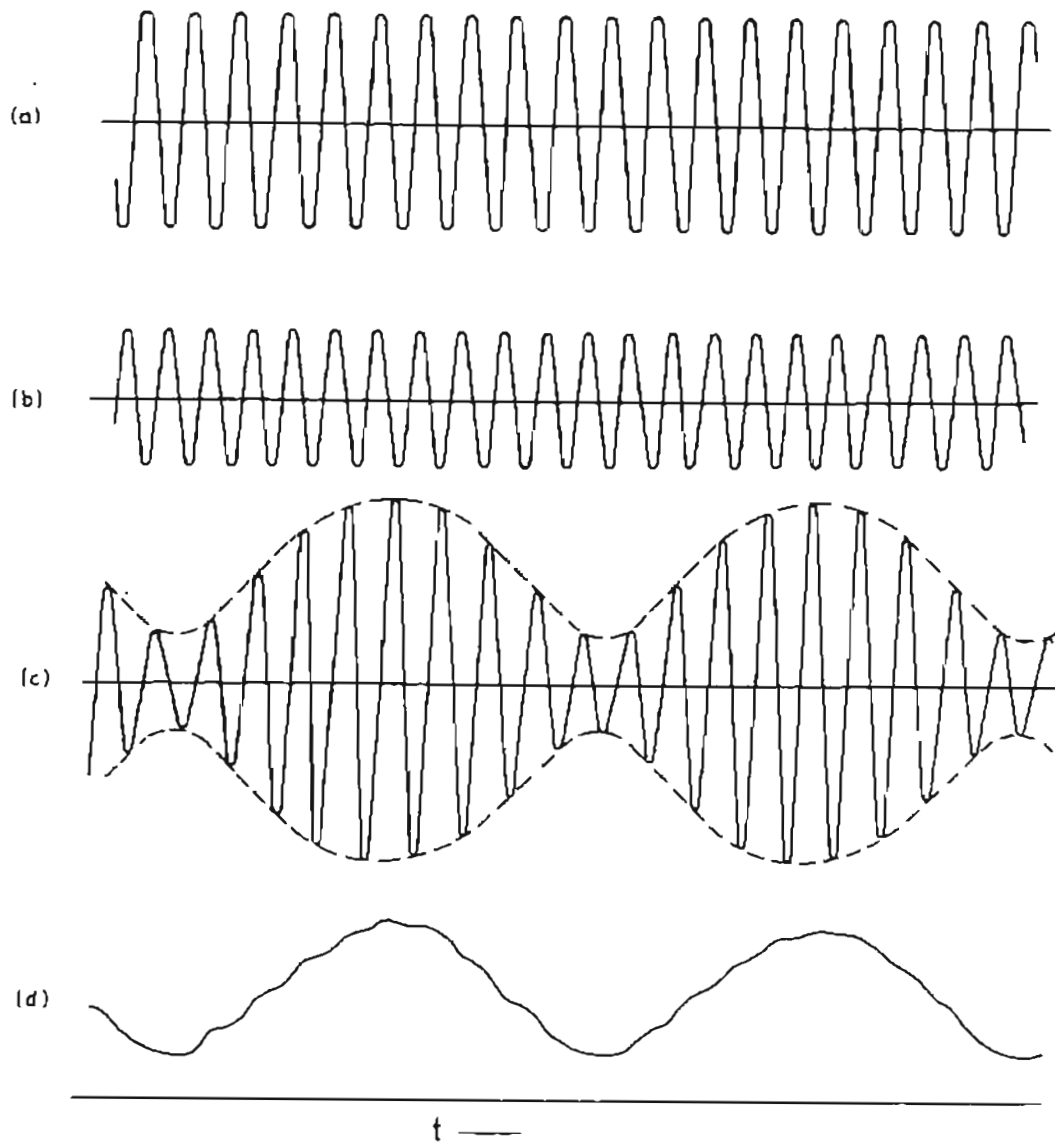


Figure 3.2 The Heterodyning of Two Frequencies [Drain, 1980]. The Addition of Signals (a) and (b) Yields Wave Form (c) Which Is Rectified to Form the Beat Signal (d).

3.3 Differential Doppler Beating

As mentioned earlier, optical beating can be detected when two beams with close frequencies intersect [Drain, 1980]. When a moving particle passes through the intersection of two focused beams of similar intensities inclined at angle α (Fig 3.3), and the scattered light (caused by a particle passing through the beams) is detected in a third direction, the Doppler frequency shift of each beam, observed by a detector, will be different. If θ_1 and θ'_1 are the angles of a moving particle with velocity of V with respect to beams A and A', and θ_2 is the angle of the moving particle with respect to the detector direction, the Doppler frequency shifts will be [Drain, 1980]:

$$\Delta \nu_A = \frac{[\cos(\theta_1) + \cos(\theta_2)] \nu V}{C} \quad (3-3)$$

$$\Delta \nu_B = \frac{[\cos(\theta'_1) + \cos(\theta_2)] \nu V}{C} \quad (3-4)$$

The difference frequency observed by the detector will be [Drain, 1980]:

$$f = \Delta \nu_A - \Delta \nu_B = \frac{[\cos(\theta_1) - \cos(\theta'_1)] \nu V}{C} = \frac{\nu \sin(\alpha/2) \cos(\beta)}{\lambda} \quad (3-5)$$

Where $\alpha = \theta'_1 - \theta_1$, the angle between the two beams, and $\beta = \frac{1}{2}(\theta'_1 + \theta_1 - \pi)$.

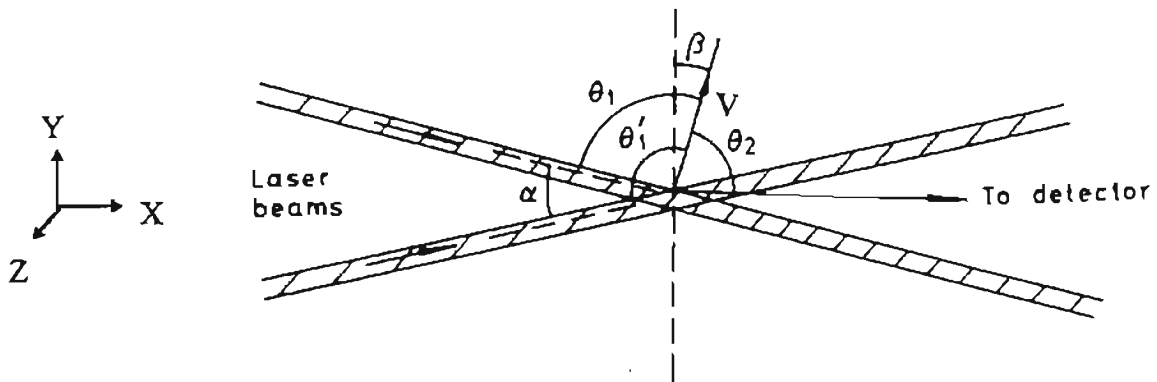


Figure 3.3 Arrangement of Illuminating Beams in the Differential Doppler Technique

[Drain, 1980].

3.4 Interference and Interpretation of Interference Fringes

The alternate constructive and destructive interference (or beating) caused by two light beams will be observed as light and dark bands, interference fringes, which represent these alternate construction and destruction interferences (Fig. 3.4). If the two beams have a well defined and consistent phase relation, the spacing of the fringes could be calculated as:

$$S = \frac{\lambda}{2\sin(\theta)} \quad (3-6)$$

Therefore a moving particle with velocity V at angle β from the normal to the fringe plane (XZ plane in Fig. 3.3) will observe a modulation of light intensity with a frequency of:

$$f = \frac{v \cos(\beta)}{S} \quad (3-7)$$

or

$$f = \frac{2v \cos(\beta) \sin(\alpha/2)}{\lambda} \quad (3-8)$$

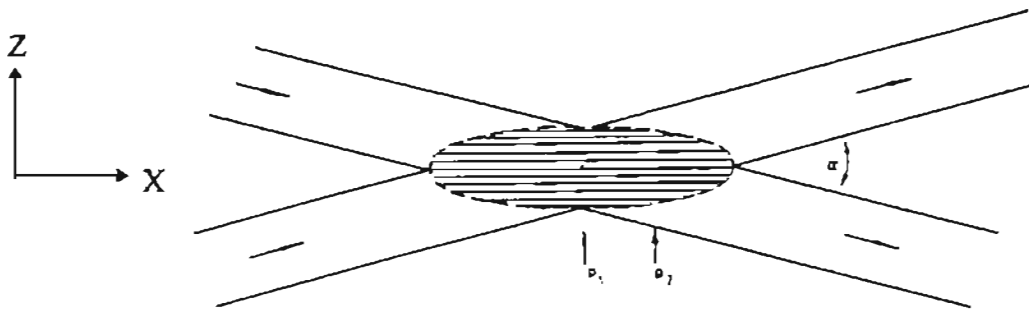


Figure 3.4 Fringe Pattern Produced by Crossing Beams in the Differential Doppler Technique [Drain, 1980].

The difference in frequencies calculated by Eq.(3-8) is called the Doppler differential frequency [Drain, 1980]. The scattered light from the particle will be modulated at this frequency.

The region where fringes are formed by crossing of the beams is called the probe volume. Usually laser beams have a circular symmetry with a Gaussian intensity distribution in the cross-sectional area. Using the interference fringe approach, a particle moving in a probe volume formed by the intersection of two laser beams with equal intensities will generate a scattered light signal as shown in Fig. 3.5a. The signal has a maximum depth of modulation possible corresponding to the high fringe contrast in the central area which appears because of high intensity in that region.

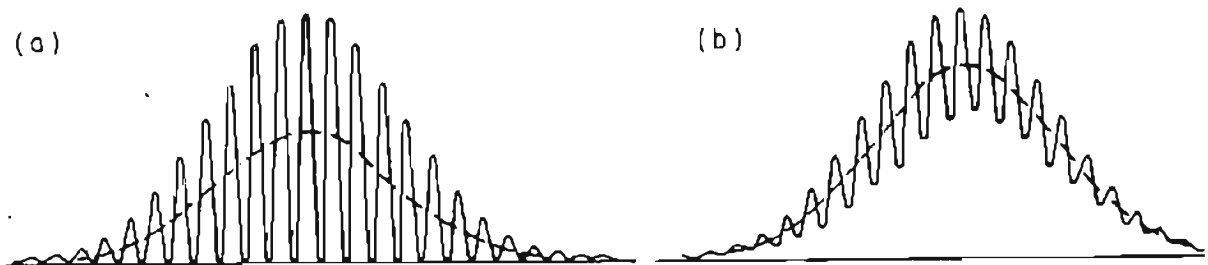


Fig. 3.5 Types of Signals from Particles Crossing a Region of Intersection of Laser Beams [Drain, 1980].

An imperfectly modulated signal (Fig. 3.5b) could arise from the beams not being of equal intensity or from a particle whose size is not small compared to the fringe spacing.

3.5 Signal Processing

The back scattered light caused by a moving particle through the probe volume is an optical signal which should be processed so that the particle velocity is obtained. Durst and Whitelaw [1976] have described different aspects of signal processing in their book. According to Durst and Whitelaw, the scattered light signal is first detected by a receiver module (RCM). The RCM converts the Doppler light signal from the receiver optics into electronic signals. The RCM contains either photodiodes or photomultiplier tubes (PMTs) which do the conversion. PMTs are typically used for signal conversion because of their high gain and low noise level. The PMT output is a voltage signal with a gain determined by the high voltage applied to it.

The electronic signal has the form shown in Fig. 3.6 [Durst and Whitelaw, 1976]. The low frequency signal variation corresponds to passage of particles through one or both light beams and the higher frequency signal, contained within various envelopes, corresponds to the velocity of individual particles passing through the region of the beam intersection observed by the PMT. In most cases, a high pass filter is used to remove the low component of the signal (Fig. 3.7). The resulting signal is then transformed into the frequency domain where the differential Doppler frequency is obtained. The velocity is then calculated using the Doppler frequency.

3.6 The Doppler Signal Analyzer

The Doppler Signal Analyzer (DSA) is used for signal processing. According to the DSA manual [1992], the DSA hardware is connected to the PMTs as well as to a computer in such a way that the system parameters can be adjusted by the DSA software installed on the computer.

The DSA system uses fast Fourier transformation for transforming the electronic signal to the frequency domain. The high voltage applied to the PMTs, the high pass filtration parameter, the frequency shift and several other parameters could be adjusted using DSA software. The DSA is also connected to an oscilloscope where the envelope signals as well as Doppler bursts can be seen.

A description of the system parameters is presented in Appendix A. The effect of each parameter on detected particle velocity and count is discussed by Anand [1997]. A brief review of optimum values for the system parameters is also presented in Appendix A.

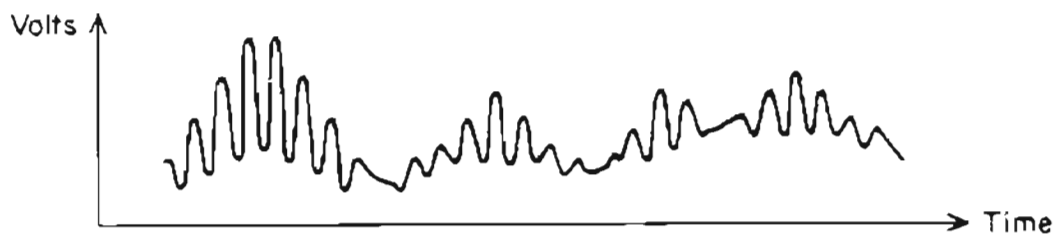


Figure 3.6 PMT Output Signal from Photodetector, Before High-Pass Filter

[Durst and Whitelaw, 1976].

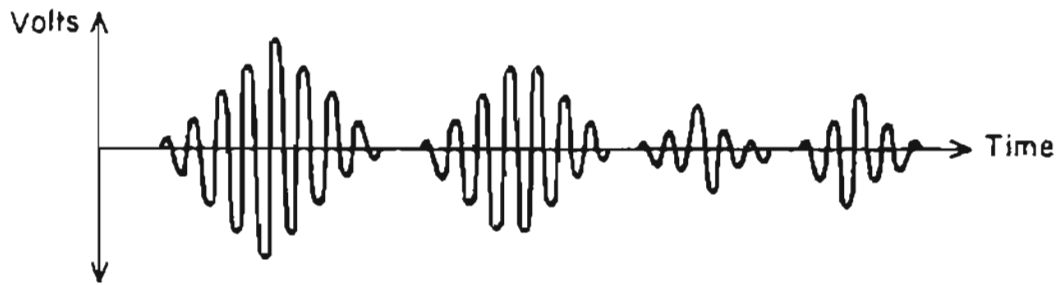


Figure 3.7 PMT Output Signal from Photodetector, After High-Pass Filter

[Durst and Whitelaw, 1976].

Up to this point, the basic principles of an LDV system have been discussed. However, different LDV systems might be used for different measurement conditions. The specification of the system used for the present measurements is described in Chapter four.

CHAPTER IV

THE EXPERIMENTAL SETUP

Details of the components and assembly of each system are presented in this chapter. The experimental setup and measurement procedures are also explained (refer to Appendix F for a list of all equipment).

4.1 Description of the System Components

The experimental setup for present measurements can be divided into two main systems: the flow system, the LDV system and the traverse.

4.1.1 Flow System

Measurements were conducted on A13192 pleated filters manufactured by Dyco-Purolator. Air flow is generated by a blower. The test housing is installed on the suction side of the blower. Ambient (room) air is sucked into the system and the blower discharge is extended to the outside of the building. As recommended by Anand [1997], the ambient room temperature is controlled so that it does not vary more than $\pm 0.5^{\circ}\text{C}$. The room temperature is controlled by the air conditioning system so that the heat generated by the blower and the air heater does not increase the room temperature.

The flow system includes the following components:

- Blower

The blower is used to maintain the air flow. As mentioned earlier, the test housing is installed on the suction side of the blower. The flow rate is controlled manually from the blower control panel.

- Six Jet Atomizer

The atomizer (made by TSI) is used for seeding the particles. 0.966 polystyrene latex spherical particles (PSL) were used as challenge contaminants. Particles are available in a solution with 10 % concentration by volume. The solution is diluted by the ratio of 1 to 100 (for example by adding 990 cm³ of distilled water to a 10 cm³ solution, making 1000 cm³ diluted solution) up to 1/50 with distilled water, depending on the required seeding rate. The diluted solution is poured into the atomizer container. The container's effective volume is about 700 cm³. The atomizer is equipped with a level gage. Compressed air with a pressure of 40 psig is supplied to the atomizer. The atomizer has a pressure regulator which should be adjusted to a value less than 30 psig as recommended by TSI. The solution is atomized by passing through the jet nozzles. The concentration of the atomized solution can be controlled by adjusting the compressed air flow rate. This can be accomplished by adjusting the air flow valve on the atomizer to get the desired air flow.

- Air Heater

Since the air coming out of the atomizer contains water droplets as well as PSL particles, in order to avoid water droplets entering the housing, the main air entering the

housing is heated by the air heater. Water droplets were vaporized by heat and only PSL particles will enter the housing. Such heating will change the air temperature. The temperature of the air entering the housing will be different for different flow rates since the heater is working with its maximum capacity. At very low flow rates, the temperature will be higher than for intermediate and high flow rates. The air temperature will affect the air viscosity which is used for Stokes number calculation. The air temperature will hardly reach 50 °C when the air entering the housing is heated by the heater. Therefore, the change in viscosity (due to the change in temperature) is so small that its effect can be neglected. For Stokes number calculations, the air viscosity at 30 °C is used. An example of the Stokes number calculation is presented in Appendix E.

- Test Housings

Two different test housings are used for the measurements: the small angle diffuser housing (Fig. 4.1) and the SAE housing (Fig. 4.2), which is constructed in accordance with SAE J726 test housing dimensions. The small angle diffuser housing will generate more uniform velocity upstream of the filter as compared to the SAE housing. Both housings were made of plexiglass. A cubic mixing box is installed upstream of the test housings in order to have a uniform particle concentration inside the test housing.

- TSI Flow Meter

The TSI flow meter is installed downstream of the test housing. It is used to measure the standard volumetric flow rate in cfm. The flow meter is calibrated for flow rates above 50 scfm with an ASME 3 inch flow nozzle. The calibration curve is shown in

Appendix D. Anand [1997] has also calibrated the flow meter for flow rates less than 50 cfm (Appendix D).

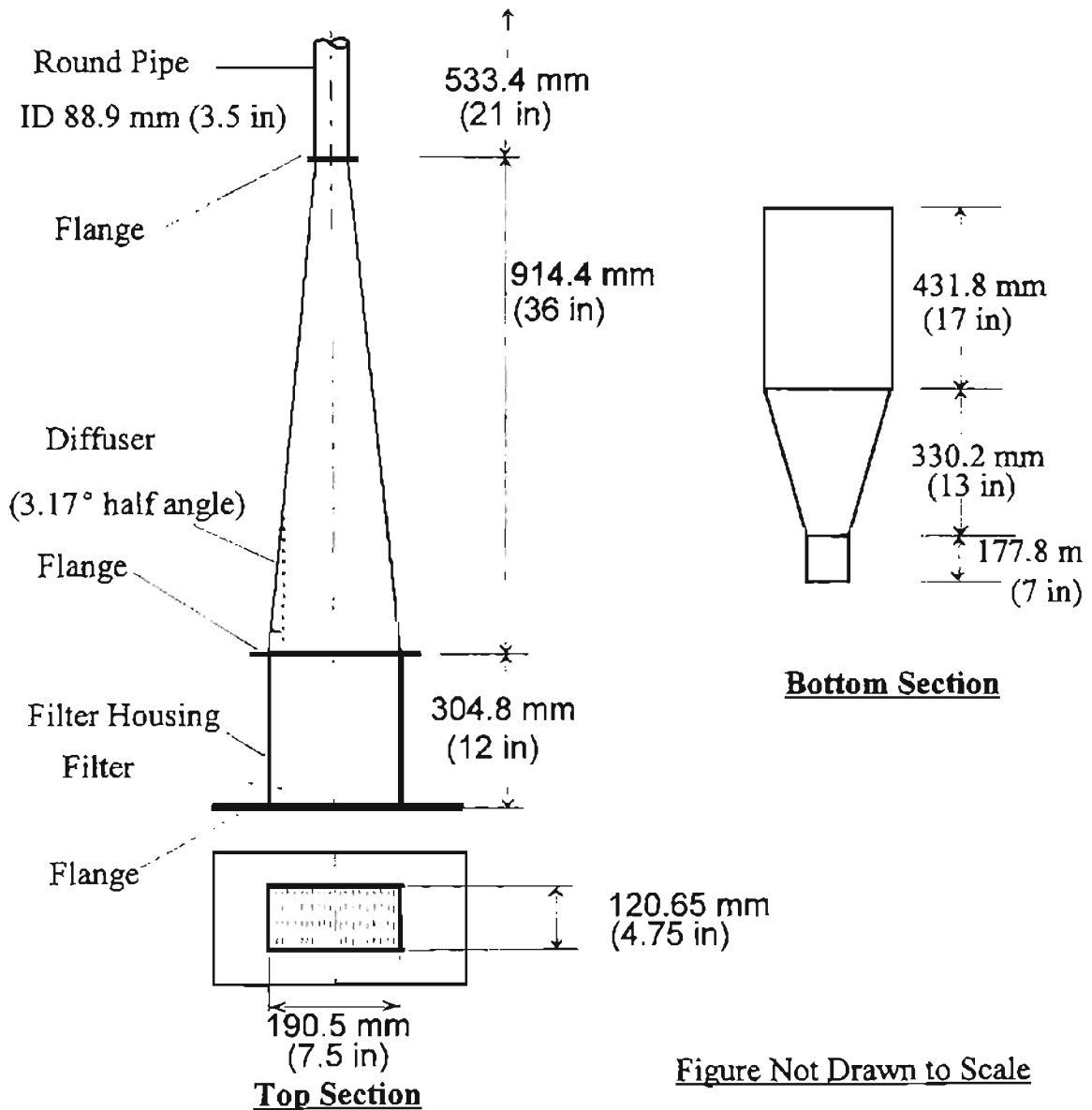


Figure 4.1 Dimensions of the Small Angle Diffuser Housing.

Figure Not Drawn to Scale

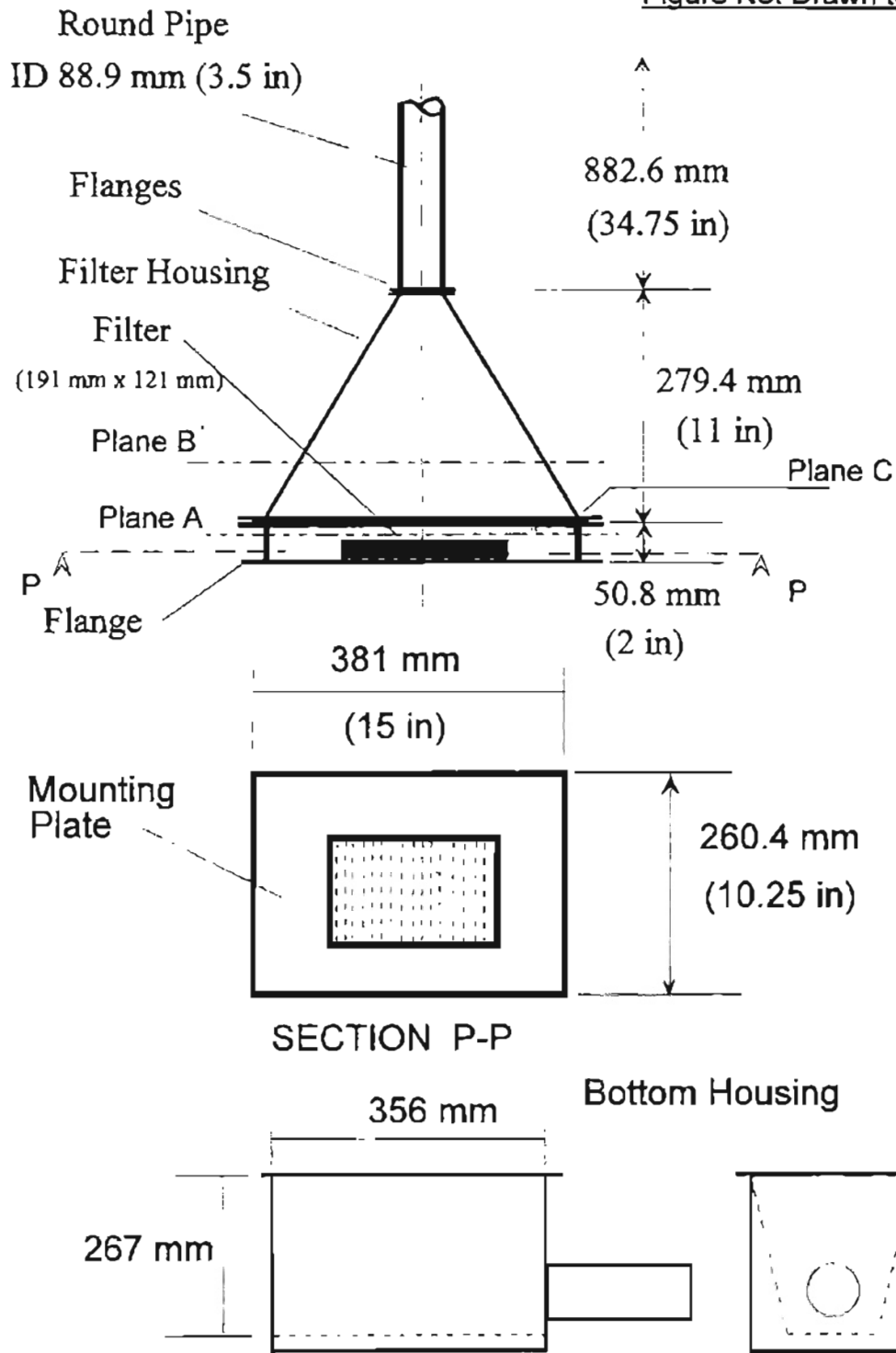


Figure 4.2 Dimensions of the SAE Housing.

- **Manometer**

In order to monitor the variation of the pressure drop across the filter, two pressure taps were installed at the top and bottom sections of the test housings, upstream and downstream of the filter. The pressure drop across the filter at the beginning of each test is measured and its variation throughout the test is monitored. The final pressure drop at the end of the test is also recorded. The amount of the pressure drop change is an indication of filter plugging which results higher efficiency values. These changes are more significant on the flat filters (Anand [1997]) as compared to the pleated filters. An inclined manometer filled with water is used for the pressure drop measurement.

- **Absolute Filter**

The absolute filter is the last piece of equipment downstream the filter before the blower suction flange. It is used to absorb the particles which have passed through the filter in order to avoid contamination of the atmosphere with PSL particles.

- **Connecting Piping**

PVC piping and rubber connectors and adapters were used for connecting the equipment to each other and guiding the flow.

- **Bypass System**

Since the blower is not capable of generating flow rates less than 25 Scfm, a bypass connection to the atmosphere with a valve is installed before the absolute filter. By setting the blower on the minimum flow rate and adjusting the bypass valve, very low flow rates could be generated to pass through the test housing (Fig. 4.3).

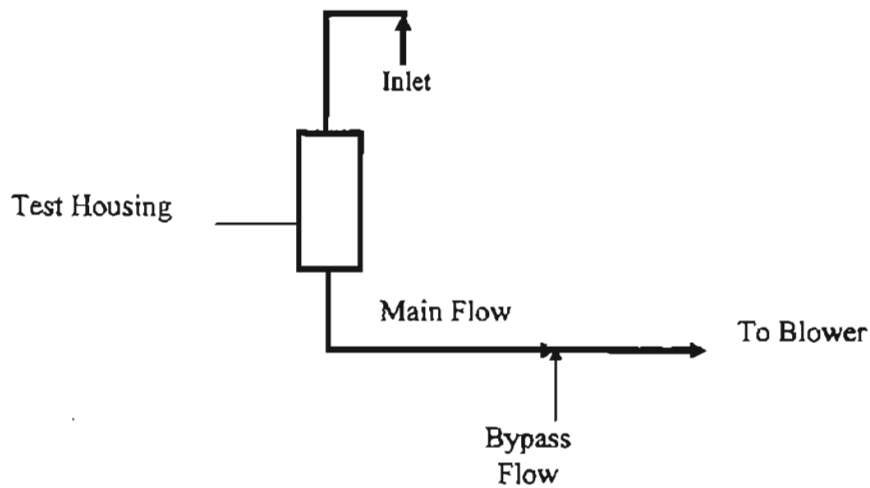


Figure 4.3 The Bypass System.

This system is more useful for very low flow rate measurements. The bypass system can provide a consistent low flow rate inside the housing as long as the pressure drop across the filter remains constant. If the pressure drop across the filter is changed, more flow will pass through the bypass and less flow will go through the system, as compared to the desired flow. Such a phenomenon is more critical on flat filter measurements.

- Test Filter

A13192 pleated filters were used as test filters. The dimensions of the A13192 filter (manufactured by Dayco-Purolator) are listed in Table 4.1. The values of the packing density and average fiber diameter were estimated values recommended by Duran [1995]. The arrangement of the pleats and the schematic view of the filter are shown in Figs. 4.4 and 4.5, respectively.

Table 4.1 A13192 Pleated Filter Dimensions [Duran, 1995].

Overall Dimensions	193 mm x 121 mm
Pleat Pitch	3.125 mm
Pleat Height	30 mm
Estimated Average Fiber Diameter	51.78 Microns
Estimated Packing Density	0.345

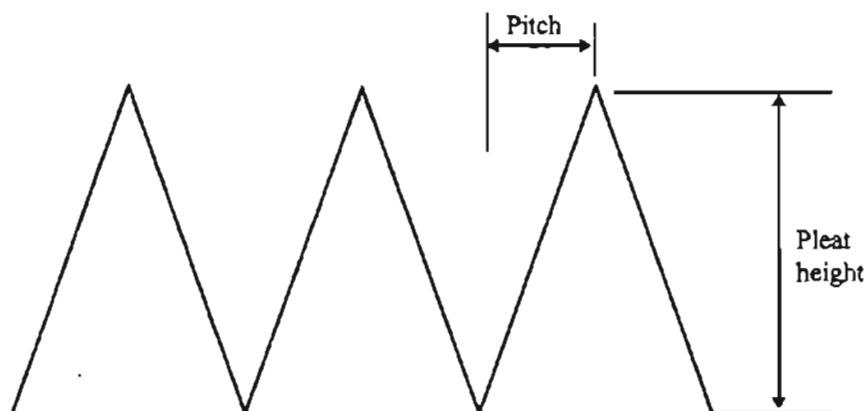


Figure 4.4 Arrangement of the A13192 Pleats.

4.1.2 The LDV System

Counts and the velocities of the particles upstream and downstream the filter were measured by the LDV system. The LDV system mainly consists of a laser, fiber drive, transceiver, DSA hardware, monitoring computers, digital oscilloscope and fiber optic cables. These components are described in this section.

- Laser

The laser is a 5 watt model Innova I 70-A argon-ion laser manufactured by Coherent. The laser power was set to 0.8 W for the current measurements.

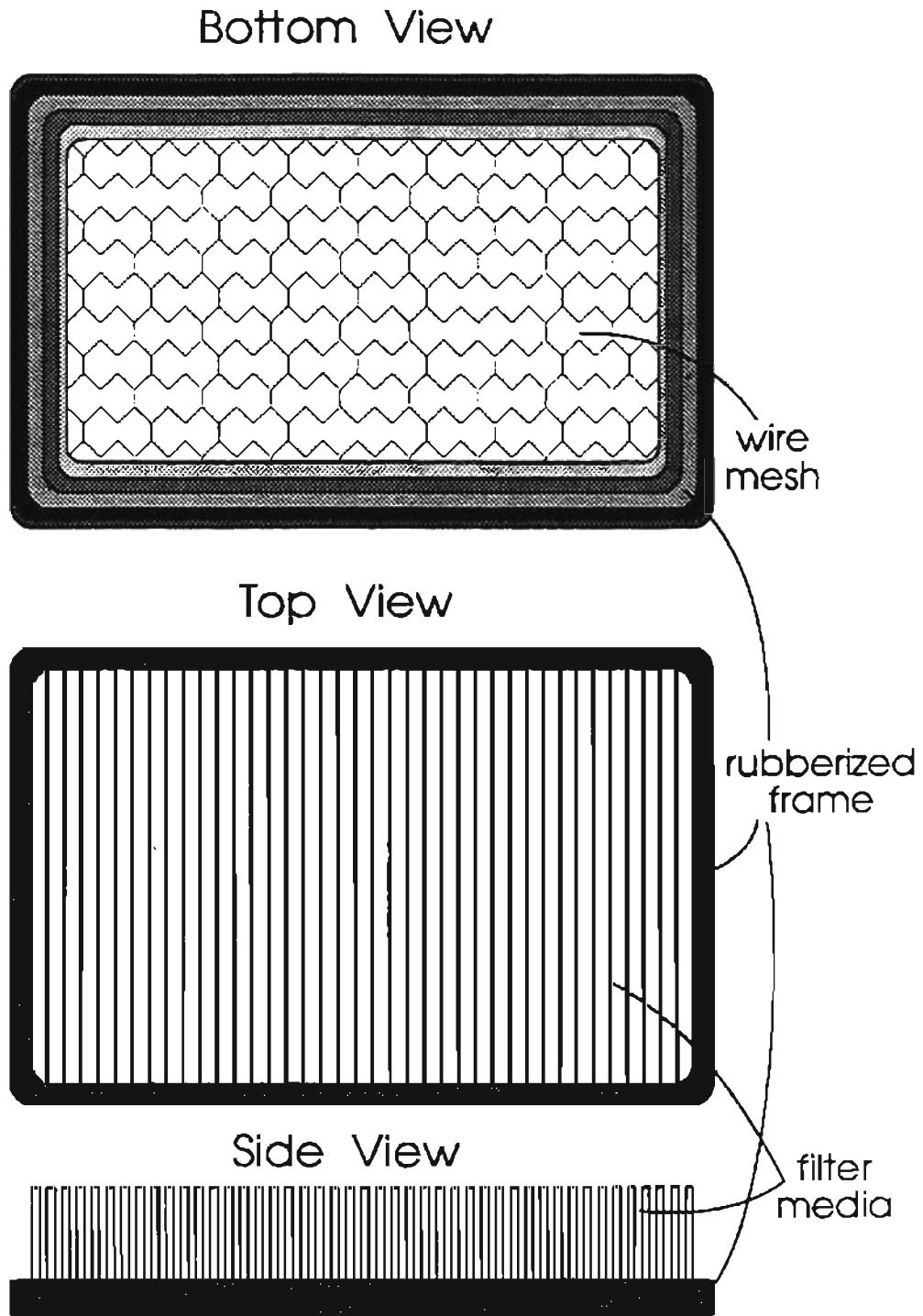


Figure 4.5 The A13192 Pleated Filter.

- Fiber Drive

The laser beam is guided by two outside mirrors to the fiber drive. The beam enters the Bragg cell which generates a second beam with a 40 MHz frequency shift. Both beams are guided to a prism which separates blue and green beam frequencies. The four beams, a blue and a green beam from the main beam (unshifted) and a set of blue and green beams from the shifted beam, will be guided to the couplers which are connected to the fiber optic cables. The beams pass through the coupler lens and enter the optic cable. The cable transfers the beams to the transceiver. Figure 4.6 shows a schematic of the fiber drive.

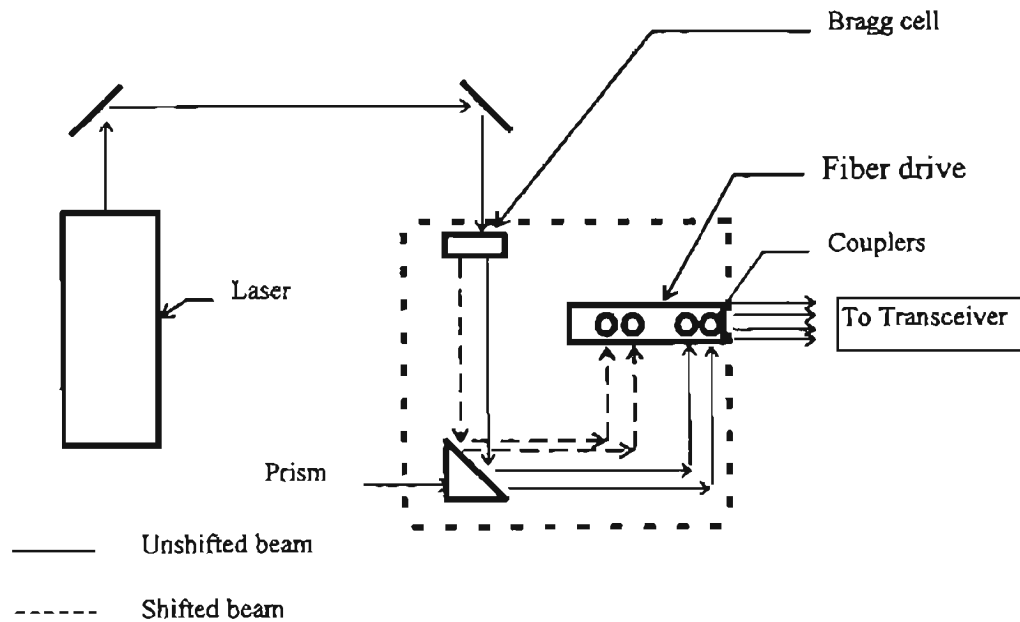


Figure 4.6 Schematic Diagram of the Fiber Drive.

- Transceiver

The four beams coming out of the fiber drive (green and blue shifted and unshifted beams) are transferred to the transceiver through fiber optic cables. As mentioned in Chapter three, the transceiver emits the four beams. The system is set so that the green beams are emitted in a vertical plane, the YZ plane, and the blue beams are emitted in a horizontal plane, the XY plane (Fig. 4.7). Also, the transceiver detects the back scattered light caused by particles passing through the probe volume. The detected light signal is transmitted to the Photo Multiplier Tubes (PMTs).

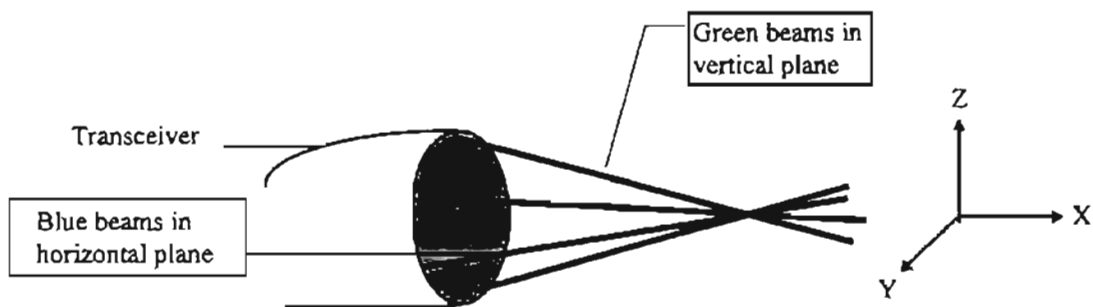


Figure 4.7 Laser Beams Emitted from Transceiver.

- PMT

The PMT's receive the back scattered light from the transceiver. The light signal is converted to an electronic signal by the PMT's. The high voltage applied to the PMT's is adjustable through the DSA software.

4.1.3 The Traverse

In order to measure local number densities. The transceiver is installed on a board (traverse) which has three dimensional movement. Three DC stepper motors are used for moving the board in three dimensions. All motors are computer controlled.

4.2 The Experimental Setup Description

The six jet atomizer is filled with desired solution. The solution is made by diluting the 10 % concentrated PSL particles (by volume) with distilled water. The dilution ratio depends on the flow rate which is used.

For most of the tests in the small angle diffuser housing and all of the tests in the SAE housing, the dilution ratio is one to one hundred. For flow rates of 313.8 and 481.8 m³/hr, the dilution ratios are 2/100 and 3/100, respectively. Higher concentrations are used at high flow rates so that enough particles are detected in a certain period of time (for example 30 seconds).

A schematic sketch of the experimental setup is shown in Fig. 4.8. The seeded particles enter the flow system through a bypass close to the housing entrance. The ambient air is sucked into the system. The heater is placed underneath of the entrance section so that the air is heated before entering the system. Heated air evaporates the water droplets which are also added to the flow together with the particles. The air passes through a mixing box before entering the housing so that the particles are mixed uniformly. The housing is connected to the mixing box and the air passes through the housing where the filter is placed.

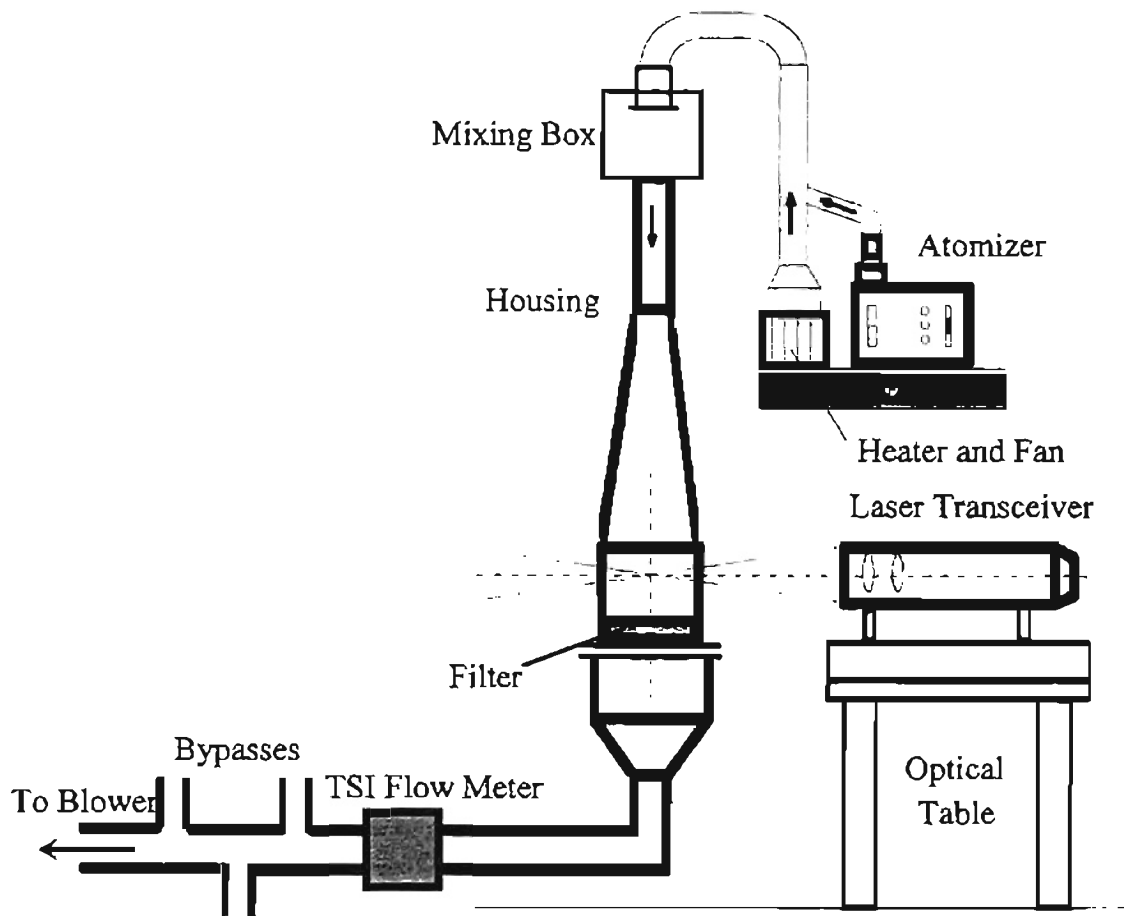


Figure 4.8 The Experimental Setup.

The housing is connected to the TSI meter. The air exiting the housing passes through the TSI flow meter (where the flow rate is measured) and the absolute filter. The particles which are not collected by the test filter will be collected by the absolute filter. Finally the air enters the blower and is vented to the atmosphere through the blower outlet.

Measurements are made at two cross-sections inside the housing: 75 mm above and 100 mm below the housing flange connections. Measurements are made at 35 grid

locations in each of these planes. The grid spacing is 16.5 mm and 20.3 mm in the X and Y directions, respectively. The X direction is the direction of the smaller side of the test filter and the Y direction is the direction of its longer side. The filter is placed such that the longer side is parallel to the transceiver lens (Fig. 4.9).

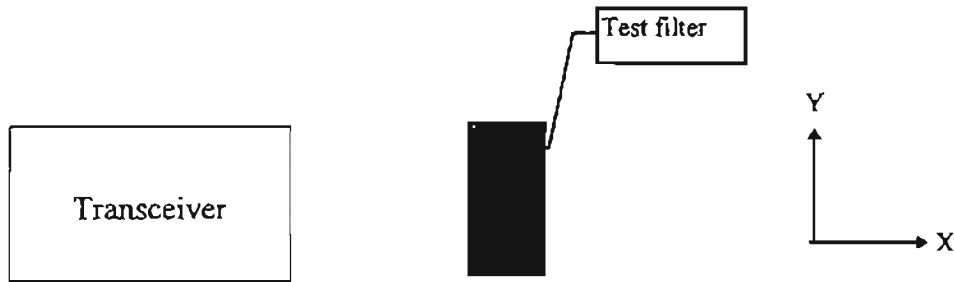


Figure 4.9 Top View of the Test Filter Positioning.

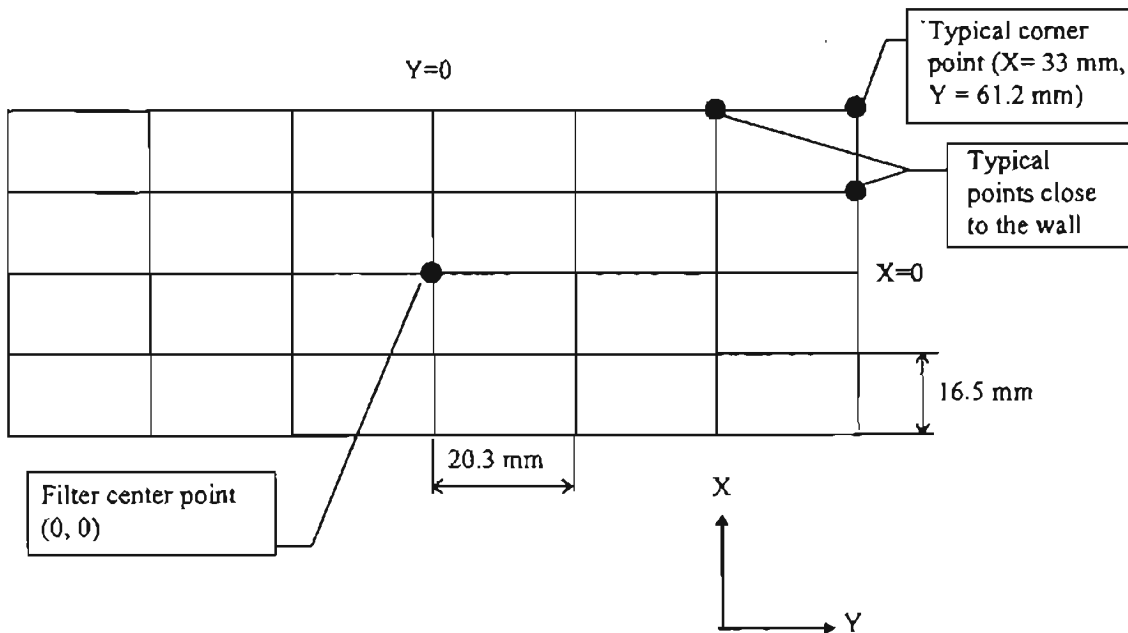


Figure 4.10 Grid Locations (Not to Scale).

4.3 Measurement Procedure

Before starting each test, the LDV system is turned on. The power of the laser beams coming out of the transceiver is checked. If the power is lower than the expected values, the couplers are aligned such that the desired power values are obtained. Alignment of the couplers is done at a laser power of 0.2 W.

For the current measurements, values of 8 mW for the green beams and 4 mW for the blue beams (at laser power of 0.2 W) are considered proper values for conducting the measurements. However, during the period which the measurements were made (about six months), the efficiency of the blue beams decreased such that the latest measurements were conducted with the blue beam powers of about 2 mW (at 0.2 W laser power). Such a reduction did not affect the quality of the measurements since the axial velocity was measured by the green beams.

The blue beams measure the transverse velocity which is usually much less than the axial velocity (more than one order of magnitude in most cases). Moreover, the number of counts are measured by green beams not the blue beams. The lower blue beam power will reduce the number of samples detected in the transverse direction but does not affect the measured velocities of the detected particles in that direction.

After the alignment of the laser beams is completed, the blower is started and is adjusted to the desired flow rate. The blower is run for at least 15 minutes in order to stabilize the flow. Then the atomizer is filled with the solution and the air to the atomizer is turned on. The atomizer pressure regulator is set to a value between 25 to 40 psig as recommended by the manufacturer.

The traverse is moved so that the probe volume is set at the center of the housing cross-section upstream the filter at the plane where measurements are conducted. Three sample runs are measured at each grid point, and the number densities are calculated. Sample measurements are continued at that grid point if the number densities are not consistent (within $\pm 5\%$ of the average of the three) until the time that three consistent measurements are obtained.

The next step is the checking of the recirculation zone. Sample runs are measured at a few grid points (usually two or three) of the two rows closest to the wall ($X=33$ mm and $X = -33$ mm, see Fig. 4.10). If the velocity profiles of the two sides are similar to each other, the main measurements are started. If not, the reference center point is relocated such that similar velocity profiles are obtained on the two rows, i.e. the velocity histograms have the same trend (not necessarily the same values).

The main measurements are conducted in a sequential manner. At each grid point, for most of the grid points, three measurements are made upstream of the filter above a grid point and after that, three measurements are conducted downstream of the filter below the same grid point.

The next chapter discusses the results and methods for efficiency calculation.

CHAPTER V

EFFICIENCY AND NUMBER DENSITY CALCULATIONS

In filtration studies, filter efficiency is typically calculated on a mass basis. In other words, if particles with total mass of M_1 are injected into the flow during a specified time, considering the portion of the total mass which passes through the filter to be M_2 , the mass collected by the filter (assuming no losses in the system) should be:

$$M_c = M_1 - M_2 \quad (5-1)$$

and the efficiency is calculated as:

$$E = \frac{M_1 - M_2}{M_1} = 1 - \frac{M_2}{M_1} \quad (5-2)$$

However, the filter efficiency might change when it is plugged by particles. Because of plugging, less area will be available for particles to pass through the filter, and the pressure drop across the filter will increase.

The present measurements are made on clean filters using 0.966 micron particles. The particle seeding rate and run time are selected so that no significant change in the pressure drop is observed. Therefore, it is assumed that the filtration efficiency does not change during the time which measurements are made. Values of pressure drop change are indicated for each measurement, and the above assumption is verified.

5.1 Calculation of Efficiencies Using Number Density

Since the seeding particles are of uniform spherical shape with a 0.996 micron diameter, the total mass of the seeding particles upstream and downstream of the filter can be written in terms of particle numbers as:

$$M_1 = \frac{4}{3} \pi R_p^3 N_1 \rho \quad (5-3)$$

$$M_2 = \frac{4}{3} \pi R_p^3 N_2 \rho \quad (5-4)$$

Therefore the efficiency will be

$$\eta = 1 - \frac{N_2}{N_1} \quad (5-5)$$

where N_1 and N_2 are the number of particles corresponding to the masses of M_1 and M_2 respectively and ρ is the density of the particles.

5.2 Local Efficiency Calculation and the Swept Volume Technique

Filtration efficiency at a specific filter location is calculated based on the number densities above and below the filter (at that location). Number density is defined as number of particles in a specific volume. Since the number densities above and below the filter should be calculated using the same volume, it is easier to calculate the number densities on a unit volume basis (see Appendix G for an alternate method-flux based). Note that since the flow is assumed to be steady-state, it is assumed that the number density is uniform throughout the probe volume (where measurements are made).

As mentioned earlier, the LDV system is used for velocity and particle count measurements. Measurements are made by focusing the probe volume on the specific

location where velocity and particle concentration are needed. The main outputs of the LDV system are: velocity histogram, number of counts and run time.

The Swept Volume Technique (SVT) is used for number density calculations. The SVT is based on the following assumptions (see Appendix G):

- The flow is steady-state, and the velocities of the particles as well as number densities do not change with time.
- Particles paths are parallel streamlines (all particles move in the same direction).
- All particles have the same velocity.

Considering a probe volume with a cross-sectional area (normal to the flow) of A_p , and assuming that the LDV system detects N particles from time $T = 0$ to time $T = T_0$ having a velocity of V , the very first detected particle (detected at $T = 0^+$) will move the distance $L = V T_0$ away from the probe volume cross-section A_p . Similarly the last particle which is detected at time $T = T_0^-$ should be at the same distance (L) upstream of the probe volume cross-section at the start time (Fig. 5.1), so that after the time T_0 , that last particle will just pass through the probe volume cross-section.

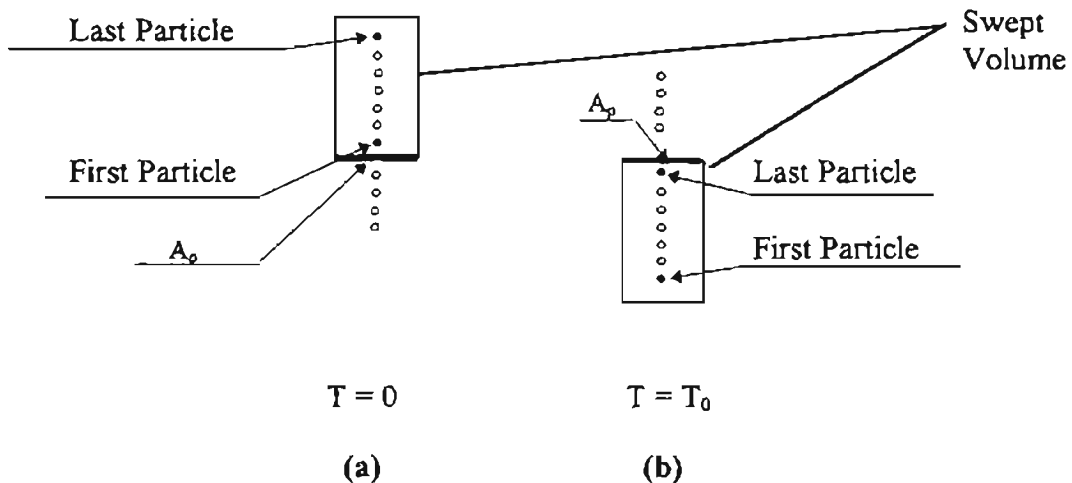


Figure 5.1 The Swept Volume Technique, (a) at $T = 0$, (b) at $T = T_0$.

Therefore, before time T_0 , all of the N detected particles would have been somewhere between the probe volume cross-section and a distance L upstream of it. In other words, all N particles existed in the volume LA_p , and the number of particles per unit volume (or number density) will be:

$$n = \frac{N}{VA_p T_0} \quad (5-6)$$

5.3 SVT for One-Dimensional Flow with Different Velocities

Consider two systems of particle flow. The first set has N_1 counts detected during time T_0 with a velocity of V_1 in the flow direction, and the second set has N_2 counts have a velocity of V_2 in the same direction and during same time, as shown in Fig. 5.2. The streams are shown separately in the figure (for clear presentation) but it is assumed that both streams pass through the same probe volume during the same time. Suppose that each block of stream #1 contains N_1 particles and each block of stream #2 contains N_2 particles. Also, assume that the whole probe volume cross-sectional area (A_p) is available for both streams and each stream does not have any effect on the other one. Considering these assumptions, we can say that N_1 particles of stream #1 (one solid block of the #1 stream) and N_2 particles of stream #2 (one solid block of the #2 stream) pass through the probe volume during the same time (T_0). The length of each block of the #1 and #2 streams (in the flow direction) will be $V_1 T_0$ and $V_2 T_0$, respectively. Using Eq. (5-6), the number density could be calculated by SVT for each set as:

$$n_1 = \frac{N_1}{V_1 A_p T_0} \quad (5-7)$$

$$n_2 = \frac{N_2}{V_2 A_p T_0} \quad (5-8)$$

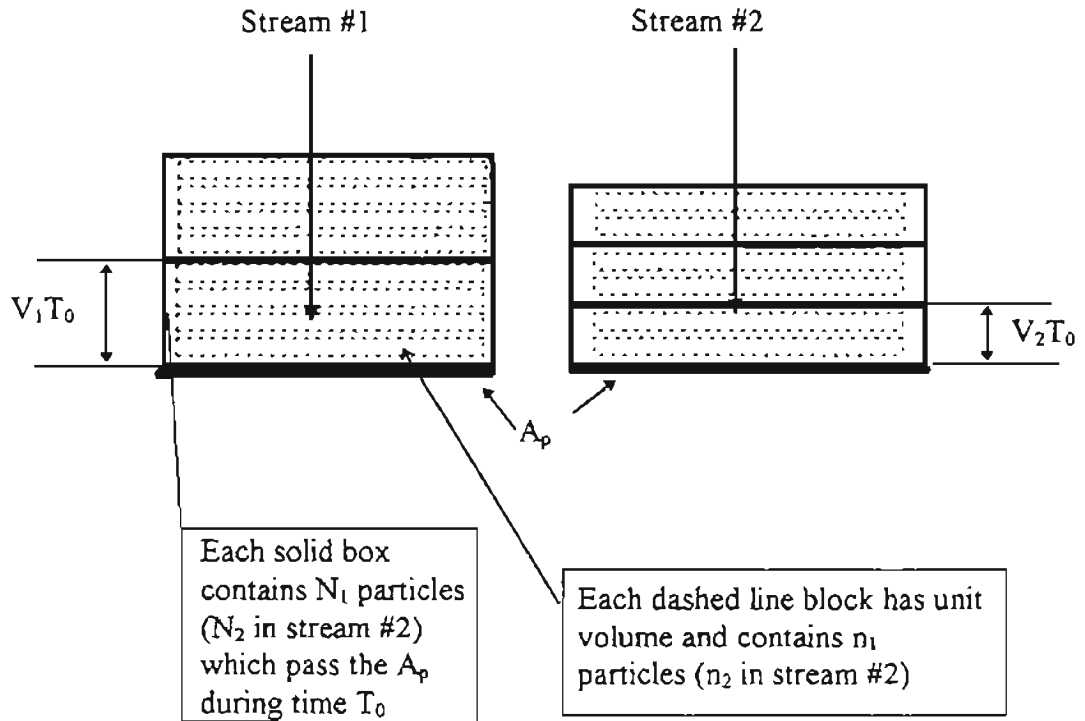


Figure 5.2 SVT for One-Dimensional Flow with Two Different Velocities.

In a unit volume upstream of the probe volume cross-section (dashed rectangles in Fig 5.2), there will be n_1 particles of stream #1 and n_2 particles of stream #2. Therefore, the total number of particles in a unit volume, the average number density for both streams, will be

$$n = n_1 + n_2 \quad (5-9)$$

The following example will explain the above calculation.

Assume that the first system has 100 particles detected in 1 second with velocity of 2 m/s and the second set consists of 600 particles detected in the same time with a velocity of 4 m/s.

Referring to Fig. 5.2, each block of stream #1 has a length of $2 \text{ (m/s)} \times 1 \text{ (sec)} = 2 \text{ m}$, and each block of stream #2 has a length of $4 \text{ (m/s)} \times 1 \text{ (sec)} = 4 \text{ m}$. If the probe volume cross-sectional area is 1 m^2 , then there will be:

- 100 particles in each solid block of stream #1 which has a volume of $2 \text{ m} \times 1 \text{ m}^2 = 2 \text{ m}^3$ with a velocity of 2 m/s (50 particles per m^3).
- 600 particles in each block of stream #2 which has a volume of $4 \text{ m} \times 1 \text{ m}^2 = 4 \text{ m}^3$ with a velocity of 4 m/s (150 particles per m^3).

Therefore, in a unit volume (1 m^3) there will be 50 particles of stream #1 and 150 particles of stream #2. The total particles in a unit volume (with a length of 1 m and cross sectional area of 1 m^2) will be $50 + 150 = 200$ particles (Fig. 5.3). Note that as stated earlier, these calculations are based on the assumptions that the total probe volume cross-sectional area is available for both streams, and that the motion of the particles in each stream does not affect the motion of the particles in the other stream.

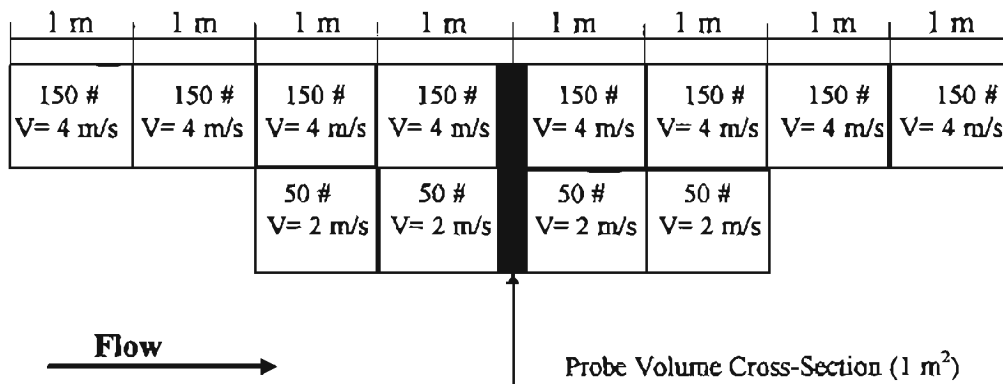


Figure 5.3 Example of Number Density Calculation for Two Streams.

5.4 SVT for One-Dimensional Flow with Gaussian Velocity Profile

The velocity histogram of the DSA usually has a Gaussian shape. The shape results from the range of velocities with their corresponding counts. For a relatively uniform flow, the histogram has symmetry with respect to the peak value. This is true upstream of the filter as well as in the central region downstream where the flow is relatively uniform.

Considering the peak velocity as V_p , there will be velocity increments, call them e where the counts are allocated to each velocity range. In other words, all particles having velocity in the range of $V_p - e/2$ and $V_p + e/2$ are considered to have a velocity of V_p . Therefore, there will be different sets of particles having velocities of V_p , $V_p - e$, $V_p - 2e$, $V_p - 3e, \dots$, $V_p - Ke$ with corresponding counts of N_0 , N_1 , N_2 , N_3, \dots , N_K (Fig. 5.4) as well as sets of particles with velocities of $V_p + e$, $V_p + 2e$, $V_p + 3e, \dots$, $V_p + Ke$ with corresponding counts of N_1 , N_2 , N_3, \dots , N_K (because of symmetry). Using the concept explained in the previous section, the total number density will be :

$$n_T = \frac{N_0}{V_p A_p T_0} + \frac{N_1}{(V_p + e) A_p T_0} + \frac{N_1}{(V_p - e) A_p T_0} + \frac{N_2}{(V_p + 2e) A_p T_0} + \frac{N_2}{(V_p - 2e) A_p T_0} + \frac{N_3}{(V_p + 3e) A_p T_0} + \frac{N_3}{(V_p - 3e) A_p T_0} + \frac{N_4}{(V_p + 4e) A_p T_0} + \frac{N_4}{(V_p - 4e) A_p T_0} + \dots + \frac{N_K}{(V_p + Ke) A_p T_0} + \frac{N_K}{(V_p - Ke) A_p T_0}$$

(5-10)

Simplifying:

$$n_T = \frac{N_0}{V_p A_p T_0} + \frac{2N_1 V_p}{(V_p^2 - e^2) A_p T_0} + \frac{2N_2 V_p}{(V_p^2 - (2e)^2) A_p T_0} + \frac{2N_3 V_p}{(V_p^2 - (3e)^2) A_p T_0} + \frac{2N_4 V_p}{(V_p^2 - (4e)^2) A_p T_0} + \dots + \frac{2N_K V_p}{(V_p^2 - (Ke)^2) A_p T_0} \quad (5-11)$$

If the lowest and highest velocity are relatively close to the peak velocity, then

$$Ke < V_p \quad (5-12)$$

As an estimate, Ke/V_p should be at least less than 0.2 for all flow rates. Then

$$(Ke)^2 \ll (V_p)^2 \quad (5-13)$$

and the total number density can be simplified as

$$n_T = \frac{N_T}{V_p A_p T_0} \quad (5-14)$$

where the total number of particles, N_T , is equal to the sum of all counts in the different sets:

$$N_T = N_0 + 2(N_1 + N_2 + N_3 + N_4 + \dots + N_K) \quad (5-15)$$

The calculated number density is based on a velocity profile. The velocity profile might not always be symmetric (Fig. 5.5). Using the superposition concept, the non-symmetric profile could be divided into two different histograms: a symmetric histogram and a non-symmetric histogram. Therefore, the total number density will be:

$$n_T = n_s + n_{ns} \quad (5-16)$$

where n_s and n_{ns} are number densities calculated based on symmetric and non-symmetric velocity histograms, respectively. If the calculated symmetric number density is one order of magnitude larger than the non-symmetric number density, then the non-symmetric part can be neglected.

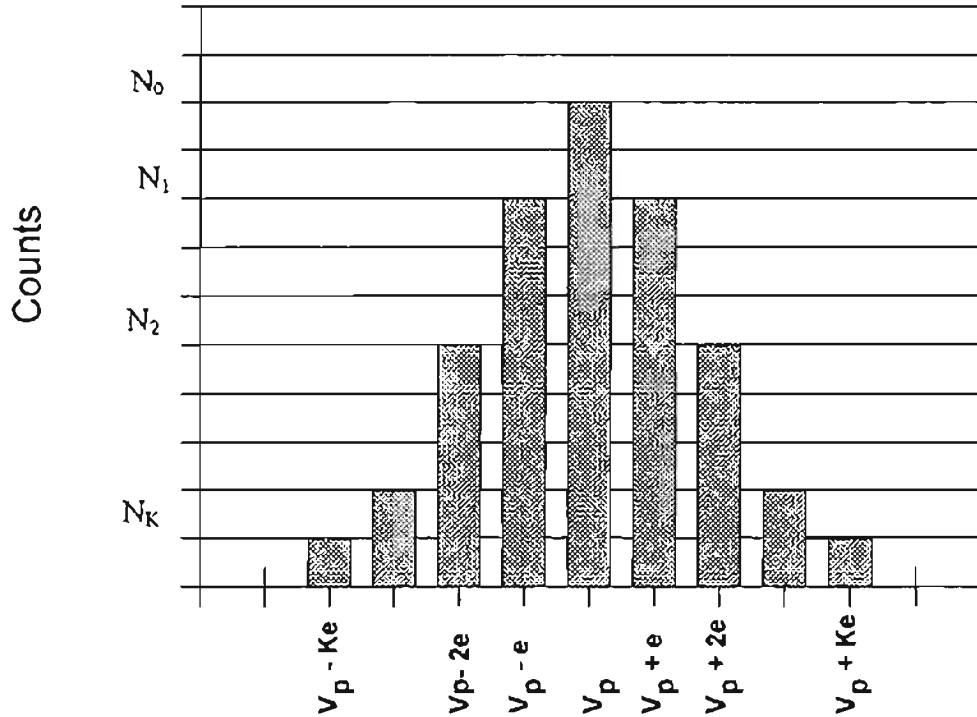


Figure 5.4 Ideal Gaussian Velocity Histogram.

This is true for the cases where both symmetric and non-symmetric histograms have average velocities on the same order, but the number of counts of the non-symmetric profile is at least one order of magnitude less than number of counts of the symmetric profile. In other words if $N_s \gg N_{ns}$ then $n_s \gg n_{ns}$ and

$$n_T \approx n_s \quad (5-17)$$

As an example, the histogram shown in Figure 5.5 could be divided into the symmetric and the non-symmetric histograms shown in Figure 5.6. As it can be seen, both

histograms have the same order of velocity averages but the number of counts of the non-symmetric histogram is less than that of the symmetric one. Since, for most of the central region of the filter, the velocity histogram has a narrow band, the error caused by such an approximation is much less than the system error (some of the system errors, such as the variation of the number density at a specific location, are discussed in Section 6.2). The quantitative evaluation of the error caused by approximation of a non-symmetric velocity profile with a symmetric one is complicated since the non-symmetric part of the histogram is not consistent at different locations and for different tests. During the current measurements, the effect of the non-symmetric portion of the velocity histogram is neglected based on visual observation of the profile on the computer screen and without any documented proof. Note that with the current version of the DSA software, it is not easy to separate the non-symmetric part of the velocity histogram from the symmetric part (in order to compare the orders of magnitude of the counts).

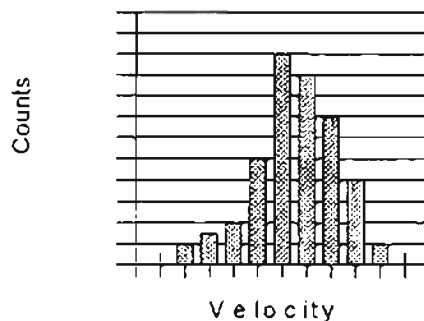


Figure 5.5 Typical Non-Symmetric Velocity Histogram.

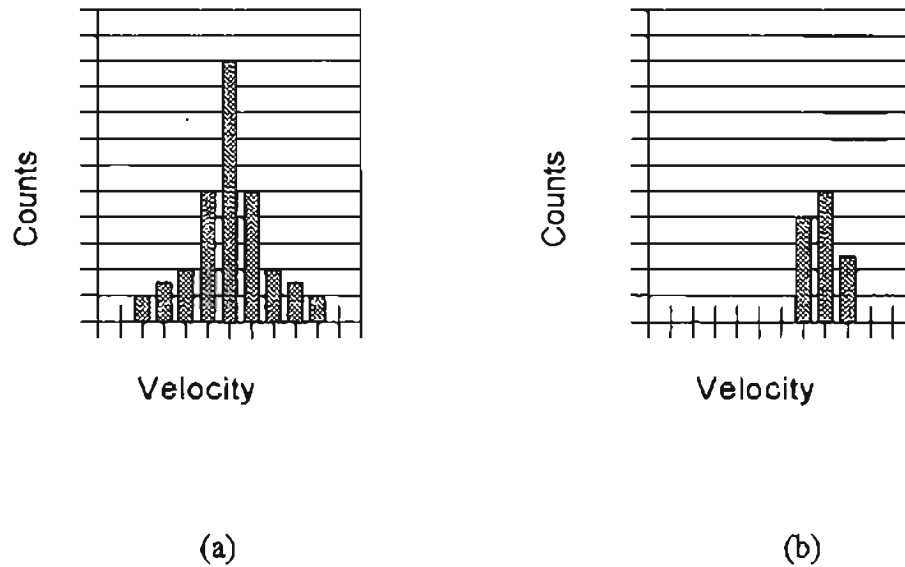


Figure 5.6 Symmetric and Non-Symmetric Parts of the Velocity Histogram of Fig. 5.5,
 (a) Symmetric Part, (b) Non-Symmetric Part.

5.5 SVT in Recirculation Zones

Flow visualization experiments have shown that recirculation zones exist at the edges of the filter [Natarajan, 1995], mainly downstream of the filter; and because of that recirculation, a uniform velocity profile might not be obtained. The axial velocities will be lower than in the central region, and in some cases, negative velocities will appear. These negative velocities will bring the average velocity to a value very close to zero which results in the calculation of very large calculated number densities. Using the SVT for a Gaussian velocity profile (Eq. (5-14)) will give unrealistic results (very large number densities in some cases). Therefore a modification is suggested to the technique so that more realistic results are achievable.

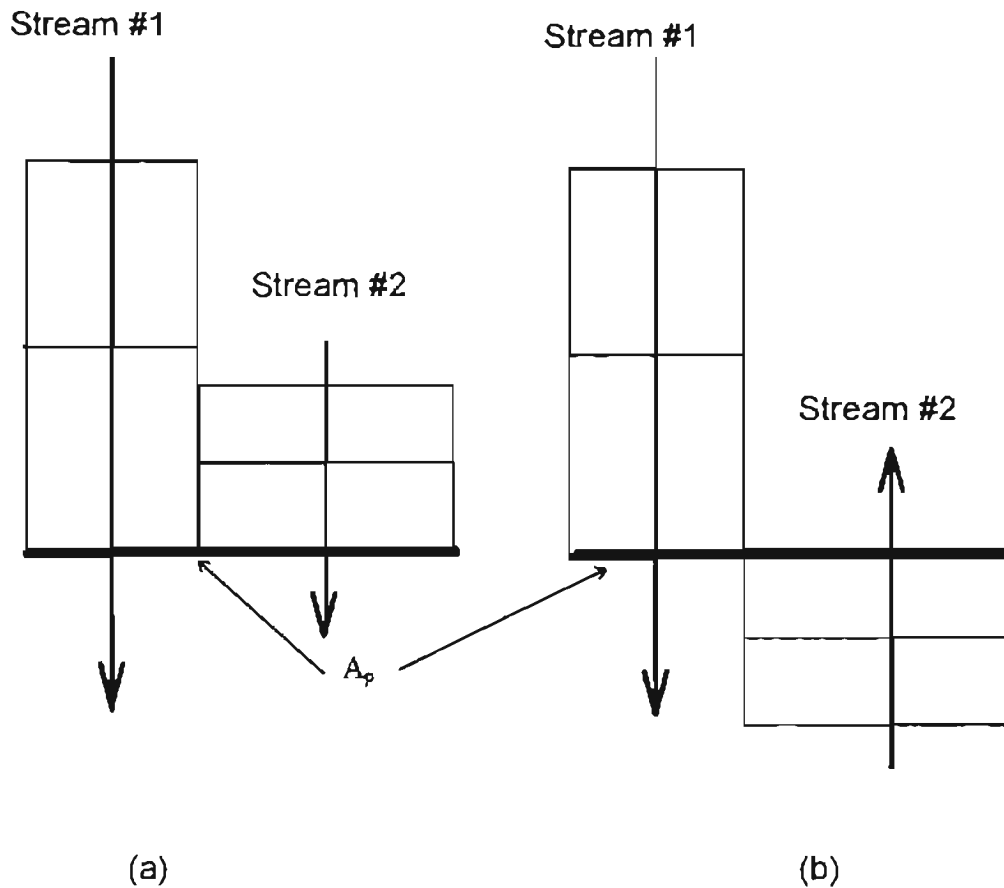


Figure 5.7 One Dimensional Flow Streams, a) Moving in the Same Direction, b) Moving in the Opposite Direction.

When two different streams are moving in the same direction, as shown in Fig. 5.7 (a), the total number density will be equal to the sum of the number densities calculated for each stream. Now, if the two sets are moving in opposite directions (relative to each other), the total number density will again be the sum of the number densities calculated for each of the streams. If the second stream shown in Fig. 5.3 (the flow stream of 100

particles detected in one second with a velocity of 2 m/s) moves in the opposite direction, the number of particles existing on each side of the probe volume will be the same as Fig. 5.3, since the flow is steady-state. This is true if the flow is one-dimensional. Therefore, for a one-dimensional flow with flow streams in the positive and negative directions, the total number density is equal to a one-dimensional flow with the two streams moving in the same direction. For each stream, Eq. (5-14) can be used for the number density calculation. A typical example is shown in Fig. 5.8. Number density for a flow with velocity histogram (a) is equal to the summation of the number densities calculated for velocity histograms (b) and (c).

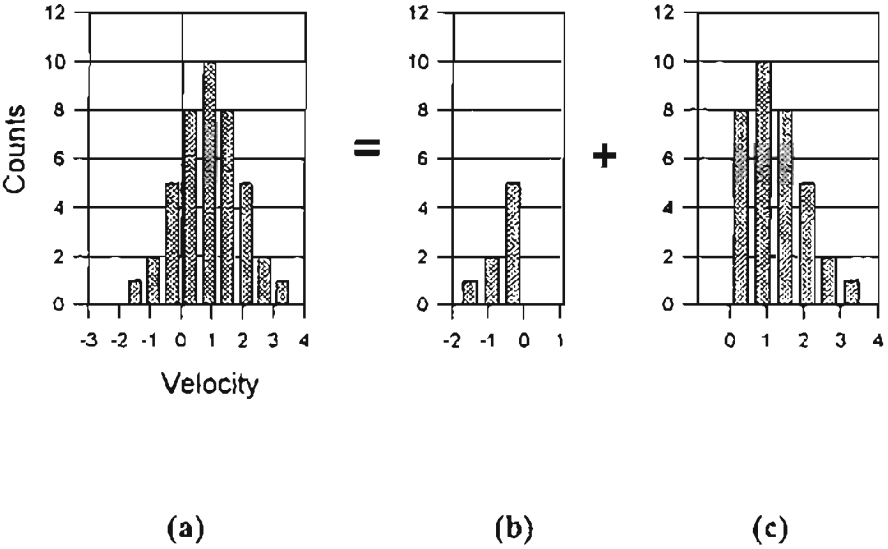


Figure 5.8 Calculation of Number Density for One-Dimensional Flow with Opposite Streams, a) Total Velocity Histogram, b) Negative Velocity Histogram, c) Positive Velocity Histogram.

5.6 SVT for Flows with Different Velocities in Different Directions

Perhaps the most general case is multi-dimensional flow which all of the particles are moving in different directions because of high turbulence intensity. This phenomena might occur at the filter corners or very close to the filter edges, especially at low flow rates. Since the particles are moving in several directions, the axial and transverse velocity histograms will have both negative and positive values, and both components are comparable to each other, so that the flow cannot be treated as a one-dimensional flow. The methods described in Sections 5.3, 5.4 and 5.5 of this chapter are applicable to one-dimensional flows. Thus, the concept of superposition of different flow streams is still valid. According to Fig. 5.9, if two flow streams are moving in two different directions, since the cross-sectional area of the probe volume is the same for particles whose entire path lays in the YZ plane (normal to the filter plane and parallel to the transceiver lens), the number densities can be calculated for each stream and then added together in order to get the total number density. The major difficulty is how to distinguish the average velocity of the different streams and calculate the needed velocity.

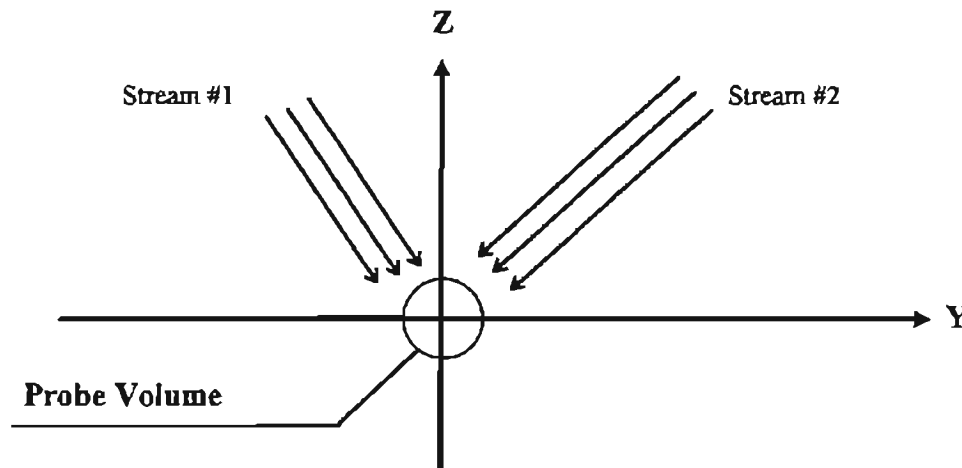


Figure 5.9 Two Flow Streams in Different Directions.

5.6 SVT for Flows with Different Velocities in Different Directions

Perhaps the most general case is multi-dimensional flow which all of the particles are moving in different directions because of high turbulence intensity. This phenomena might occur at the filter corners or very close to the filter edges, especially at low flow rates. Since the particles are moving in several directions, the axial and transverse velocity histograms will have both negative and positive values, and both components are comparable to each other, so that the flow cannot be treated as a one-dimensional flow. The methods described in Sections 5.3, 5.4 and 5.5 of this chapter are applicable to one-dimensional flows. Thus, the concept of superposition of different flow streams is still valid. According to Fig. 5.9, if two flow streams are moving in two different directions, since the cross-sectional area of the probe volume is the same for particles whose entire path lays in the YZ plane (normal to the filter plane and parallel to the transceiver lens), the number densities can be calculated for each stream and then added together in order to get the total number density. The major difficulty is how to distinguish the average velocity of the different streams and calculate the needed velocity.

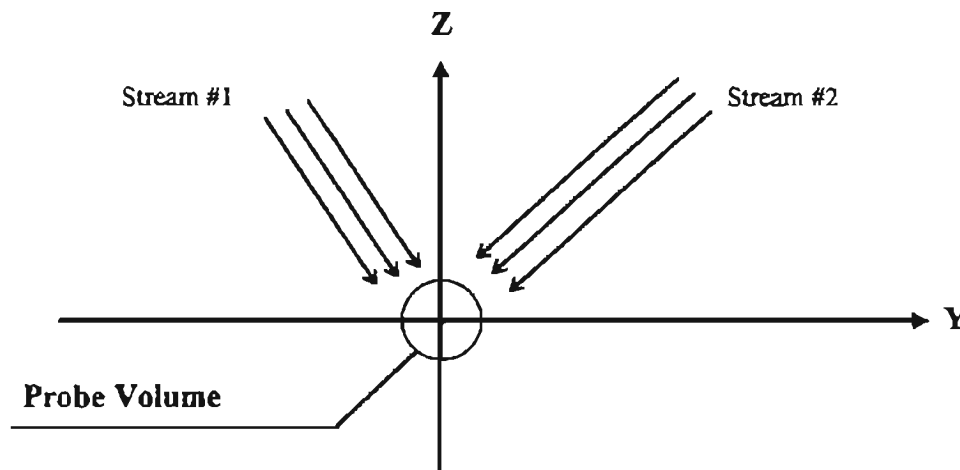
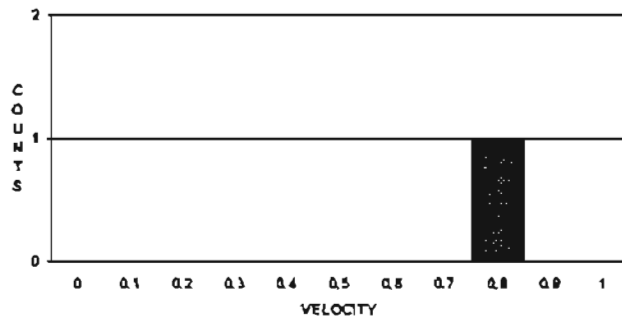
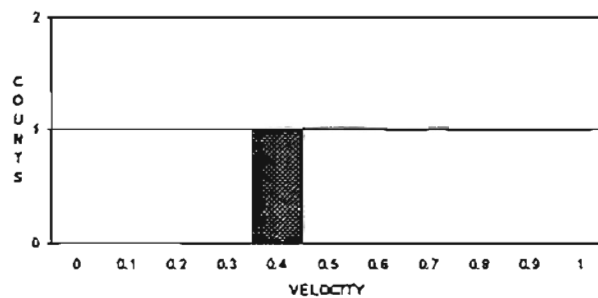


Figure 5.9 Two Flow Streams in Different Directions.

The LDV system measures the axial and transverse velocities of all counted particles, and it is not easy to verify what are the corresponding transverse velocities of particles having a specific axial velocity. Moreover, since the power of the laser beams measuring axial velocities and counts (green beams) are different than those measuring transverse velocities (blue beams), the number of particles detected by the two channels will not be the same. The only way to measure the particles' axial and transverse velocities together is to set the system for detection of one particle only. Also, coincidence should be on, so that the transverse and axial velocities correspond to the same particle (Figure 5.10).



(a)



(b)

Figure 5.10 Typical Example of Measurement of One Particle Velocity,

a) Axial Velocity, b) Transverse Velocity.

From a statistical point of view, in order to obtain the complete histogram, a sufficient number of particles should be detected. As an example, using 1000 samples will be suitable for statistical calculations. This means that data should be acquired 1000 times at each individual location; but this is not practical because of the limited test time.

Number densities were measured at a few locations using this method with 200 samples. Results show that, in most cases, the axial and transverse velocities are such that the average velocity of 30 samples at a specific point does not change more than 10% when the number of samples are increased to 200. In other words, the average for the total velocities of 30 samples taken from one point is within 10% of the average of 200 samples. The following example explains this method in greater detail.

Consider four flow streams as follows:

- Stream A with an axial velocity of 1 m/s and transverse velocity of 0.1 m/s;
- Stream B with an axial velocity of -1 m/s and transverse velocity of -0.1 m/s;
- Stream C with an axial velocity of 0.1 m/s and transverse velocity of -1 m/s;
- Stream D with an axial velocity of -0.1 m/s and transverse velocity of 1 m/s.

If all four streams are such that 1 particle is detected in one second to cross a unit cross-sectional area of 1 m², all four streams will have the same number densities since the number of counts, run time and the total velocities are the same. The total velocities are:

$$V_A = V_B = V_C = V_D = \sqrt{(1)^2 + 1.01^2} = \sqrt{1.01} \approx 1 \quad (5-18)$$

and the individual number densities will be:

$$n_A = n_B = n_C = n_D = \frac{N}{VA_p T_0} = \frac{1}{(1)(1)(1)} = 1 \quad (5-19)$$

then the total number density will be the sum of all four number densities, 4 particles per cubic meter. Figure 5.11 shows the velocity streams. Velocity histograms are shown in Fig. 5.12.

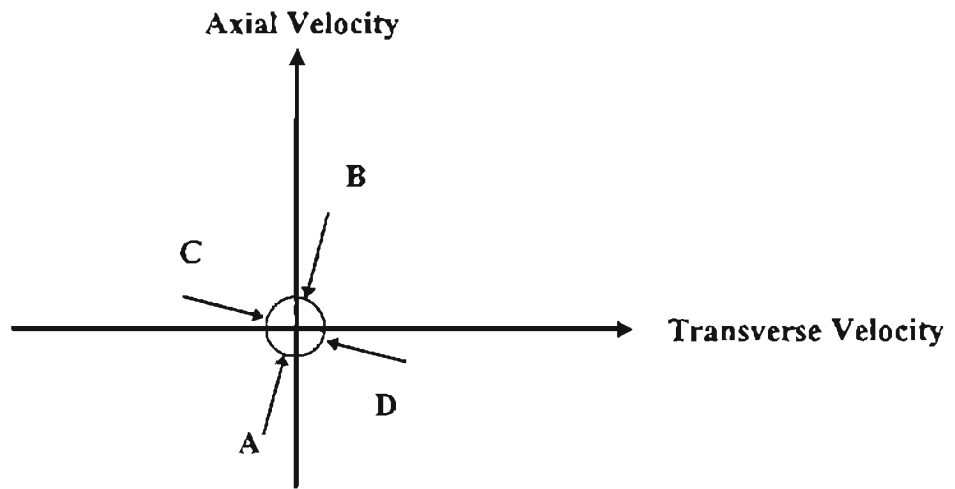
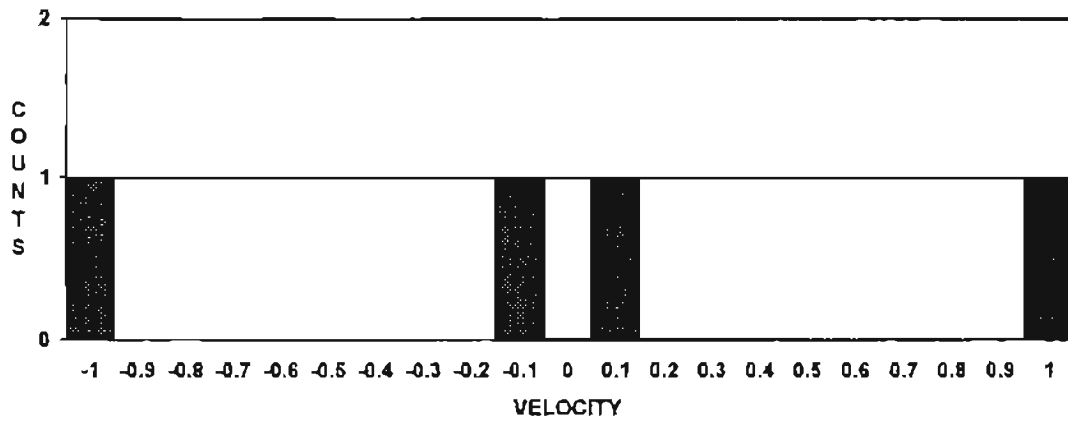


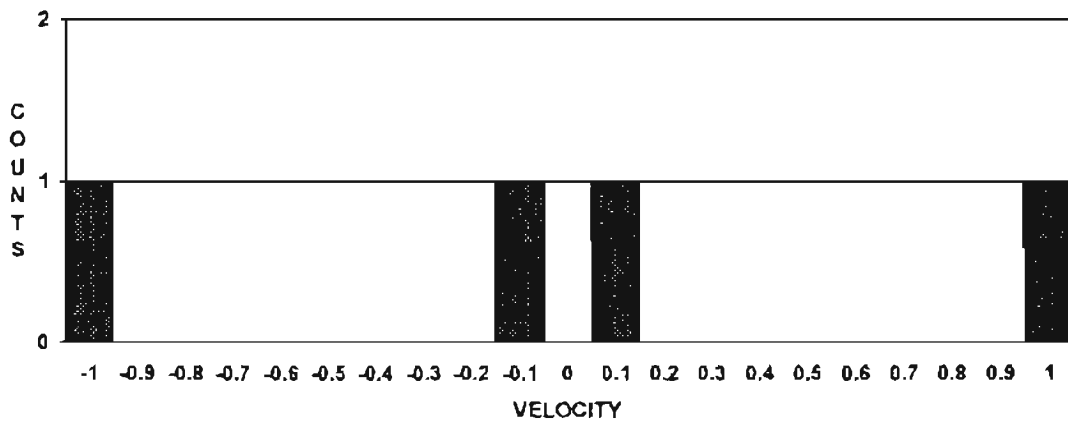
Figure 5.11 Velocity Streams for the Example of Four Flows in Different Directions.

The number densities cannot be calculated based on the average velocities since the average velocities are zero. Using the method mentioned in Section 5.4 for a one-dimensional velocity profile and considering the axial velocity only, an errant number density can be calculated as:

$$n_T = n_A + n_B + n_C + n_D = \frac{1}{(1) (1) (0.1)} + \frac{1}{(1) (1) (1)} + \frac{1}{(1) (1) (0.1)} + \frac{1}{(1) (1) (1)} = 22 \quad (5-20)$$



(a)



(b)

Figure 5.12 Velocity Histograms for the Example of Four Flows in Four Different Directions, a) Axial Velocity, b) Transverse Velocity

which is greater than 4, the actual number density. Considering the histograms, there are four counts with two different axial and transverse velocities: 0.1 m/s and 1 m/s. So it is possible to have two particles with total axial and transverse velocities of 0.1 m/s which

gives a total velocity of 0.141 m/s and two particles with transverse and axial velocities of 1 m/s (which gives a total velocity of 1.41 m/s). The number densities calculated based on these values are quite different than the actual numbers. Therefore, if the total velocity of each particle is measured first (which will be approximately one for all particles in my example), the calculated number density will be the same as the actual number density. Thus the methods described in Sections 5.4 and 5.5 cannot be used at grid locations in recirculation zones.

In summary, for number density calculations in recirculation zones, it is recommended to measure velocities of individual particles (at least 30 runs at each grid point with measuring one sample per run) and use the average of the measured total velocities for number density calculation.

The third component of the velocity is not measured because the present LDV system is equipped only for two-dimensional measurements. If the third velocity component values are of the same order of the other two, there will be additional errors in the measurements.

The grid points of the present measurements are selected such that most of the points fall outside of the recirculation zones where velocities could be considered one-dimensional (since the transverse velocities are at least one order of magnitude lower than the axial velocities). However, since the thickness of the rubber edgings of the filters are not consistent and vary from filter to filter, in a few tests there have been a few grid locations which fall into (or too close to) recirculation zones. This happens downstream of the filter only.

The present measurements were conducted based on the following procedure in order to calculate number densities at different grid locations more accurately.

Before starting each test, the velocity profiles at the grid locations close to the housing walls were measured and recorded. These profiles were reviewed. For grid points at which the axial velocities were at least one order of magnitude greater than the transverse velocities, number densities were calculated based on the following:

- SVT method described in Section 5.4 was used if the velocities were all positive or all negative (the histogram did not intersect with zero velocity line).
- SVT method described in Section 5.5 was used for velocity if some of the samples had positive velocities and some negative velocities.

For particles whose axial and transverse velocity profiles were on the same order, the SVT method described in Section 5.6 was used. 30 runs (with one sample per run) were measured for velocity calculation.

Number densities for all grid locations other than the ones close to the housing wall were calculated based on the one-dimensional SVT (Section 5.4).

CHAPTER VI

CONSISTENCY MEASUREMENTS

One of the most important goals of the present measurements is to prove the repeatability of the data. If the measurement conditions are the same for two different tests, the results should be comparable to each other within a reasonable range. In the past, the major problem was repeatability of the measurements. As stated by Williams [1996] and Natarajan [1995], the results obtained from two different tests for the same conditions have relative errors ranging from 20% up to 300%. Consistency measurements are made on uniform flows so that the factors affecting the data and causing the errors could be investigated. Also system parameters have been varied so that their effects on the calculated number density could be verified.

Anand [1997] conducted consistency measurements at a specific location in two different flows:

- A uniform flow coming out of the atomizer exposed to the atmosphere (water droplets were used as seeding particles).
- A uniform flow inside the small angle diffuser housing (without the filter) using 0.966 micron particles.

He also made measurements at two different locations inside the small angle diffuser housing without the filter. One location was at the center of a plane located 40 mm above the filter, and the other location was at the center of a plane 50 mm below the filter. These measurements are called zero efficiency measurements since a zero value for efficiency is expected. Measurements are then extended to all of the grid points by measuring number densities at 35 grid points upstream and downstream of the filter placement cross-section. Detailed discussion of the consistency measurements is presented by Anand [1997]. A brief review of the test procedures and the results as well as the effect of system parameters on the measurements is presented in this chapter.

6.1 Factors Affecting Measured Data

When number density at a specific location in a uniform flow is measured, it might be affected by a variation in one of the following factors:

- the power of the laser beams,
- DSA parameters,
- polarization angle of the beams,
- flow rate and particle seeding rate, and
- possible leaks.

The effect of each of these items on the measurements and the calculated number density was investigated by Anand [1997]. Most of the material presented in this section is based on his work.

6.1.1 The Power of the Laser Beams

The number of counts per unit time changes when the power of the beams coming out of the transceiver is varied. The power is adjusted to its maximum value for a given laser power, i.e., maximum efficiency of the fiber drive, by aligning the fiber drive. Anand [1997] has shown that a slight change in the room temperature will reduce the power of the beams which results in a reduction of the detected sample rate (number of counts per unit time). He examined the effect of the temperature change on the power of the beams. He found out that the laser power is reduced when the room air temperature is raised by 0.5°C.

Temperature change is believed to cause flexing of the breadboard which holds the fiber drive and affects the alignment of the couplers on the fiber drive (giving lower fiber drive efficiency). Since the beams have a Gaussian cross-sectional intensity distribution (low intensity on the periphery), when the power is reduced, the particles which are not passing through the central region of the probe volume might not generate back-scattered light strong enough for detection. Such a signal is considered to be noise and the particle is not detected. This problem is solved by maintaining the room temperature at a specific value. Measurements show that a variation of temperature more than 0.5° C might cause power reduction.

Vibration could also affect the power. Vibration caused by the blower is believed to be transferred to the board and fiber drive either from the ground or by air (acoustics). No measurements were conducted for determination of the amount of the vibrational

noise. However, it was tested by isolating the system using pneumatic vibration isolators and installing them under the breadboard, the effect of the ground vibration was reduced.

6.1.2 DSA Parameters

As described in Chapter three and Appendix A, the DSA parameters should be adjusted to appropriate values in order to achieve the optimum conditions for measurements. Variation of any of these parameters might change either the velocity profile or the sampling rate. Variation of number density due to each of them is examined by Anand [1997]. The effects of a few important parameters are described below.

6.1.2.1 High Voltage

High voltage controls the gain of the PMT output signal. Below a certain HV level, many signals will not be detected, and above a certain limit, noise in the signal might become dominant. We found these low and high levels to be 350 and 400 volts, respectively. The optimum value of high voltage was found to be a value which corresponds to a validation in the range of 90 to 95% of the maximum achievable validity. For example, if a validity of 100% is obtained by setting the HV to a specific value, it should be changed so that a validity of 90 to 95% is achieved. The validity decreases when the HV is increased, so according to the above discussion, the HV should be increased to a new value corresponding to 90 - 95% validity.

6.1.2.2 Threshold

The threshold determines the minimum signal amplitude required to cause a burst detection. Variation of threshold will also change the validity as well as the sample rate and velocity profile. Low threshold may cause additional noise to be added to the signal,

so that one Doppler burst might be detected as several individual bursts. High threshold will eliminate valid signals which are valid but have low gains. By starting with a very low value of the threshold and increasing the value up to the point where the burst signal does not have a break and where the validity reaches 90 to 95% of its maximum achievable value, the optimum threshold can be obtained.

6.1.2.3 Velocity Range

Velocity range should be selected in such a way that no count is invalid because of having a velocity out of the selected range. The velocity range should be set to the maximum value (-14.2 m/s to 14.2 m/s) in the beginning. Once data for a few points is acquired, the velocity range could be adjusted so that velocities of all detected particles fall within the selected range. As an example, if the velocity profile is in the range of 1 to 3 m/s, the maximum and minimum velocities could be set to 5 and -5 m/s, respectively. Usually the maximum and minimum are set to the same absolute values, but with opposite signs so that the location of the velocity histogram with respect to the origin can be easily seen on the screen.

6.1.2.4 Coincidence

The LDV system is setup in such a way that the number of particles and their corresponding velocities could be measured in each direction (normal to a filter or transverse to a filter) independent of the other direction. The power of the green laser beams (which detect the particle count and velocity in the normal direction) is different than that of the blue laser beams (which detect particle count and velocity in the transverse direction). Since the number of counts is dependent on the laser beam power, the sample

rates measured in the two different directions will not be the same. In order to measure the same number counts in both directions and obtain their corresponding velocity components in each direction, the coincidence of the LDV must be turned on. With coincidence turned on, the same particles will be detected (in both the normal and traverse directions) for each run. If the number of samples is set to one, for each run, only one particle will be detected in both directions. The particle's velocity components will be measured by the system if the coincidence is turned on.

6.1.2.5 Other Parameters

Some of DSA parameters were set to fixed values independent of the flow conditions. The frequency shift, burst filter, sample frequency and number of samples are examples of these parameters. The definitions of these items as well as their values are presented in Appendix A.

6.1.3 Polarization Angle of the Beams

As discussed in Chapter two, in order to get a Doppler burst or beat signal, the two crossing beams (i.e., both green beams or blue beams) should have the same phase relation and the same polarization angle. The polarization angle of the beam can be measured by a simple polarizing filter. By locating the polarizer in front of the beam and measuring the power of the beam coming out of the polarizer, we could set the polarizer to a maximum power position. The polarization angle will be the position which corresponds to the maximum measured power. Once the angle is determined on one beam, the other beam should be checked to have maximum power at the same angle. If it does not have the same angle, the optic fiber connected to the couplers should be rotated

in a way such that by redoing the above procedure, the same angle is obtained for maximum power as for the first beam.

When the polarizer is placed in front of a specific beam and rotated, different power values will be obtained. The maximum power coming out of the polarizer corresponds to an angular position 90 degrees away from the minimum power location. The optimum polarization condition is a situation where the ratio of the maximum achievable power of the polarized beam to the minimum achievable power of the same beam (obtained by rotating the polarizer 90 degrees from the maximum power position) is more than 100. Further details regarding the optimization of the polarization angle are presented by Anand [1997].

6.1.4 Flow Rate and Particle Seeding Rate

As described in Chapter three, the air flow rate is maintained by a blower, and the test section is located on the blower's suction side. Ambient (room) air is sucked into the housing while being heated by the heater. The flow rate is measured by a TSI flow meter which measures the standard flow rate corresponding to a temperature of 70°F and 29.2 mm Hg absolute pressure. Since the air is heated before entering the system, it is possible that the temperature of the air flowing in changes throughout the test, thus resulting in a change in the flow rate. Experiments show that the flow rate decays during a period of time after the blower is turned on, and it is recommended that the blower be run for at least 30 minutes before starting the test. Present measurements were made with a flow rate variation of ± 2 to 3% during the test.

The amount of particles fed to the flow per unit time (particle seeding rate) should also be constant. The six-jet atomizer seeds particles at a uniform rate (with a maximum error of $\pm 5\%$) into the flow. This has been verified by consistency measurements conducted by Anand [1997]. It has been seen that when the volume of the solution in the atomizer container goes below a certain level (about 300 ml) during the test, the rate of particles fed to the flow is increased. This has caused termination of a few tests. Measurements show that the maximum solution consumption rate does not exceed 100 ml/hr. Knowing the maximum effective capacity of the atomizer to be 900 ml, a test should not take longer than 6 hours. Note that it is more difficult to control all of the parameters in a test for a very long time. If a test is going to take longer than six hours, it is recommended to connect the atomizer solution container to an additional container so that more solution can be available.

Before starting an actual test, a short test should be conducted with the atomizer filled with water only. If water droplets are detected by the LDV system, the heater should be rearranged so that all water droplets coming out of the atomizer are vaporized before reaching the filter. In that case, no particles will be detected.

6.1.5 Possible Leaks

The system should be checked for possible leaks. There could be possible leaks causing air flow into the system from a leaking point. The system should be tested for leaks by pressurizing the housing and checking joints by applying a soap bubble solution and looking for evidence of growing bubbles due to leakage. The small angle diffuser housing is pressurized by a small blower when the main blower is turned off. The whole

system is pressurized when the small blower is turned on. Leak tests were performed on the system with a differential pressure of 6 inches of water. Maximum differential pressure of the current tests does not exceed 5.0 inches water in most of the tests.

6.2 Consistency Measurements

The items listed in Section 6.1 affect the calculated number density. By controlling all of these parameters and optimizing them, one should get a consistent number density at a specific location. The intention of consistency measurements is to verify this concept and calculate the overall system errors. Anand [1997] has made a series of consistency measurements with different values of the DSA parameters as well as efficiency measurements without a filter present. A few of his measurements are described below.

6.2.1 Consistency Measurements on Air Flow with Water Droplets

Using water droplets as seeding particles, Anand measured the sampling rate and velocity profile at the center of the flow coming out the atomizer (vertical flow) exposed to the atmosphere. He acquired data in different sets of 30 or 50 consecutive measurements. A typical plot of calculated sample rates is shown in Fig. 6.1. In order to examine variation in the sample rates measured by Anand, the normalized sample rates (sample rate for each run divided by the average sample rates of all runs) for each test are plotted using box and whiskers (Fig. 6.2). The lower and higher end of each box presents the 25 percentile and 75 percentile of each test, respectively. The high and low end whiskers present 90 and 10 percentiles respectively. The median of each test is specified by a line in each box. Points outside of the 10 to 90 percentile range are plotted as circles.

These points are called out-lyers and in most cases represent the maximum deviation from the average. It is the author's opinion that the 10-90 percentile range should be taken into account for error calculations. Figure 6.2 shows that for all tests, at least 90 percent of the measured samples fall within $\pm 5\%$ of the average. Each test consists of 30 runs.

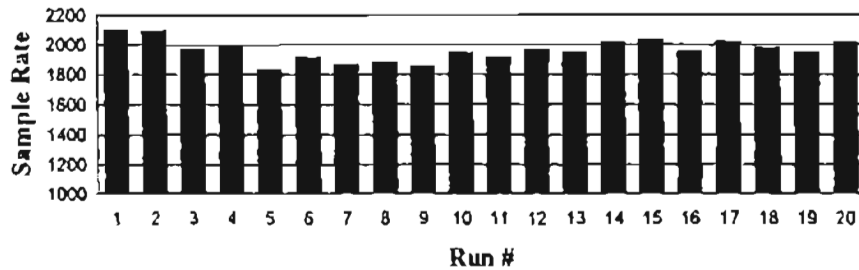


Figure 6.1 Consistency Measurements in Open Air Flow with Water Droplets, Valid Samples/Run = 20000, Validity = 93%, Laser Power = 0.8 W.

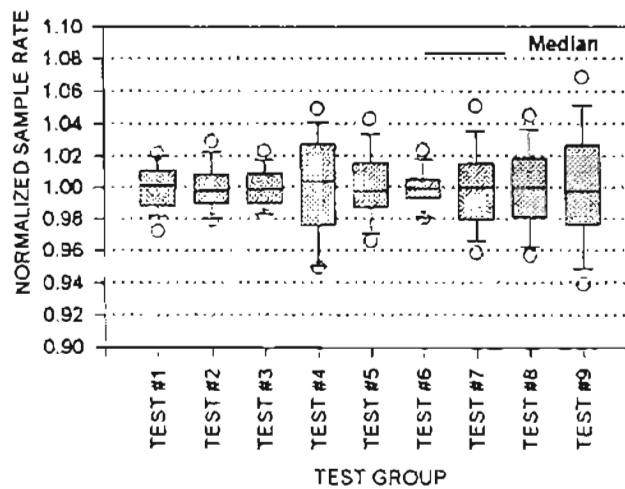


Figure 6.2 Summary of the Consistency Measurements for Flow with Water Droplets (30 Runs per Test).

6.2.2. Consistency Measurements in Particle Flow

The same method was applied to measure sampling rate at the center point of two different cross-sections, upstream and downstream of the filter placement inside the housing. 0.966 micron PSL particles were used for these measurements. This type of measurement was also repeated with different DSA parameter settings. A typical plot of the measured data is presented in Fig. 6.3.

Measurements were made at upstream and downstream locations for each run using 1000 valid samples. The box plots presenting normalized sample rates for different tests with particles are shown in Fig. 6.4.

Comparing the box plots for flow coming out of the atomizer (with water droplets only) with flow inside the housing (with PSL particles), it can be concluded that the deviation of the sample rates from the average for both flows are in the same range (maximum $\pm 6\%$ to $\pm 8\%$). Therefore, it can be concluded that the error presents the system error and is independent of particle concentration, flow velocity and measurement location.

The sample rates of the two flows are different than each other since the number of samples are different. For open flow with water droplets, because of the high concentration of water droplets, the number of valid counts are set to 20000 while for the flow inside the housing with PSL particles, this number is set to 1000. However, since the error values are relative to the average, they are comparable to each other.

The consistency measurements were extended to two points. one in the center of a plane upstream of the filter placement and the other at the center of a plane downstream

of the filter placement, without the filter. These measurements are called “zero efficiency” measurements since the efficiency should be zero if the flow is uniform.

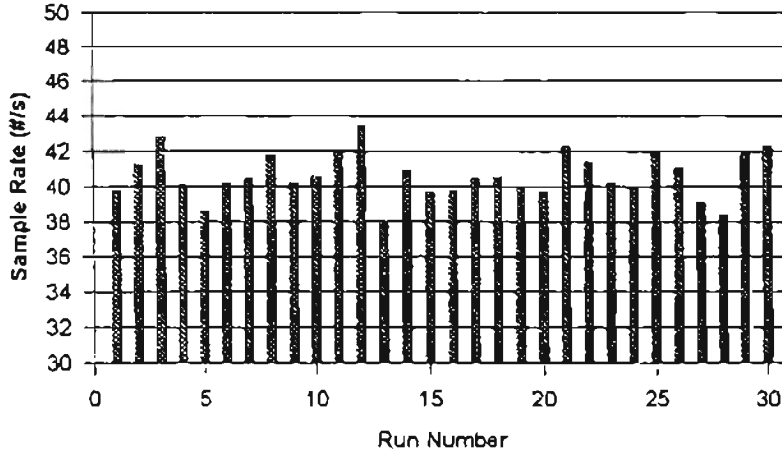


Figure 6.3 Consistency Measurements for Flow inside the Housing with PSL Particles, Valid Samples/Run = 1000, Validity = 92%, Laser Power = 0.8 W .

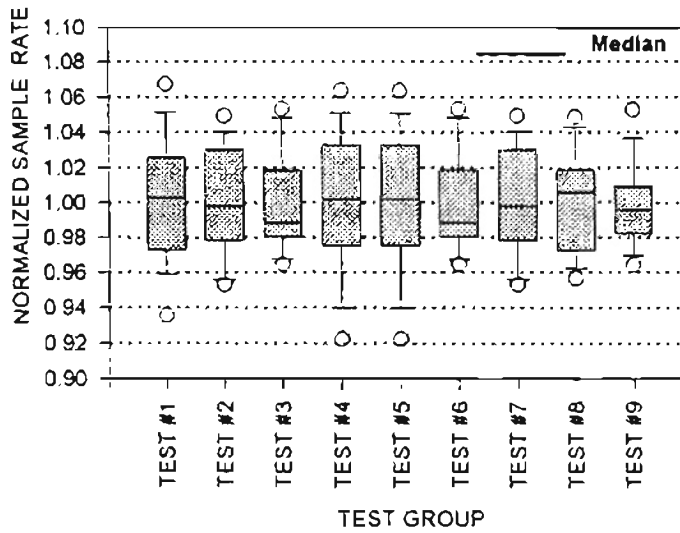


Figure 6.4 Summary of the Consistency Measurements for Flow with Particles inside the Housing (30 Runs per Test).

6.2.3 Zero Efficiency Measurements at the Center of the Housing

Anand [1997] has conducted the zero efficiency measurements. A typical plot of his measurements is shown in Fig. 6.5. Sample rates are measured at two locations, one at the center of a plane 40 mm above the filter placement plane and the other at the center of a plane 50 mm below the filter placement plane (exactly below the first point). The efficiency was then calculated by Eq. (5-2), but instead of number densities, the sample rates were used. Measurements showed that the velocity of the particles at the above mentioned locations are the same since there is no filter to affect the velocity. Therefore sample rates were used for efficiency calculation (instead of number density).

During the tests, all of the parameters mentioned in the previous section (Section 6.1) were controlled and optimized Anand [1997]. The ambient temperature was maintained constant within ± 0.5 °C. The power of the laser beams was checked several times in order to make sure that the measurements were not affected. The measured sample rates have maximum errors of $\pm 6\%$, which conforms to the previous results of consistency measurements. Measured sample rates have random fluctuations within the error band. Since there is no filtration, a zero value for efficiency is expected. Therefore the two sample rates (upstream and downstream the filter placement) should be equal.

Applying the fluctuation error to each of the measured sample rates in order to get the error in the efficiency, there will be two worst cases for which the efficiency has its highest error value. If s_1 and s_2 are the number densities corresponding to locations above and below the filter, then for zero efficiency:

$$s_1 = s_2 \tag{6-1}$$

Introducing s_1' and s_2' as measured number densities with error, the worst cases will be:

1. The case where $s_1' = 0.95 s_1$ (an error of -5%) and $s_2' = 1.05 s_2$ (an error of +5%)

$$\eta = 1 - \frac{s_1'}{s_2'} = 1 - \frac{0.95s_1}{1.05s_2} \approx 9.5\% \quad (6-2)$$

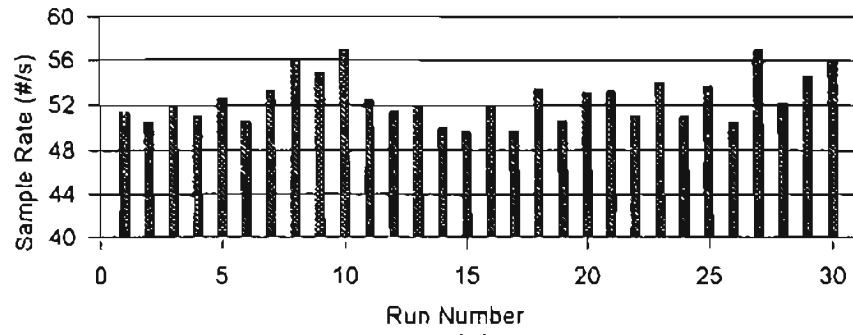
2. The case where $s_1' = 1.05 s_1$ (an error of + 5%) and $s_2' = 0.95 s_2$ (an error of -5%)

$$\eta = 1 - \frac{s_1'}{s_2'} = 1 - \frac{1.05s_1}{0.95s_2} \approx -10.5\% \quad (6-3)$$

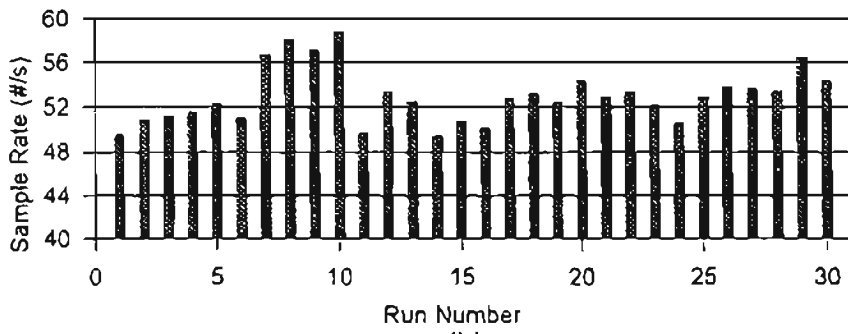
In other words, if zero efficiency is expected and the sampling error is $\pm 5\%$, the worst fluctuation from zero will be 9.5 % to -10.5 %. These values will be obtained if a peak of the measurement at one point matches with a valley when measuring at its corresponding point above or below the filter. The probability of measurement with these errors is low. However, within several samples, there could be a few with either of the above stated conditions.

6.2.4 Zero Efficiency Measurements at All Grid Points

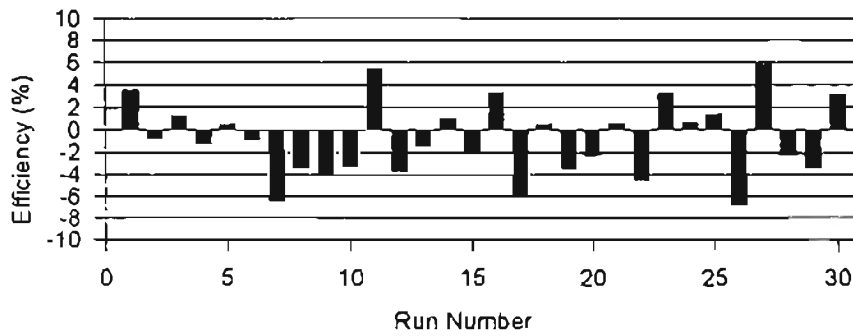
Using a rectangular grid spacing of 19.05 mm x 19.05 mm, Anand [1997] conducted zero efficiency measurements for all grid points. The grid consisted of 5 rows in the X direction and 7 rows in the Y direction (a total of 35 points). At each point, three sample sets were taken and the average of the three calculated number densities was used for the efficiency calculation. The overall efficiency was -0.22%. He repeated the zero efficiency measurements with the same grid spacing. The overall efficiency obtained was -0.36%, which demonstrates the repeatability of the tests.



(a)



(b)



(c)

a) Upstream, b) Downstream, c) Efficiency

Figure 6.5 Zero Efficiency Measurements at One Location inside the Housing with Flow Rate = $103.7 \text{ m}^3/\text{hr}$, Valid Samples/Run = 1000, Validity = 92%, Laser Power = 0.8 W, 3/19/96.

CHAPTER VII

RESULTS AND DISCUSSION

The experiments on the A13192 filter were conducted using 0.966 micron PSL particles as the challenge contaminant. Measurements were mainly made in the small angle diffuser housing described in Chapter four. A few tests were conducted in the SAE housing (Chapter four) in order to compare the two diffusers. The DSA parameters were set to their optimum values as recommended by Anand [1997]. The detailed discussion of the results and comparison with previous theoretical models and experimental measurements is presented in this chapter.

7.1 Summary of the Tests in the Small Angle Diffuser Housing

At least two complete tests were conducted for each selected set of measurements. Values of initial pressure drop as well as the pressure drop change were recorded for each test. Table 7.1 summarizes the measurements. At least three runs were recorded at each location if the run time did not exceed 30 seconds. For longer time runs, one or two measurements were made (instead of three) because of the limited test time. The number densities were calculated based on the average velocities (discussed in Section 5.4) for most cases. The modified SVT discussed in Section 5.5 was used for measurements in

recirculation zones. The two-dimensional SVT (described in Section 5.6) was used at a few points only because of the test time limitations.

Table 7.1 Summary of the Small Angle Diffuser Housing Tests.

TEST	TEST DATE	FLOW RATE (Sm ³ /hr)*	AVERAGE EFFICIENCY WHOLE FILTER (%)	AVERAGE EFFICIENCY CENTRAL REGION (%)	INITIAL PRESSURE DROP (mm water)	FINAL PRESSURE DROP (mm water)
F15	7/1/96	5.68	37.63	36.58	2.54	3.81
F16	7/2/96	5.68	42.63	36.86	3.81	3.81
F11	8/24/96	29.48	37.53	35.6	3.3	4.57
F12	6/25/96	29.48	39.7	38.3	3.05	3.81
F23	7/16/96	53.27	30.98	27.7	3.81	5.08
F22	7/15/96	53.27	39.03	35.8	5.08	5.34
F24	7/17/96	53.27	39.26	35.33	3.81	5.08
F9	6/19/96	77.06	33.26	30.84	N/A**	N/A**
F10	6/20/96	77.06	36.01	35.2	6.35	8.89
F20	7/5/96	103.69	33.86	32.9	10.16	11.43
F19	7/5/96	103.69	37.34	37.56	19.05	21.59
F1	5/8/96	145.7	44.1	47.02	N/A**	N/A**
F4	5/14/96	145.7	46.2	44.7	N/A**	N/A**
F2	5/13/96	145.7	50.02	48.27	N/A**	N/A**
F18	7/4/96	187.72	51.59	57.1	N/A**	N/A**
F21	7/8/96	187.72	60.95	62.05	21.59	24.13
F5	5/21/96	187.72	72.56	72.99	N/A**	N/A**
F7	6/7/96	313.75	74.48	79.16	N/A**	N/A**
F8	6/18/96	313.75	82.17	84.1	N/A**	N/A**
F14	6/28/96	481.8	89.41	95.34	119.4	127
F17	7/3/96	481.8	90.45	95.22	129.54	134.62

*Flow rate at standard conditions; 101 kpa and 27°C at sea level.

**Data was not measured.

7.2 Results of Measurements in the Small Angle Diffuser Housing

As listed in Table 7.1, measurements were conducted using 9 different flow rates ranging from 5.68 to 461.8 standard m^3/hr . The initial and final pressure drops across the filter are also listed in the table. As can be seen from the values, the pressure drop does not change more than 7.5 mm of water which is at the highest flow rate with an initial pressure drop of 120 mm of water. The velocity and number density plots for the tests as well as efficiency plots are presented in Appendix B. However, in order to discuss the general trend of the measurements, plots of three sets of measurements (at low, intermediate and high flow rates) are presented in this chapter.

The velocity profiles upstream of the filter are relatively uniform (within the filter area where the velocities were measured). The velocity was lower along the edge rows, grid locations closer to the housing wall. Figures 7.1 and 7.2 present the velocity profiles upstream and downstream of the filter for test F15. The test was conducted on Purolator filter A13192 using 0.966 micron PSL particles. The flow rate was 5.68 m^3/hr . This was the lowest flow rate among the present tests. The average upstream and downstream velocities for this test were 0.203 and 0.328 m/s, respectively. The maximum and minimum velocities downstream the filter were 0.523 and 0.088 m/s, respectively. The minimum velocity was at the corner grid point which is one of the closest points to the housing walls. The maximum and minimum velocities upstream the filter were 0.24 and 0.17 m/s, respectively. The variation in the downstream velocity significantly affected the number densities, because of the velocities were closer to zero as compared to those for the higher flow rates.

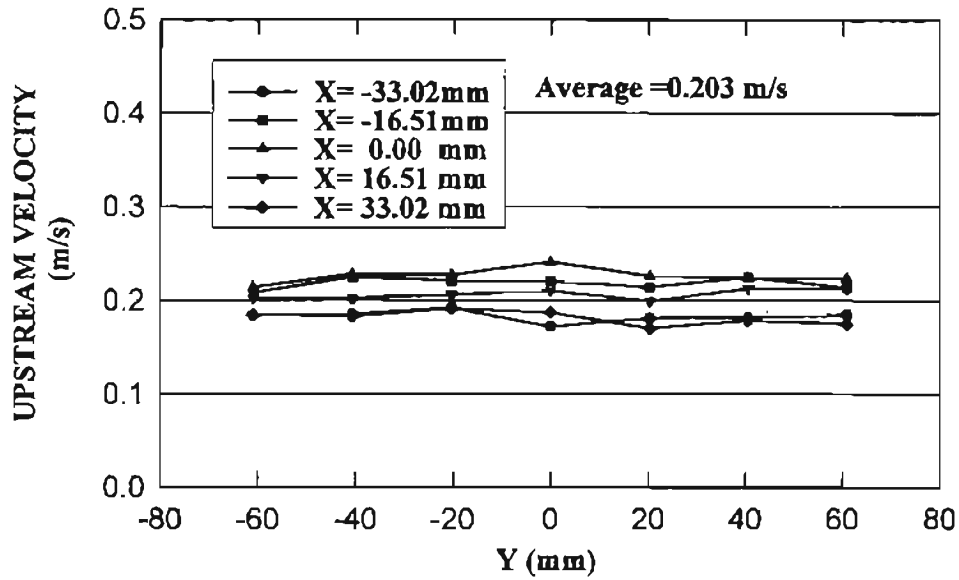


Figure 7.1 Upstream Velocity Profiles for Test F15, Flow Rate = 5.68 m³/hr.

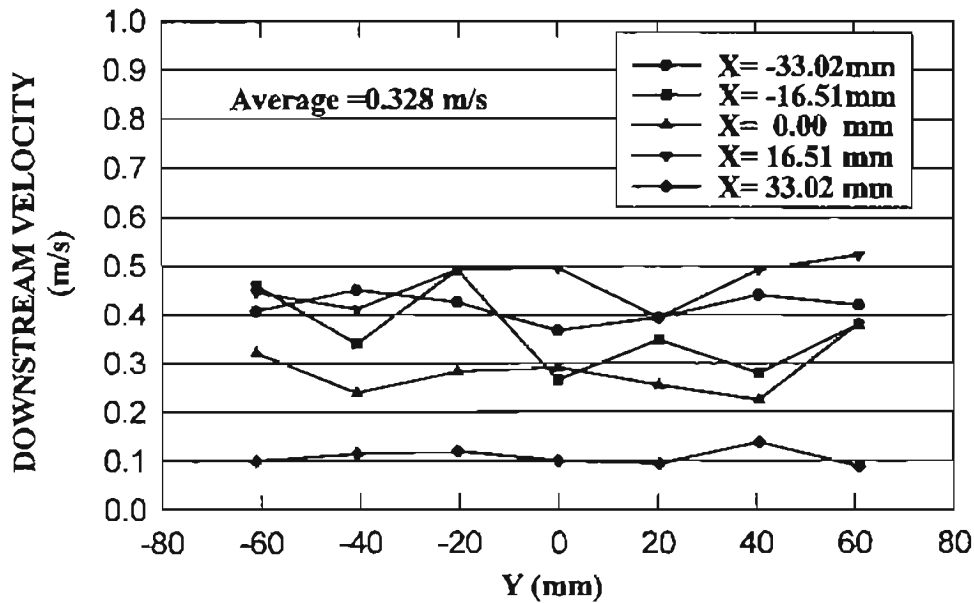


Figure 7.2 Downstream Velocity Profiles for Test F15, Flow Rate = 5.68 m³/hr.

Number density plots upstream and downstream of the filter are shown in Figs. 7.3 and 7.4. Number densities for upstream grid locations as well as downstream grid points, except grid points at $X = -33.02$ mm downstream the filter, were calculated based on the average axial velocity. The number densities for grid points at $X = -33.02$ mm were calculated based on the average of the absolute values of the velocities (the modified SVT method described in Section 5.5).

The upstream number density plots show that the variation in number density was within $\pm 20\%$ of the average number density upstream of the filter. The downstream variation was also about the same. The number density upstream the filter had its greatest value at this flow rate ($5.68 \text{ m}^3/\text{hr}$) as compared to the other flow rates. This was mainly due to the fact that with velocities as low as 0.2 m/s upstream of the filter, a slight change in velocity, like 0.05 m/s , will change the number density by 25% since the velocity was changed 25% .

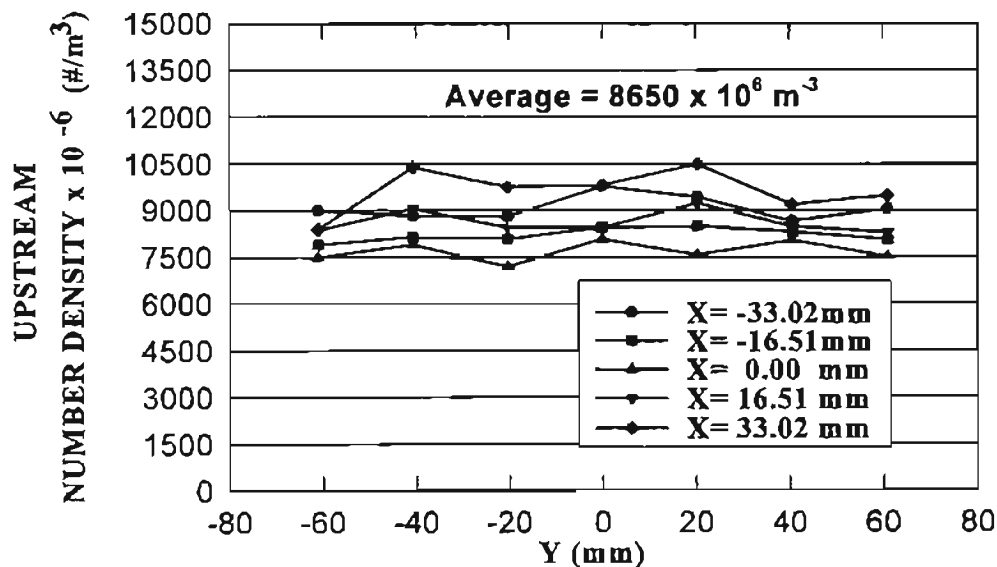


Figure 7.3 Upstream Number Density Plot for Test F15, Flow Rate = $5.68 \text{ m}^3/\text{hr}$.

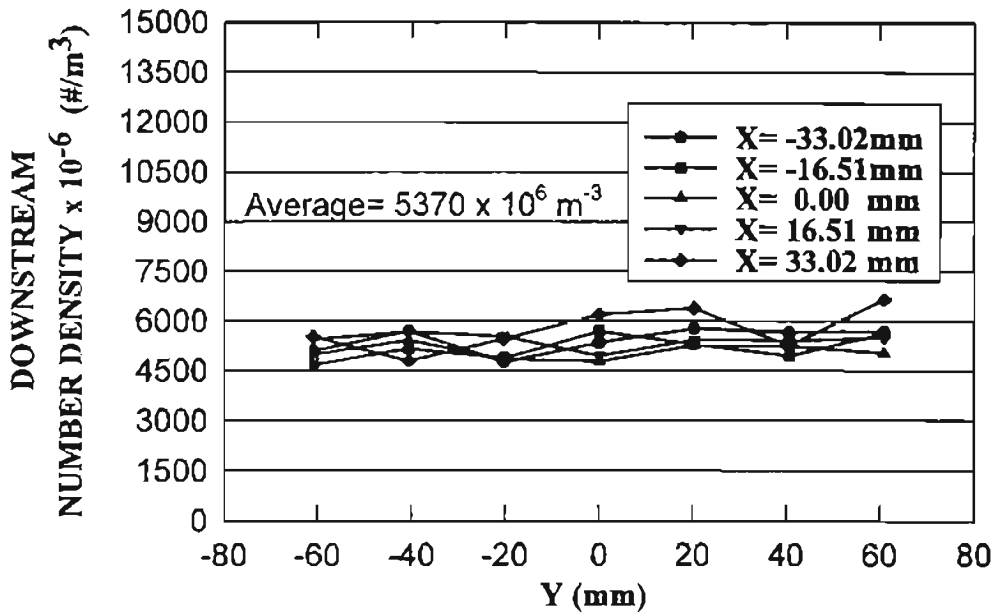


Figure 7.4 Downstream Number Density Plot for Test F15, Flow Rate = 5.68 m³/hr.

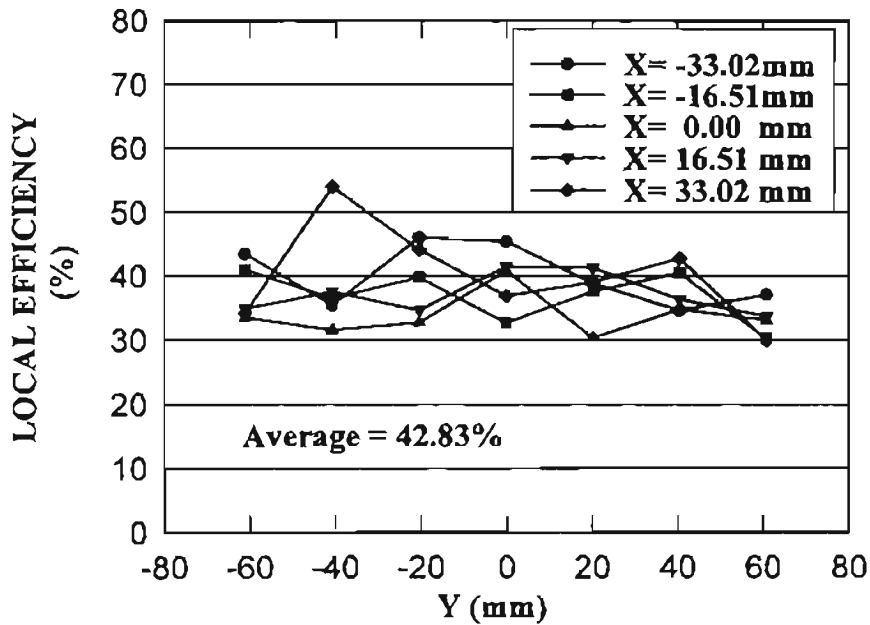


Figure 7.5 Efficiency Plot for Test F15, Flow Rate = 5.68 m³/hr.

For most of the points, the local efficiencies varied from 30% to 50% for this test.

Results of testing with intermediate and higher flow rates show that the local velocities and number densities upstream of the filter were more uniform (relative to the averages at each flow rate). The next series of plots, Figs. 7.5 to 7.10 present the velocities, number densities and efficiency plots for the test conducted at an intermediate flow rate of $187.7 \text{ m}^3/\text{hr}$ (Test F5). The test conditions were the same, 0.966 micron particles with the A13192 filter, and only the flow rate was changed. Results show that the upstream velocity was relatively uniform with a maximum deviation of $\pm 6\%$ from the average. However, the variation of the downstream velocities was more than that of the upstream. As can be seen from Fig. 7.7, the downstream velocities at $X=33.02 \text{ mm}$ were lower than at the other grid points.

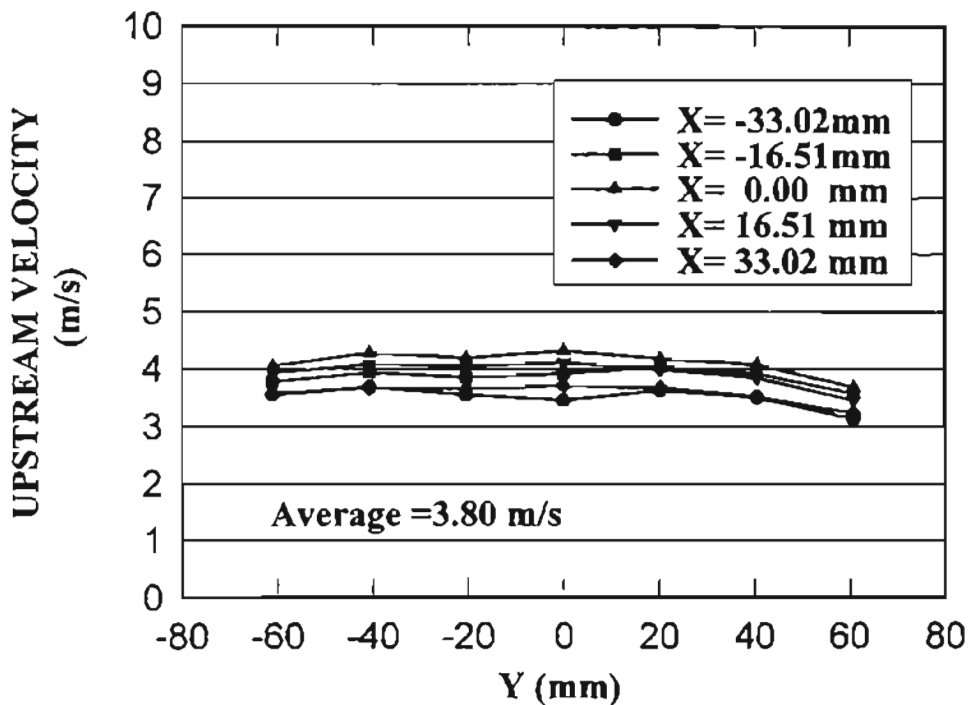


Figure 7.6 Upstream Velocity for Test F5, Flow Rate = $187.7 \text{ m}^3/\text{hr}$.

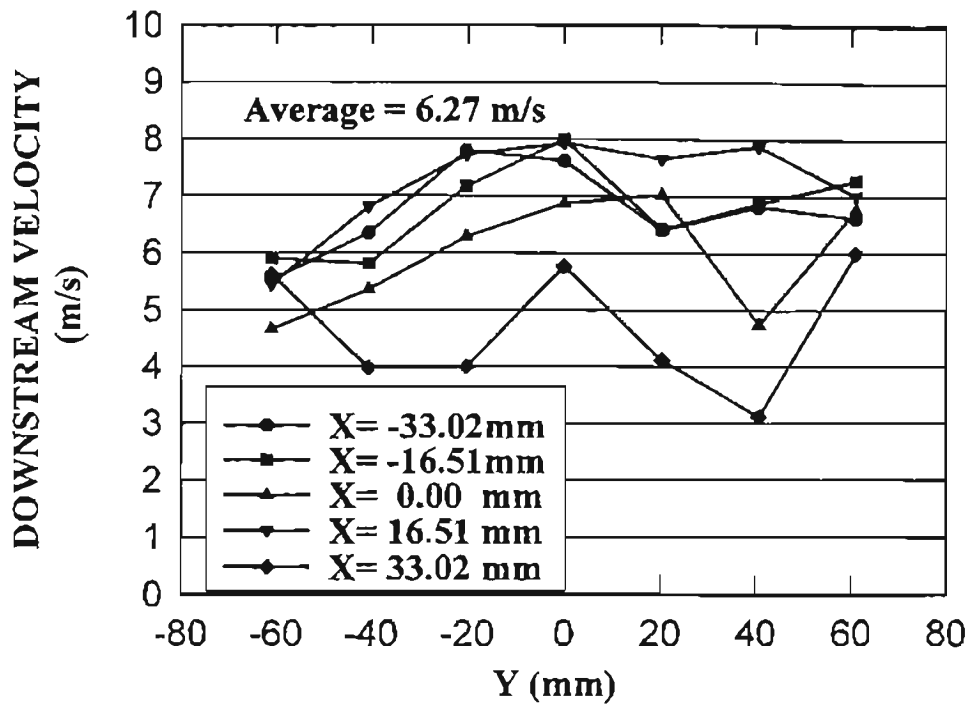


Figure 7.7 Downstream Velocity for Test F5, Flow Rate = 187.7 m³/hr.

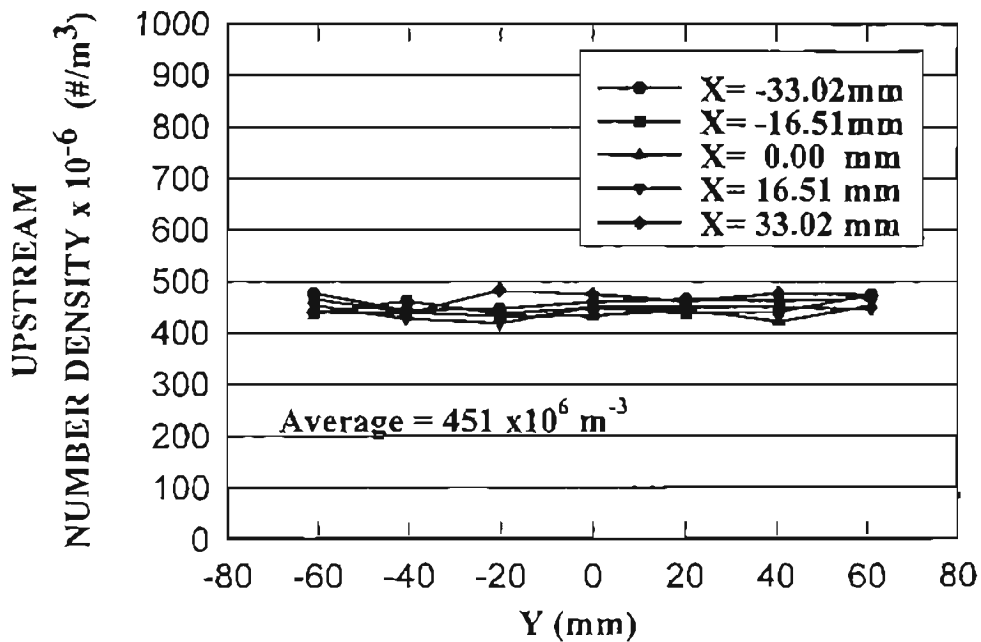


Figure 7.8 Upstream Number Density Plot for Test F5, Flow Rate = 187.7 m³/hr.

These lower velocities for the $X = 33.02$ mm grid points were mainly due to the fact that those grid points were inside the recirculation zone. This symptom is not observed on $X = -33.02$ mm since these points are not in the recirculation zone. Although the grid points are arranged symmetrically with respect to the filter center, the rubber edging on the bottom periphery of the filter is not symmetric with respect to the center of the filter. The edging is also not in a straight line. So it is possible that a single grid point falls into the recirculation zone while the neighboring grid points do not.

The trend in the number densities upstream and downstream of the filter mainly follow the velocity trends. As shown in Figs. 7.8 and 7.9, number densities are more uniform upstream of the filter than downstream. The efficiency plot (Fig. 7.10) shows that the efficiencies remain within a band of 70% to 80 % with the average of 72.56 %. Since the efficiency is defined as a function of upstream and downstream number density ratio, three factors will determine the variation in the local efficiency. These factors are:

- Order of magnitude of the ratio of the downstream number density to the upstream number density compared to one.
- Range of variation of the upstream number density.
- Range of variation of downstream number density.

If the ratio of the number densities (downstream to upstream) is much less than one, say on the order of 0.01, the efficiency will be on the order of 99%. Now if the downstream number density varies by a factor of five from one point to the other and the upstream number density remains on the same order, the ratio will be on the order of 0.05 (versus 0.01) and the efficiency will change from 99% to 95%. It can be concluded that,

in such cases, the variation in the downstream number density will not affect the efficiencies significantly.

Now consider a case for which the number densities upstream and downstream of the filter are close to each other, say the downstream number density is 0.9 that of upstream. The ratio is 0.9 and efficiency is 10%. Using the same reasoning, as for the previous case, a 25% decrease in the downstream number density from one point to another will change the ratio to 0.675. The efficiency will change from 10% to 32.5%. A 25% increase in the downstream number density in this example will result negative efficiencies.

Concluding the above discussion, a larger variation in the local efficiencies is expected for flow rates for which the number densities upstream and downstream of the filter are close together as compared to the case wherein the flow rates are far apart. Measurements show that higher flow rates have higher average efficiencies, which is an outcome of lower number density ratios (downstream to upstream). Therefore, the efficiency variation is less for higher flow rates.

The number densities calculated by the various Swept Volume Techniques (described in Sections 5.4, 5.5 and 5.6) might be quite different. For lower flow rates, the transverse velocities will be closer to the axial velocities, and the one-dimensional Swept Volume Technique for downstream number density calculations might not be as accurate as for higher flow rates. Even calculating the total velocity outside of the recirculation zones could be less accurate. This is due to the fact that the transverse velocities will have positive and negative values (although the axial velocities are not negative). So the best way to calculate the number density accurately is to use the multidimensional SVT,

and measure the total velocity as discussed in Section 5.6. Such measurements are not practical for all grid points because of limited test time. Increasing the test time might allow variation of test conditions such as temperature, flow rate, and most important, the pressure drop across the filter due to plugging, which changes the efficiency.

Figures 11 through 15 present the velocity and number density profiles and efficiencies for test F8. This test was conducted at the same conditions: the A13192 filter, 0.966 micron PSL particles, and a flow rate of 313.75 m³/hr. As can be seen from the figures, number densities upstream and downstream of the filter have more uniform profiles as compared to the 5.68 m³/hr test results.

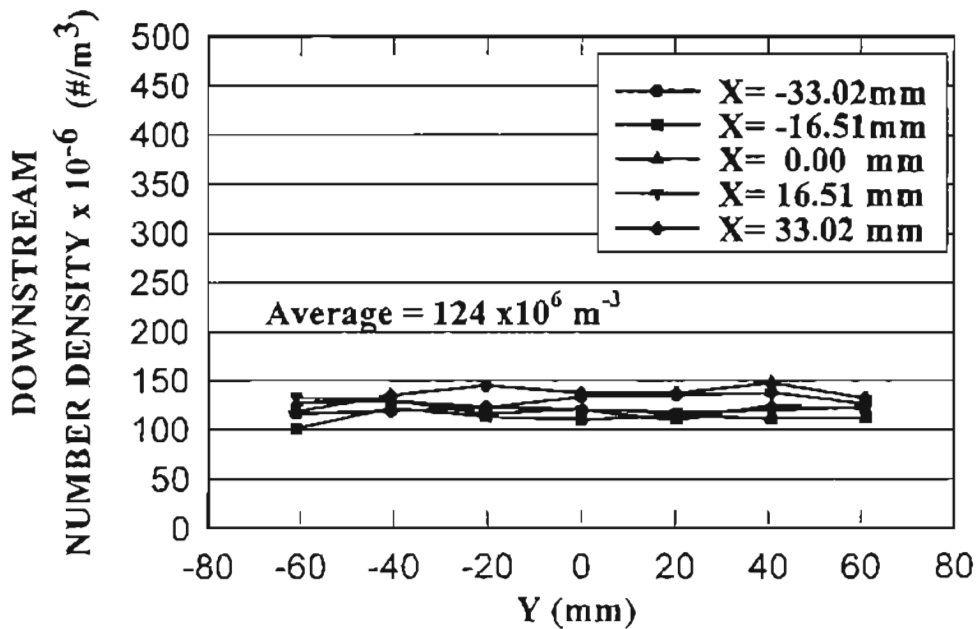


Figure 7.9 Downstream Number Density Plot for Test F5, Flow Rate = 187.7 m³/hr.

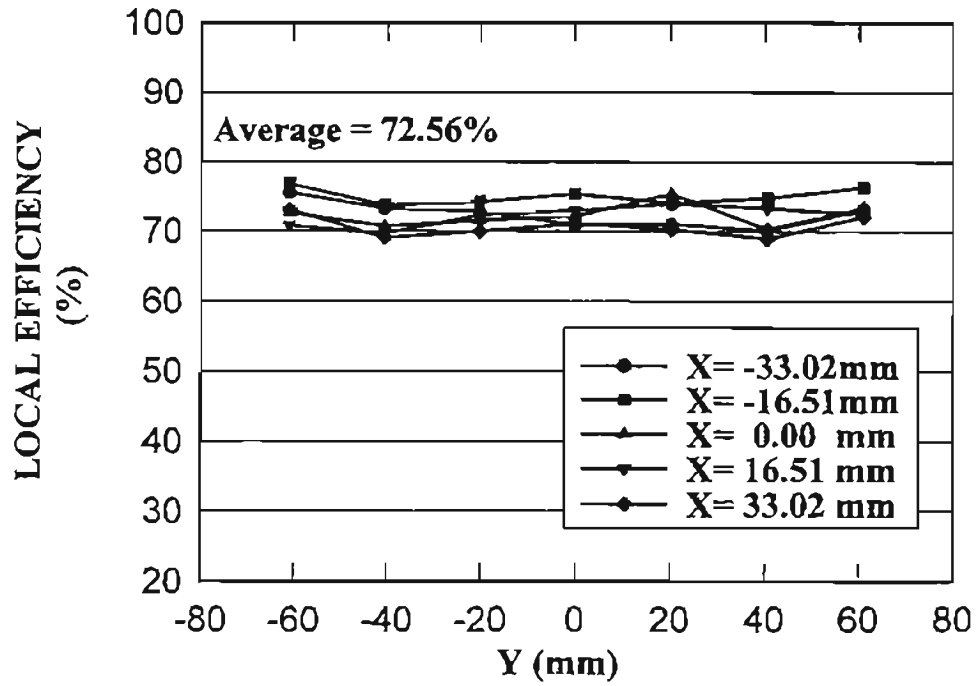


Figure 7.10 Efficiency for Test F5, Flow Rate = 187.7 m³/hr.

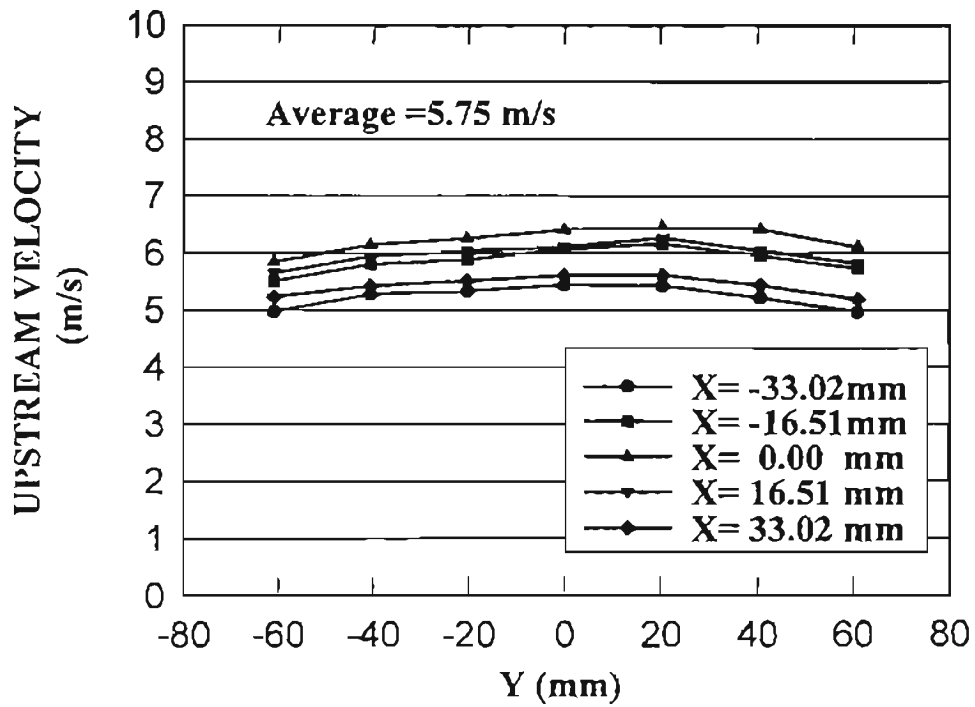


Figure 7.11 Upstream Velocity for Test F8, Flow Rate = 313.75 m³/hr.

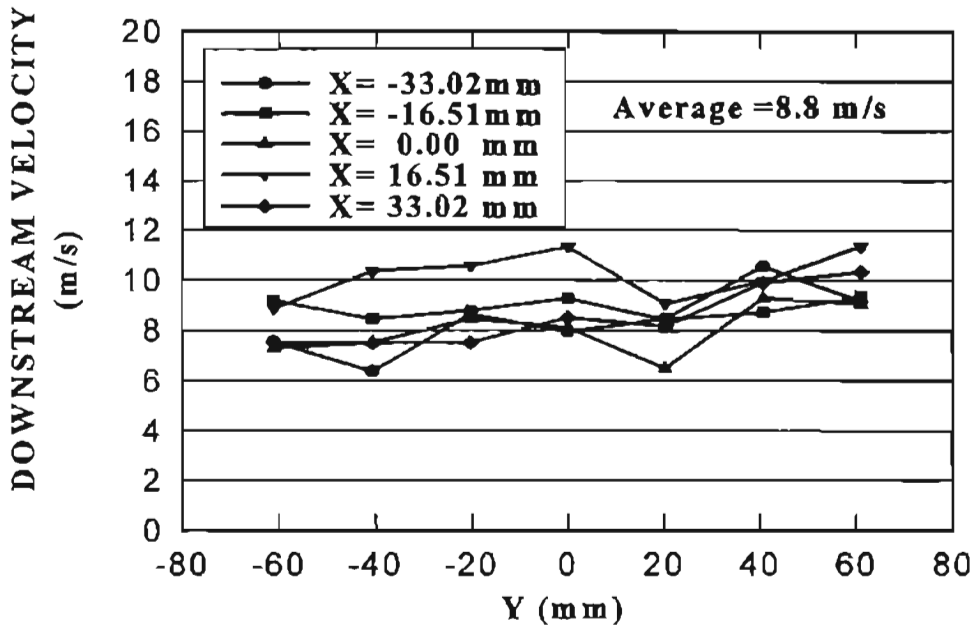


Figure 7.12 Downstream Velocity for Test F8, Flow Rate = 313.75 m³/hr.

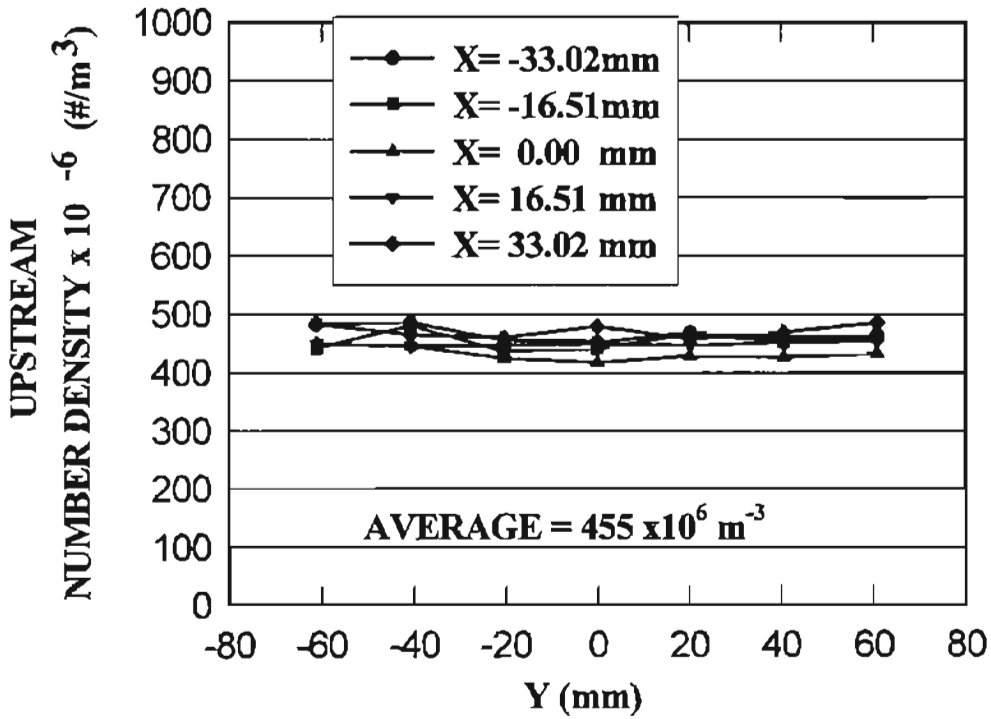


Figure 7.13 Upstream Number Density Plot for Test F8, Flow Rate = 313.75 m³/hr.

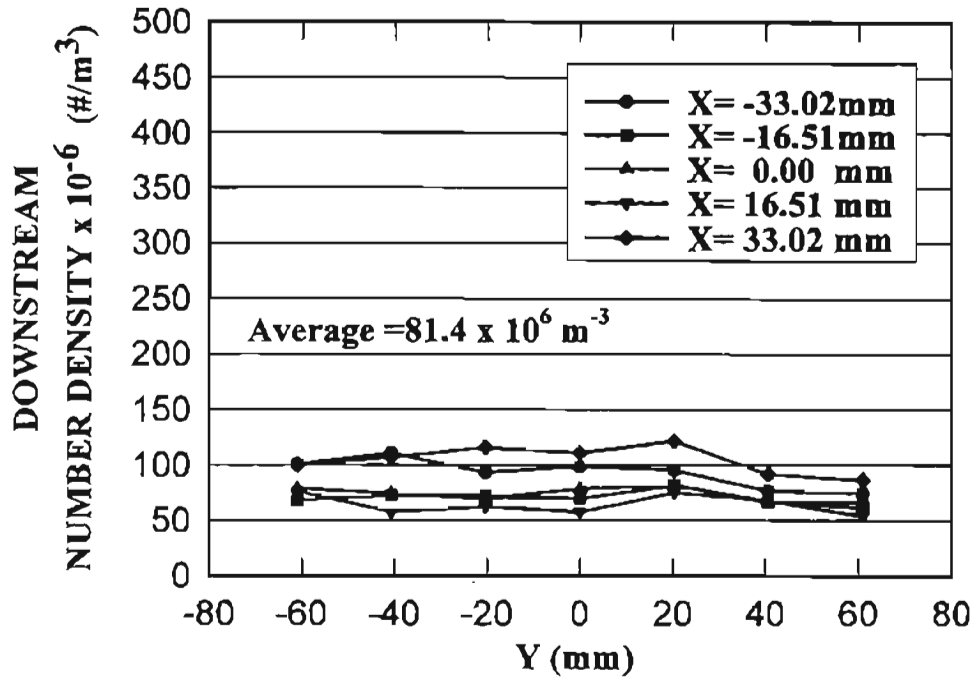


Figure 7.14 Downstream Number Density Plot for Test F8, Flow Rate = 313.75 m³/hr.

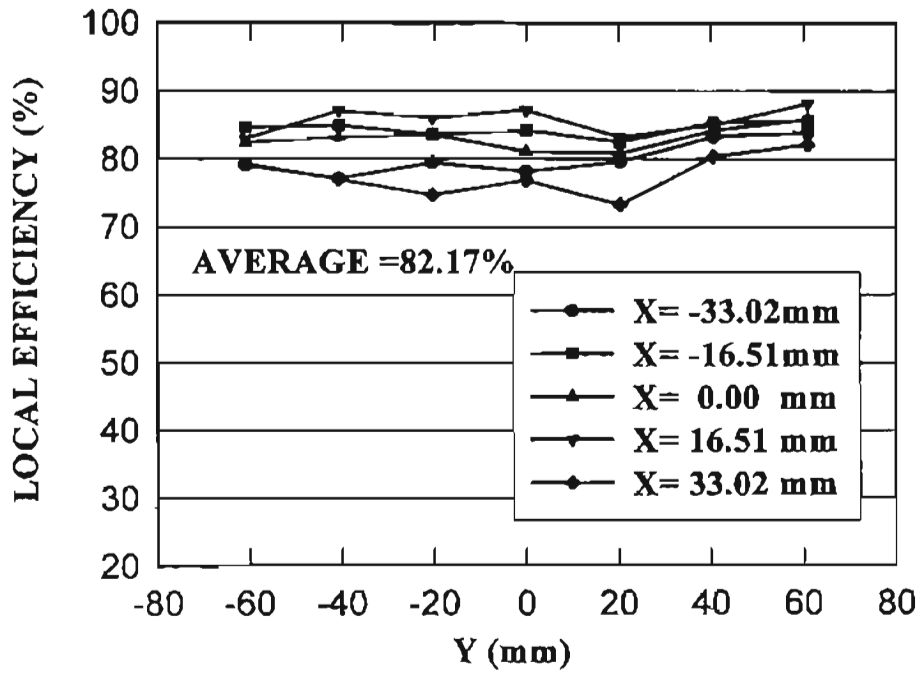


Figure 7.15 Efficiency for Test F8, Flow Rate = 313.75 m³/hr.

7.3 Three Point Measurements

In order to eliminate the effect of recirculation zones, non-uniformity of the different filters used, and other variable parameters which might increase the measurement error, a series of three point measurements were conducted. These measurements were made to achieve the following goals:

- verify the consistency of the whole filter measurements;
- see how accurately a small number of local measurements represent the “whole filter” measurements;
- investigate the effect of the recirculation zones on the overall efficiency;
- have a better picture of the efficiencies in a uniform flow in the central region of the housing;
- compare the results with the theoretical models.

These measurements were made on one filter, at three grid locations, the filter center and the two neighboring points in Y-direction (the long axis of the filter). Measurements were made at different flow rates ranging from 5.68 m³/hr to 649.9 m³/hr. The initial and final pressure drops were also recorded (Table 7.2). The test was conducted in a short period of time. Three measurements were made at each location. The same particles (0.966 PSL) and the same housing (small angle diffuser) were used. The comparison of these results with the whole filter measurements is presented in Fig. 7.16.

As can be seen from the figure, the three point measurements efficiency plot versus the flow rate is a smooth S shaped curve while the total filter measurements

slightly deviate from them. The major difference between the three point measurements and the total filter measurements is due to the fact that the whole filter measurements include some points inside or close to the recirculation zones where the efficiencies are different than in the central region of the filter.

Comparing the efficiency curves of the three point measurements with whole filter measurements, the author believes that the three point measurements efficiencies present the behavior of a clean filter (in a uniform flow) with less error as compared to whole filter measurements. Therefore, the author suggests that the results of three point measurements be used for Stokes number analysis instead of those from whole filter measurements.

Table 7.2 Summary of the Three Point Measurements.

Flow rate (m³/hr)	Efficiency (%)	Initial pressure drop (mm Water)	Final Pressure drop (mm Water)
2.5	29	0.5	0.5
5.7	29.2	1	1
29.5	27.8	1.9	1.9
53.3	28.3	4.1	4.1
77.1	30.1	6.1	6.1
103.7	33.3	10.4	10.7
145.7	40.9	14.2	14.2
187.7	49.6	21.1	21.1
229.7	62.2	30.5	30.5
280.1	79.6	42.9	43.4
313.8	83.4	50.0	51.3
397.8	92.1	76.2	76.7
481.8	92.1	105.9	107.2
649.9	95.1	180	186.7

The author believes that the difference between the overall efficiencies of the whole filter tests and three point measurements at low flow rates (or low Stokes numbers), is mainly due to the errors in the calculation of downstream number density at grid locations other than central region. The error is introduced by choosing an average velocity (calculated based on one-dimensional SVT) which is different than the actual average at grid points other than central region. The overall efficiencies averaged over 15 grid locations at the central region of the filter are listed in Table 7.1. These efficiencies are compared with the whole filter average efficiencies in Appendix H. Note that the error could be also due to the effect of the diffusion mechanism which was neglected. As stated earlier, it is not possible to use multi-dimensional SVT at all grid points (due to limited test time).

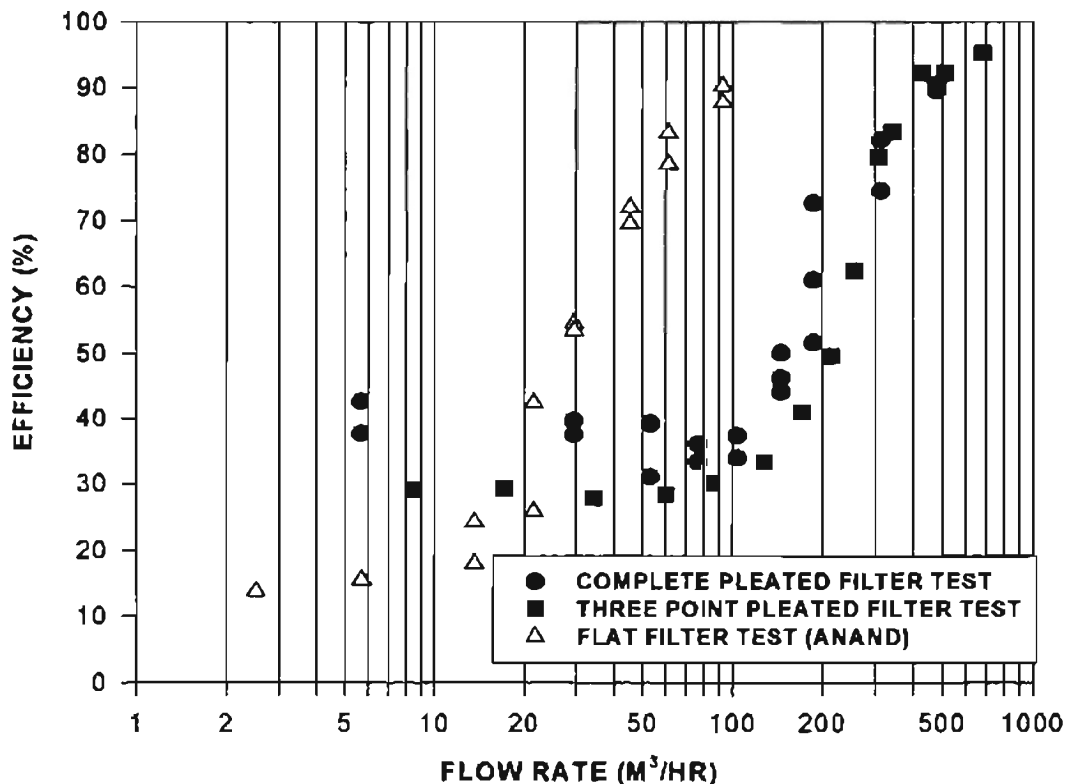


Figure 7.16 Comparison of the Filter Efficiencies.

7.4 SAE Housing Measurements

Local efficiency measurements were also conducted in the SAE J726 test housing. These measurements were conducted at three different flow rates, low flow rate ($61.2 \text{ m}^3/\text{hr}$), intermediate flow rate ($187.7 \text{ m}^3/\text{hr}$) and high flow rate ($313.8 \text{ m}^3/\text{hr}$). Typical plots of the upstream and downstream velocity profiles as well as the efficiency plot are shown in Figs. 7.17 to 7.21 (for a flow rate of $187.7 \text{ m}^3/\text{hr}$). Plots for two other flow rates (61.2 and $313.75 \text{ m}^3/\text{hr}$) as well as summary of the SAE housing tests are presented in Appendix C.

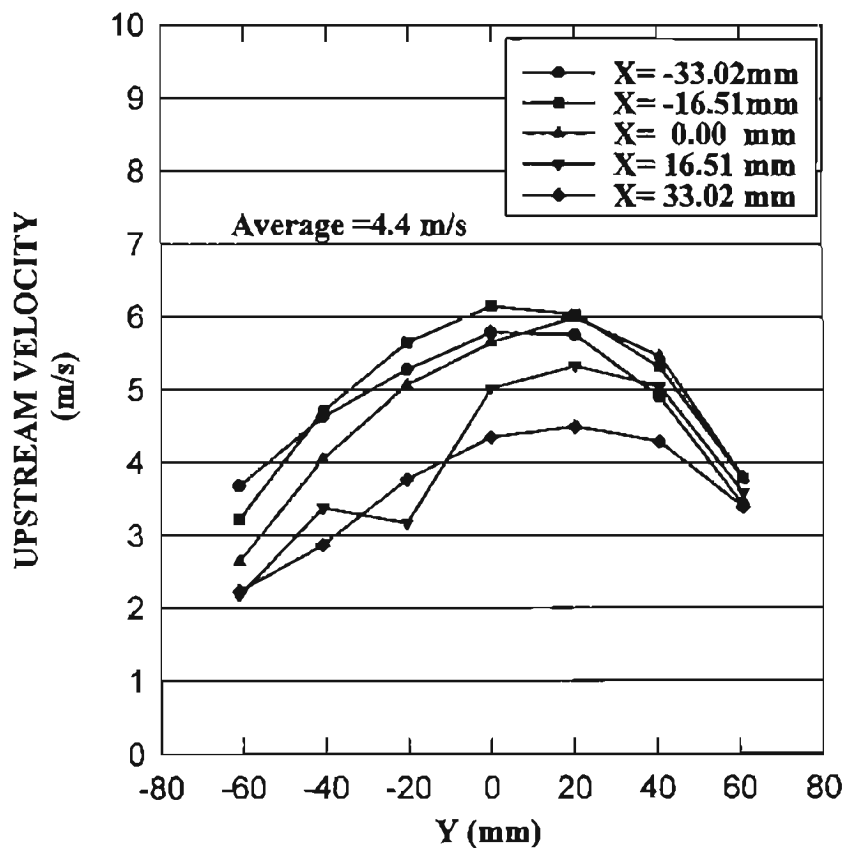


Figure 7.17 Upstream Velocity for Flow Rate = $187.7 \text{ m}^3/\text{hr}$, SAE Housing.

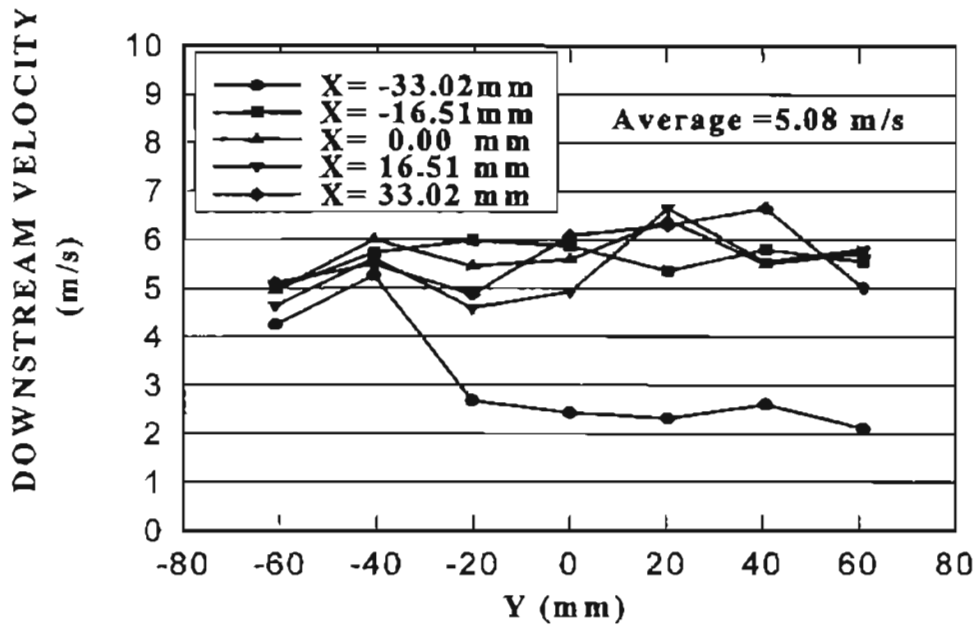


Figure 7.18 Downstream Velocity for Flow Rate = 187.7 m³/hr, SAE Housing.

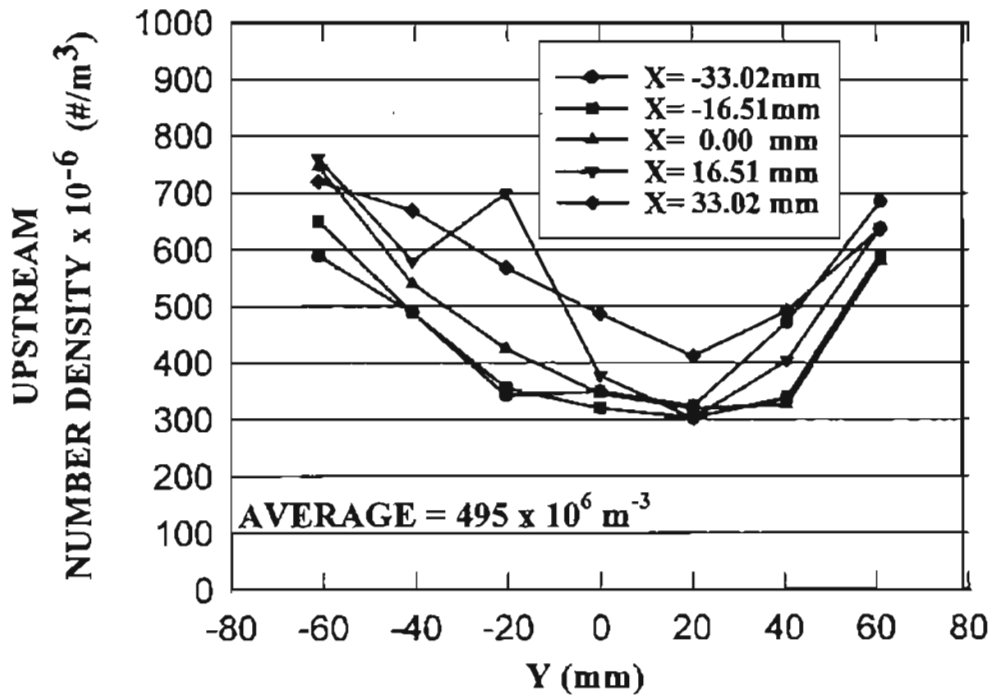


Figure 7.19 Upstream Number Density Plot for Flow Rate = 187.7 m³/hr, SAE Housing.

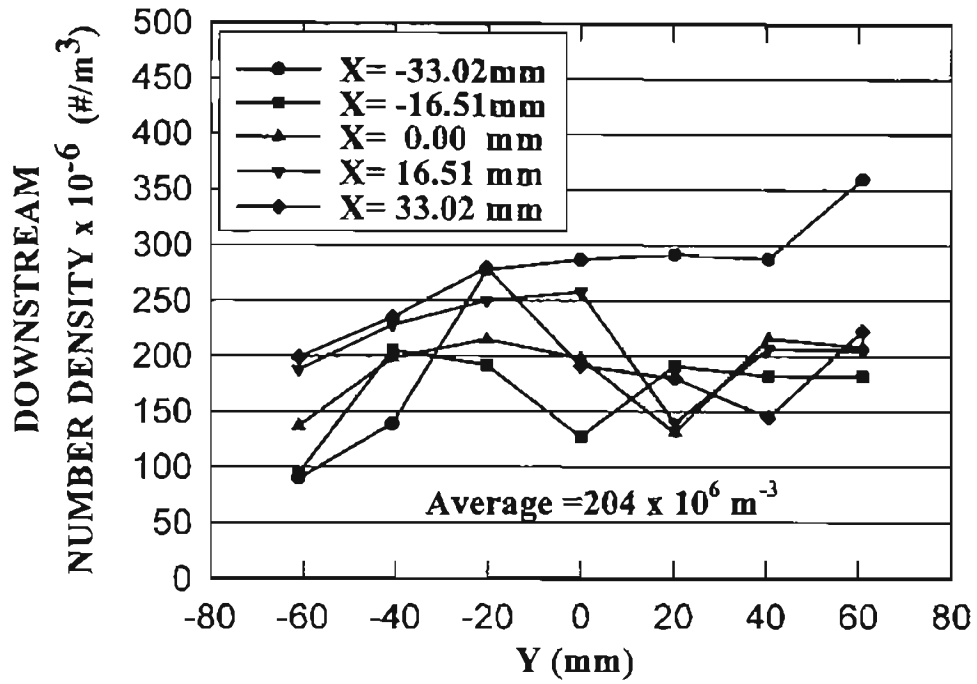


Figure 7.20 Downstream Number Density for Flow Rate = 187.7 m³/hr, SAE Housing.

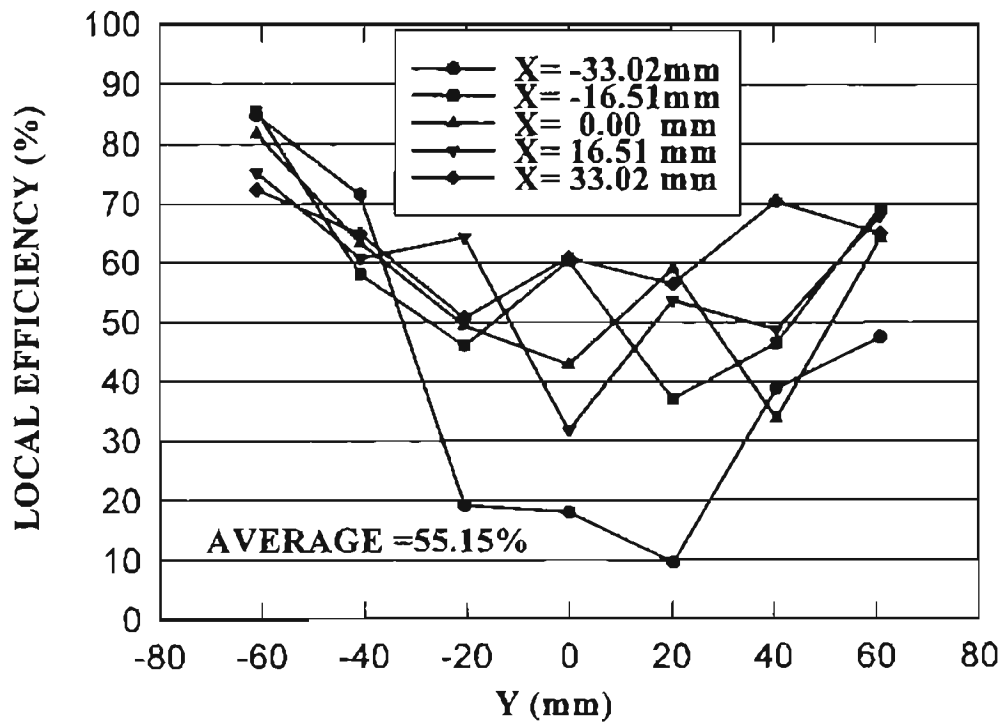


Figure 7.21 Efficiency for Flow Rate = 187.7 m³/hr, SAE Housing.

7.5 Comparison of Results with Previous Studies

The current measurements are compared with previous theoretical and experimental data in this section.

7.5.1 Comparison with Theoretical Models

Results of the present measurements and calculations are compared with the theoretical studies in this section.

7.5.1.1 The Single Fiber Efficiency

The single fiber efficiencies were calculated using Eq. (2-2) with different packing densities and the filter thickness of 700 microns (thickness suggested by Duran [1995]). Two different packing densities were used: a value of 0.345 which was suggested by Duran and a value of 0.153 which was calculated based on the following modeling.

Assuming that the pleated filter behaves like a flat filter with an area equal to its unfolded area, the volume of the filter paper is:

$$V_{FF} = T_{FF} A_{FF} \quad (7-1)$$

where

$$A_{FF} = 19.3 A_{PF} \quad (7-2)$$

The total volume occupied by the filter is:

$$V_{PF} = A_{PF} H_p \quad (7-3)$$

In the above equations, T_{FF} is the filter paper thickness, H_p is the pleat height, V_{FF} and V_{PF} are the volume of the filter paper (flat filter) and the pleated filter, respectively,

and A_{PF} and A_{FF} are the pleated filter area and the area of the unfolded filter. The volume fraction of the filter paper will be V_{FF}/V_{PF} , and the packing density will be the ratio multiplied by the packing density of the flat filter. Calculating the final packing density:

$$C = 0.345 \frac{V_{FF}}{V_{PF}} = 0.345 \frac{T_{FF}(19.3A_{PF})}{A_{PF}H_p} = 0.345 \frac{(0.7)(19.3)}{30} = 0.153 \quad (7-4)$$

This packing density is calculated based on the concept that the pleated filter could be replaced by a flat filter (with the above packing density) and have the same total efficiency as the pleated one at different flow rates. The thickness of the imaginary flat filter is not considered as the pleat height since the flow passes through the filter paper once.

As shown in Fig. 7.22, the pleated filter is modeled with a low packing density flat filter at each pleat cross-section (the dashed line in Fig. 7.22a) with a thickness equal to the filter paper thickness. It is not modeled as in Fig. 7.22b, in which the filter thickness is equal to the pleat height since the flow is not filtered through such thick media. Figure 7.23 presents the single fiber efficiencies based on two different packing densities. The single fiber efficiencies were calculated by Eq. (2-2), using total efficiencies obtained from three point measurements in the small angle diffuser housing. The calculated values are plotted versus Stokes number. The Stokes number is calculated based on Eq. (2-3) and the average velocity inside the housing (duct velocity) since the pleated filter is modeled as a flat filter, with the same area as if a flat filter was placed inside the housing, but with reduced packing density. Results are compared with Sabnis' single fiber efficiency model. As can be seen from the model, the single fiber efficiency of the current three point measurements match better with the Sabnis prediction for

packing density of $C = 0.153$, where the Stokes number calculations are based on duct velocity.

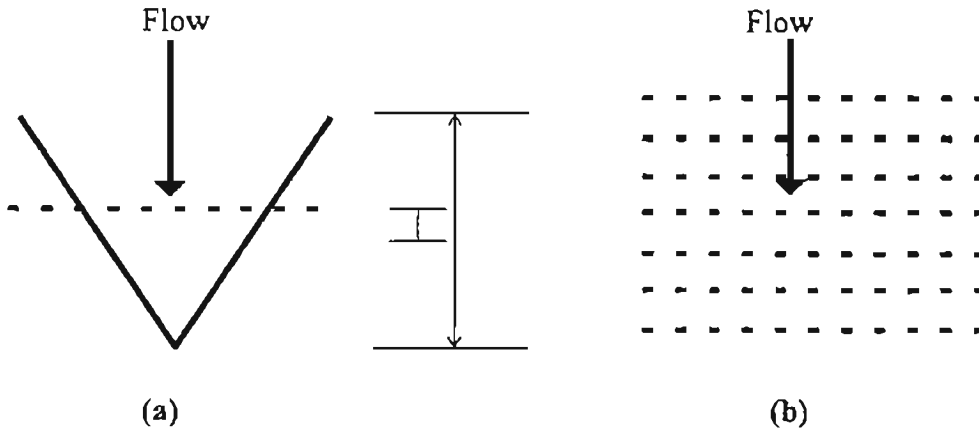


Figure 7.22 Pleated Filter Modeling with Different Thicknesses,

a) Filter Paper Thickness, b) Pleat Height Thickness.

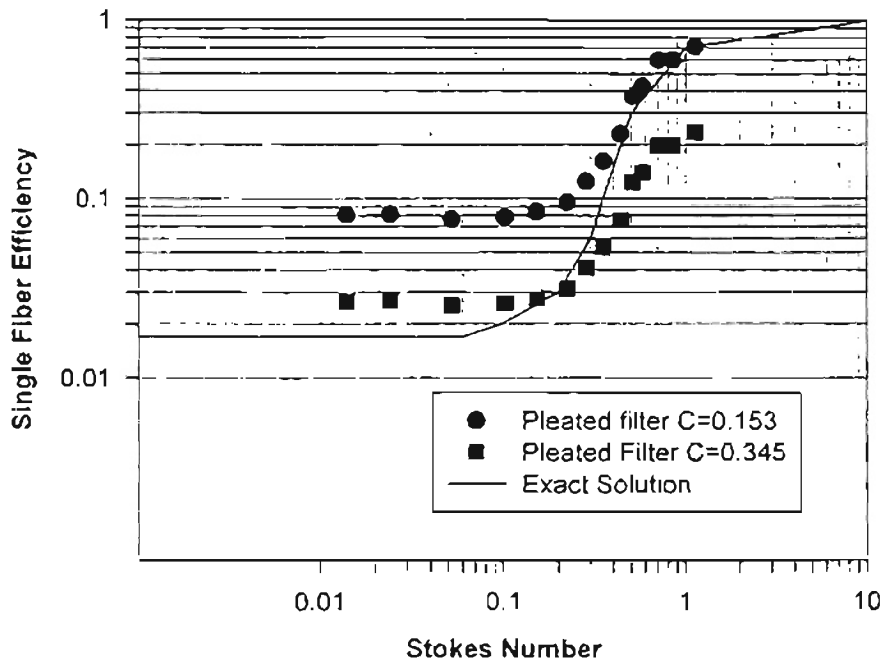


Figure 7.23 Comparison of Single Fiber Efficiencies.

Filters with different packing densities will have different efficiencies at a specific flow rate. However, the single fiber efficiency should be the same if all other conditions except the packing density (such as approach velocity, etc.) should be the same. Therefore, as suggested by Lee [1977], the total efficiencies of the two different filters (even with the same fiber diameter) could not be compared. Also, the analysis of the variation of the efficiency with Stokes number is not meaningful if the single fiber efficiency is not calculated. Anand [1997] has plotted the measured efficiencies over a flat filter versus the Stokes number. His results show that the S shaped efficiency curves appears at very low Stokes numbers. His results are shown in Fig. 7.16. As can be seen from the figure, the flat filter efficiencies at most of the grid points have the same trend as the present measurements but they are shifted by an approximate factor of 4 to the left.

7.5.1.2 Comparison of Results with Duran's Model

Duran [1995] has predicted the overall efficiency of an A13192 pleated filter. His model gives an average efficiency of 0.25% for a flow rate of 204 m³/hr using a packing density of 0.235 and 0.966 micron PSL particles. However, efficiencies calculated based on his model for 2.5 micron particles, a packing density of 0.345, and a fiber diameter of 51.75 are close to the current measurements. Figure 7.24 presents the average efficiencies versus upstream velocity. Since the fiber diameter, air viscosity and particle density are constant, the Stokes number will be a function of the velocity only. As can be seen from the figure, the efficiencies of the current measurements have the same trend as predicted by Duran's model. However, since Duran's model is based on 2.5 micron particles, the Stokes numbers for the current measurements will be 6.25 times smaller

than the corresponding values of Duran's model (considering the same fiber diameter). In other words, plotting the efficiency curve versus the Stokes number, the present measurements should be shifted to the left by factor of 6 as compared to Duran's efficiencies. The local efficiencies calculated by Duran's model using one micron particles were less than 5% for intermediate flow rates (204 m³/hr) [Duran, 1995]. The author was not able to explain the significant difference between the present measurements and the local efficiencies which were calculated by Duran's model.

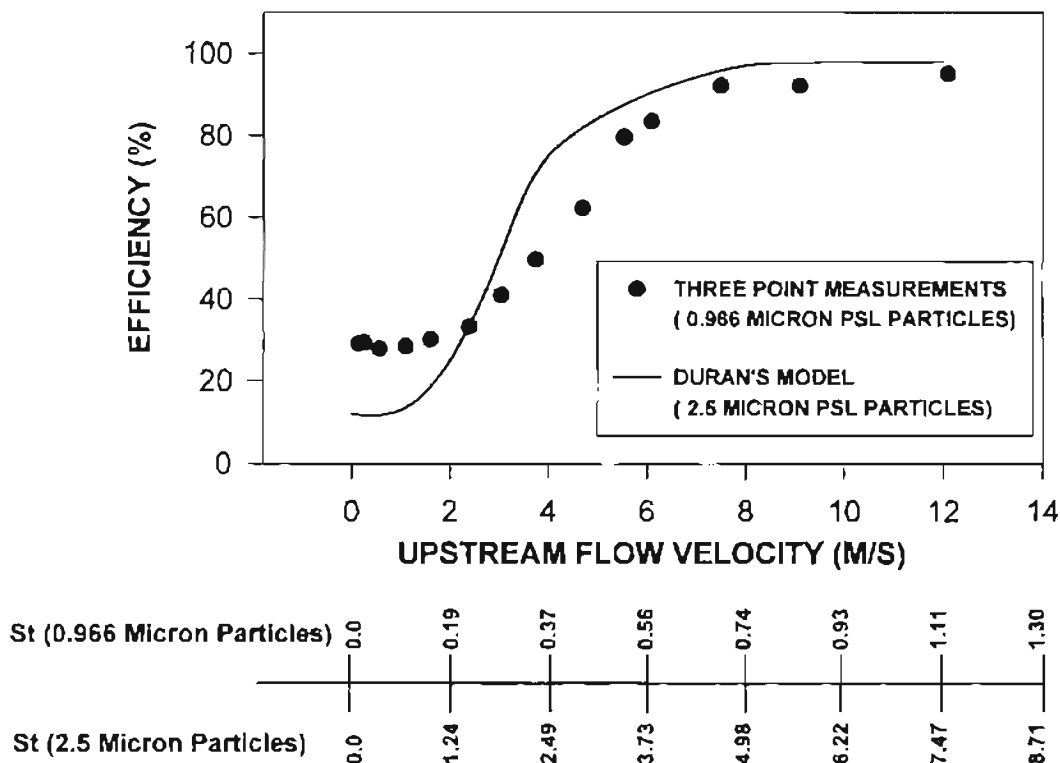


Figure 7.24 Comparison of Efficiencies with Duran's Model.

7.5.2 Comparison with Experimental Data

Anand [1997] has conducted similar measurements on flat filter media. His results are compared with the three point measurement efficiencies in Fig. 7.16. As can

be seen, the current measurements show the same trend provided that the pleated filter curve is shifted to the right by a factor of 4 approximately.

Natarajan [1996] has conducted similar tests on the pleated filters. However, because of variation in the system parameters and small efficiencies in the recirculation zones (calculated based on one-dimensional SVT), his results show a variation in efficiency between 25% and 79%. The upstream velocity profiles and number densities were not as uniform as for the current measurements. Figure 7.25 presents the present whole filter measurements as well as Natarajan's results.

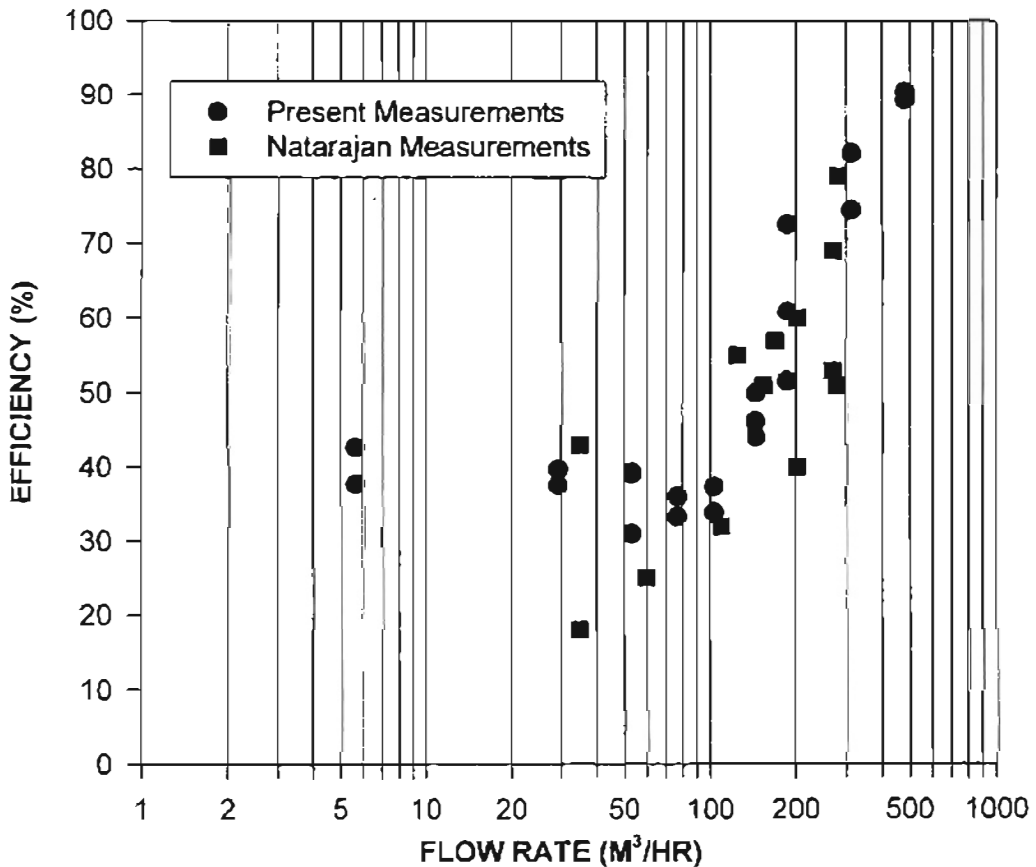


Figure 7.25 Comparison of Present Measurements with Natarajan Measurements.

By comparing the present pleated filter measurements in two different housing, it can be concluded that the average efficiencies obtained from measurements in the two different housings at the same flow rates are close to each other. However, the upstream velocity profile in the SAE housing is not as uniform as for the small angle diffuser upstream velocities. In the SAE housing, the peak upstream velocity is at the center and velocity reduces substantially at the edges. The number density profile is inverted as compared to the velocity pattern in the SAE housing. The downstream velocity profiles are different as well. In the SAE housing, because the flow is exiting at the side of the housing, there is a relatively large recirculation zone on the opposite side of the exit duct (downstream) where the velocities are lower. This situation does not exist in the small angle diffuser housing where the flow is exiting at the center of the lower part of the housing.

7.6 The Stokes Number Analysis

As stated earlier, it is common to plot the single fiber efficiencies based on the Stokes numbers. Stokes numbers are calculated based on Eq. (2-3). Liu and Lee [1982] suggested that the velocity used for the Stokes number calculation should be the ‘undisturbed velocity’. For flat filter media, this velocity is equal to the duct velocity. For pleated filter, two different velocities may be used:

- the duct velocity or the velocity obtained by dividing the flow rate by the duct area; or
- the face velocity, which is the velocity calculated by dividing the flow rate by the total unfolded filter area.

Knowing that the pleats of the A13192 filter are such that the total unfolded filter area is 19.3 times larger than the duct area, the calculated face velocity will be 19.3 times lower than the duct velocity. Such velocities will give smaller Stokes numbers.

As stated earlier, comparing the efficiency curves of the flat and pleated filter, it was concluded that the curves will match if the pleated efficiency curves are shifted by a factor of about four (i.e., the flow rates should be multiplied by 4). In other words, if the filtration mechanisms are identical on pleated and the flat media for a given efficiency value:

- the available filtration area is 19.3 times greater than that of the pleated filter, but this area is not normal to the flow;
- considering the same efficiencies, the calculated Stokes number for the pleated filter is about four times larger than that of the flat media (based on duct velocity).

The following conceptual models are introduced to justify these observations. These models were not proven, are discussed in a qualitative manner, and need to be explored in the future. They are based on the observations and findings of the current measurements as well as Anand's results on flat media. However, they might be used as a guide for future study and investigation.

These models are based on the fact that there is a velocity profile distribution along the pleats which is neither the duct velocity nor the face velocity.

1) The Velocity Profile Concept

According to Chen et al. [1994], there is a velocity distribution profile along the pleats and the velocity of the air approaching the filter paper is different at different cross-sections, but they did not discuss the trend of the distribution (increasing or decreasing along the pleat) in their paper. It is the authors belief that the effective velocity for comparison with flat filter media shall be the integrated average of the normal velocities along the pleats. This velocity (the effective velocity) is neither the duct velocity nor the face velocity. Based on the current measurements, the order of the effective velocity is four times less than the duct velocity, or five times more than the face velocity.

2) The Flat Filter Model with Variable Packing Density Concept

According to Liu and Lee [1982], the velocity of the air flow before entering the pleats should be used for Stokes number calculation. Therefore the pleated filter may be modeled as a flat filter, with a thickness equal to the filter paper. In this case, the duct velocity will be the proper velocity for the Stokes number calculation. This model was described in Section 7.3.1 of this chapter. As can be seen from Fig. 7.23, the single fiber efficiencies calculated based on this model fairly matches with the exact solution calculated by Sabnis [1993].

3) The Pressure Drop Concept

Perhaps this is the most practical concept as compared to the previous ones. Anand's results [1997] and present measurements indicate that the same initial pressure drop across the pleated and flat filters will result in the same efficiencies. Note that, in order to get the same initial pressure drop across the pleated and the flat media, different flow rates should be used. Since the filter material is the same for both the flat and

pleated filters, and the efficiency is a function of the pressure drop across the filter (which depends on the flow rate), the pleated filter in a specific air flow rate could be modeled as if it were a flat media in a different flow rate which has the same pressure drop as the pleated filter. In other words, the effective velocity for Stokes number calculation for a pleated filter is the duct velocity over the flat media which gives the same initial pressure drop as that of the pleated filter. Figure 7.26 presents the current measured efficiencies as well as efficiencies measured by Anand [1997] for the flat media as a function of the initial pressure drop. It should be noted that the local efficiency values obtained by Anand are lower at the central region and higher at the areas further away from the center. Anand has suggested that such a difference is mainly due to filter plugging, since he started his measurements from the center of the filter and worked toward the outer edges. Therefore, the flat filter efficiencies shown in Fig. 7.26 might be slightly higher than the actual values of the clean filter efficiencies.

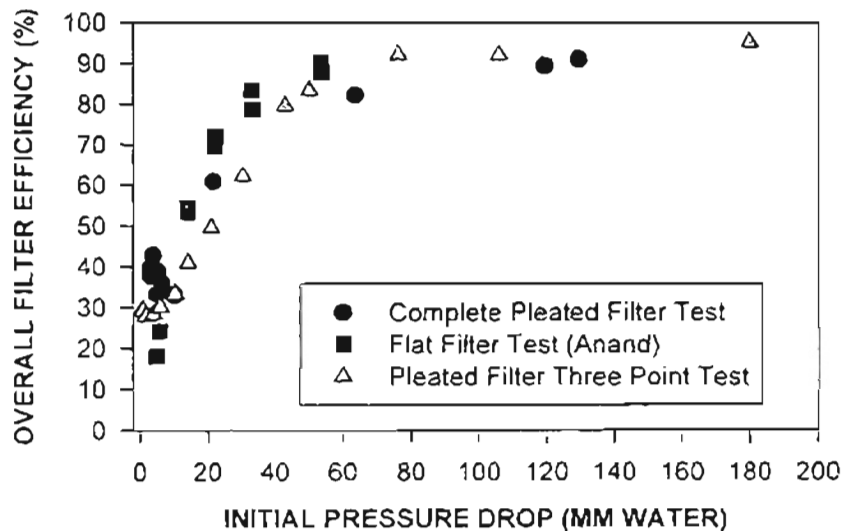


Figure 7.26 Efficiency Versus Initial Pressure Drop for Flat and Pleated Filters.

CHAPTER VIII

CONCLUSIONS

8.1 Summary

The results of the present measurements and the comparisons are summarized in this section:

- The local efficiency of the pleated filters is relatively uniform across the filter except in the recirculation zones (Section 7.1).
- Different Swept Volume Techniques should be used for calculation of the downstream number densities at different areas. Methods described in Section 5.4 (one-dimensional SVT with velocities in the same direction) should be used at the central regions and SVT methods described in Sections 5.5 and 5.6 should be used along the edge rows where the axial and transverse velocities are on the same order (Section 5.6) or the axial velocities of the detected particles have both positive and negative values (Section 5.5).
- Overall efficiency plots versus the Stokes number for pleated filters may not be conclusive since the velocities of the particles approaching the filter paper (between the pleats) are not precisely known (Section 7.4).

- Only single fiber efficiencies of flat and pleated filters can be compared to each other (not the overall efficiencies), when they are plotted versus the Stokes number. Filters with different packing densities will behave differently under similar test conditions and will have different efficiency curves. The differences can be seen when the overall efficiencies are plotted versus the Stokes numbers. However, the single fiber efficiencies should be the same if the fiber diameter and the testing conditions are identical (Section 7.3.1).
- In the reviewed literature (such as Harrop and Stenhouse [1969]), variation of the single fiber efficiency versus the Stokes number is with constant particle Reynolds number (by maintaining the multiplication of the particle diameter and its velocity constant, the particle Reynolds number will remain constant, see Fig. 2.5).
- The present measurements suggest that the integrated average velocity of the flow approaching the filter pleats is on the order of 20 % of the duct velocity.
- The same initial pressure drop across the pleated and flat media will result in very similar efficiencies. In order to have the same pressure drop across the A13192 pleated filter and the flat filter media, the flow rate for the pleated filter has to be approximately four times that of the flat filter flow rate.
- By choosing the optimum system parameters, the errors in calculated number densities can become on the order of $\pm 5\%$ or less (for grid points in the central region of the filter).

8.2 Recommendations for Future Work

The following recommendations may improve the quality of the future measurements:

- Improvement of the test setup equipment. The SAE and the small angle diffuser housings should be rebuilt and tested for leaks. The present housings have some cracks on the connecting flanges. Although these cracks were repaired and sealed, new housings will be more reliable for future measurements. Flow and pressure measurements should be automatically taken from the computer. The pressure drop measurements should have a better accuracy, with a maximum error of one millimeter of water, in order to investigate the variation of the pressure drop across the filter more accurately (both the present measurements and Anand's [1997] results indicate that the pressure drops across the clean filter for flow rates less than $30 \text{ m}^3/\text{hr}$ are on the order of 1 mm of water or less).
- More research may be needed in order to find the actual velocity profile of the flow approaching the pleats. Velocity measurements inside the pleats for filters with different pleat counts, height and/or material are needed.
- Efficiency measurements for different particle sizes are needed in order to vary the Stokes number (over a greater range) by changing the particle size and compare the elemental efficiencies with available data in the literature. Also efficiency measurements with combinations of different particle sizes should be conducted.
- More research is needed for improvement of the Swept Volume Technique. If possible, a computer code should be written in order to extract velocities of a large

number of samples individually (from DSA output files), in order to calculate the average velocity more accurately.

- The temperature of the flow approaching the flow meter should be measured in order to avoid errors in flow rate measurements. The thermometer should be installed close to the TSI flow meter so that the temperature of the air flow (whose volumetric flow rate is being measured by TSI) can be recorded.
- Constant ambient temperatures should be used during each test in order to keep the power of the laser beams coming out of the transceiver constant.
- Dust measurements should be conducted. The Wright dust feeder should be used for seeding the dust particles. SAE fine dust is recommended for starting the dust measurements. The downstream number densities should be measured first in order to minimize the effect of filter plugging and time dependent variation of the filter efficiency. The author was not successful in conducting measurements with dust particles because the filters plugged early after starting the test.
- Complete measurements in the SAE housing at more flow rates with one micron particles as well as larger size particles (such as 5 micron) are needed. Measurements should be repeated so that the reliability of the measurements can be verified.
- Investigation of the velocity profile along the pleats using CFD models is recommended. Also, experiments should be conducted in order to measure the velocity along the pleats (at different cross-sections). A pleated filter from flat sheet filter paper should be constructed (with a pleat angle larger than that of the A13192 pleated filter), so that the velocity can be measured along the pleats.

REFERENCES

- Aerometrics (1992), Doppler Signal Analyzer for Phase Doppler Particle Applications User's Manual, Sunnyvale, CA, draft 2.
- American Society for Testing and Materials (1989), "ASTM F 1215-89, Standard Test Method for Determining the Initial Efficiency of a Flatsheet Filter Medium in an Airflow Using Latex Spheres," Annual Book of ASTM Standards, Vol. 14.02, Philadelphia, PA.
- Anand, S. (1997) "Filtration Efficiency Measurements on Flat Sheet Filters," M.S. Thesis, School of Mechanical and Aerospace Engineering, Oklahoma State University, Stillwater, Oklahoma.
- Anand, S., Jadbabaei, F. M. and Dougherty, R. L. (1997), "Comparison of Filtration Efficiency Measurements for Pleated and Flat Sheet Filters," presented at the 1997 SAE International Congress and Exposition, SAE Technical Paper #970671, (SP-1252), SAE, Inc., Warrendale, PA.
- Benedict, R. P. (1984), Fundamentals of Temperature, Pressure, and Flow Measurements, Third Edition, Wiley-Interscience, New York.
- Brown, R. C. (1993), Air Filtration: An Integrated Approach to the Theory and Applications of Fibrous Filters, Pergamon Press, Oxford.
- Chen, Da-Ren, Pui, D. Y. H. and Liu B. Y. H. (1994), "Optimization of Pleated Filter Design," American Filtration Society Conference, Minneapolis St. Paul, Minnesota.
- Chen, Da-Ren, Pui, D. Y. H. and Tang Y. M. (1996), "Filter Pleating Design for Cabin Air Filtration," SAE Technical Paper #960941, Aspects of Automotive Filtration (SP-1165), SAE, Inc., Warrendale, PA.
- Davies, C. N. (1973), Air Filtration, Academic Press, New York.
- Drain, L. E. (1980), The Laser Doppler Technique, John Wiley and Sons, London, U. K..
- Duran, R. (1995), "Improvement of Flow Uniformity and Modeling of Filtration Efficiencies for Automotive Air Filter Test Housings," M. S. Thesis, School of Mechanical and Aerospace Engineering, Oklahoma State University, Stillwater, Oklahoma.

Durst, F., Melling A. and Whitelaw J. H. (1976), Principles and Practice of Laser Doppler Anemometry, Academic Press, London.

Ensor, D. S., Krafthefer, B. C. and Otteney, T. C. (1994), "Changing Requirements for Air Filtration Test Standards," *ASHRAE Journal*, June, pp. 52-60.

Gidley, D. (1993), "The Selection Process and Comparative Air Filter Performance Testing for Combustion Turbine Inlet Air Filters," International Gas Turbine and Aeroengine Congress and Exposition, Cincinnati, Ohio.

Gustavsson, J. (1996), "Cabin Air Filters: Performances and Requirements," SAE Technical Paper #960941, Aspects of Automotive Filtration (SP-1165), SAE, Inc., Warrendale, PA.

Hoppel, J. (1959), "Viscous Flow Relative to Arrays of Cylinders," *AICHE Journal*, Vol. 5, pp. 174-177.

Harrop, J. A. and Stenhouse, J. I. T. (1969), "The Theoretical Prediction of Inertial Impaction Efficiencies in Fibrous Filters," *Chemical Engineering Science*, Vol. 242.

Hsieh, Ker-Ching, Wu, T., Connors, P. and Tang, Y. M. (1996), "Performance Enhanced Electret Media," SAE Technical Paper #960534, Aspects of Automotive Filtration (SP-1165), SAE, Inc., Warrendale, PA.

Jaroszcyk, T. (1987), "Experimental Study of Nonwoven Filter Performance Using Second Order Orthogonal Design," *Particulate Science and Technology*, Vol. 5, Hemisphere Publishing Corporation, pp. 271-287.

Jaroszcyk, T., Wake, J. and Connor, M. J. (1993), "Factors Affecting the Performance of Engine Air Filters," American Society of Mechanical Engineers, Energy Sources Technology Conference and Exhibition, Houston, Texas.

Kline, S. J. and McClintock, F. A. (1953), "Describing Uncertainties in Single-Sample Experiments," *Mechanical Engineering*, January, pp. 3-8.

Kuwabara, S. (1959), "The Forces Experienced by Randomly Distributed Parallel Circular Cylinders or Spheres in a Viscous Flow at Small Reynolds Numbers," *Journal of the Physical Society of Japan*, Vol. 14, pp. 527-532.

Landahl, H. D. and Hermann, R. G. (1949), "Sampling of Liquid Aerosols by Wires, Cylinders, and Slides, and the Efficiency of Impaction of the Droplets," *Journal of Colloidal Science*, Vol. 4, pp. 103-136.

Lee, K. W. (1977), "Filtration of Submicron Aerosols by Fibrous Filters," Ph.D. Thesis, University of Minnesota, Twin Cities, Minnesota.

Lee, K. W. and Liu, B. Y. H. (1982), "Experimental Study of Aerosol Filtration by Fibrous Filters," *Aerosol Science and Technology*, Vol. 1, Elsevier Science Publishing Co., Amsterdam, pp. 25-76.

Liang, F. (1994), "Particle Counting and Sizing with LDV for Automotive Air Filters," Ph.D. Qualifying Exam Report, School of Mechanical and Aerospace Engineering, Oklahoma State University, Stillwater, Oklahoma.

Liang, F. (1997), "Particle Counting and Sizing with LDV for Automotive Air Filters," Ph.D. Thesis, School of Mechanical and Aerospace Engineering, Oklahoma State University, Stillwater, Oklahoma.

Liang, F., Natarajan, B., Tian, Y. and Dougherty, R. L. (1995), "Local Efficiency Measurements Applicable to Both Automotive Engine and Cabin Filtration," *Particulate Science and Technology*, Taylor and Francis Publishers, Vol. 12, No. 4, April, pp. 333-350.

Liu, B. Y. H. and Lee, K. W. (1982), "Experimental Study of Aerosol Filtration by Fibrous Filters," *Aerosol Science and Technology*, Vol. 1, Elsevier Science Publishing Co., Amsterdam, pp. 25-76.

Liu, B. Y. H., Rubow, K. L. and Pui, D. Y. (1985), "Performance of HEPA and ULPA Filters," Proceedings of the 31st Annual Technical Meeting of the Institute of Environmental Sciences, Kingwood, Texas, pp. 537-542.

Liu, G. (1995), "Velocity Measurements and CFD prediction of Flow Redistribution Through Air Filter," M. S. Thesis, School of Mechanical and Aerospace Engineering, Oklahoma State University, Stillwater, Oklahoma.

Löffler, I. F. (1970), "Separation Efficiency and Pressure Loss of Filter Materials of Different Structure, at Differing Conditions," *Staub-Reinhalt. Luft*, Vol. 30, No. 12, December, pp. 27-31.

McLaughlin, C., McComber, P. and Gakwaya, A. (1986), "Numerical Calculation of Particle Collection by a Row of Cylinders in a Viscous Fluid," *Canadian Journal of Chemical Engineering*, Vol. 64, April, pp. 205-210.

Natarajan, B. (1995), "Local Efficiency Measurements of Automotive Air Filters Using Laser Doppler Velocimetry," M. S. Thesis, School of Mechanical and Aerospace Engineering, Oklahoma State University, Stillwater, Oklahoma.

Natarajan, B., Liang, F., Williams, J. C. and Dougherty, R. L. (1995), "Local Efficiency Measurements Flat Filter Media: Application to Automotive Cabin and Engine Air Filters," presented at the American Filtration and Separation Society Meeting, April 24-36, Nashville, Tennessee.

Nicholson, R. M. and Weisert, L. E. (1986), "A Review of the Use of SAE Standard J726 in Heavy Duty Engine Air Cleaner Testing," *Fluid Filtration: Gas*, Vol. I, ASTM STP 975, American Society for Testing and Materials, Philadelphia, pp. 266-274.

Newman, R. A. (1994), "Uniformity of Air Flow in an Automotive Air Filter Test Housing and Its Effect on the Efficiency of Fibrous Filters," M. S. Thesis, School of Mechanical and Aerospace Engineering, Oklahoma State University, Stillwater, Oklahoma.

Person, J. F. and Cashin, A. H. (1994), "Recent Developments in Cabin Air Filtration," American Filtration Society Conference, Chelmsford, MA.

Ptak, T. J. and Jaroszczyk, T. (1990), "Theoretical-Experimental Aerosol Filtration Model for Fibrous Filters at Intermediate Reynolds Numbers," Proceedings of the Fifth World Filtration Congress, Nice, France, pp. 566-572.

Ptak, T. J., Wake, J. and Jaroszczyk, T. (1994), "An Experimental Evaluation of the Factors Influencing the Performance of Car Interior Air Filters," SAE Technical Paper #930014, SAE, Inc., Warrendale, PA.

Reinhart, C. O. and Weisert, L. E. (1983), "Measurement of Engine Air Cleaner Efficiency Using Airborne Particle Size Analysis," SAE Technical Paper 831262, International Off-Highway Meeting and Exposition, Milwaukee, Wisconsin, Sept.

Rodman, C. A. (1992), "Historical Perspective of Automobile Air Filters," *Fluid Particle Separation Journal*, Vol. 5, pp. 27-30.

Rodman, C. A. and Lessmann, R. C. (1988), "Automotive Nonwoven Filter Media: Their Constructions and Filter Mechanisms," *Tappi Journal*, Apr., pp. 161-168.

Sabnis, R. D. (1993), "Effects of Non-Uniform Air Flow Through Filters on Filtration Efficiency," M. S. Thesis, School of Mechanical and Aerospace Engineering, Oklahoma State University, Stillwater, Oklahoma.

Sabnis, R. D., Cai, Q. and Chambers, F. W. (1994), "Diagnosis of the Flow Fields in a Housing for Automotive Air Filter Performance Testing," presented at the ALAA 32nd Aerospace Sciences Meeting, Paper #94-0117, Jan. 10-13, Reno, Nevada.

Society of Automotive Engineers (1987), "SAE J726 Air Cleaner Test Code - SAE Recommended Practice," SAE, Inc., Warrendale, PA.

Society of Automotive Engineers (1993), "SAE J1669 Passenger Compartment Air Filter Test Code - SAE Recommended Practice," Proposed Draft, SAE, Inc., Warrendale, PA.

Stechkina, I. B., Kirsh, A. H. and Fuchs, N. A. (1969), "Investigation of Fibrous Filters For Aerosols," *Colloid Journal, USSR*, Vol. 31, pp. 97-101.

Stenhouse, J. I. T. (1975), "Filtration of Air by Fibrous Filters," *Filtration and Separation*, May/June, pp. 268-274.

Stinson, J. A., Meyers, M. N., Jaroszczyk, T. and Verdegan, B. M. (1989), "Temporal Changes in Oil and Air Filter Performance Due to Dust Deposition," *Filtration and Separation*, Sept./Oct., pp. 368-371.

Tebbutt, C. B. (1995), "CFD Model of Flow Through Air Filter Pleats," M. S. Thesis, School of Mechanical and Aerospace Engineering, Oklahoma State University, Stillwater, Oklahoma.

Tian, Y. (1995), "TSTEP - Three Dimensional Traverse Software," performed as part of the OCAST Applied Research Project on Automotive Air Filtration, Oklahoma State University, Stillwater, Oklahoma.

Wake, J. and Jaroszczyk, T. (1991), "Experimental Study of Dust Filtration in Surface-Type Nonwovens," *Particulate Science and Technology*, Vol. 9, Hemisphere Publishing Corporation, pp. 31-44.

Walker, M. and Ptak, T. J. (1996), "Particulate Filter Performance in the North American Environment," SAE Technical Paper #960940, Aspects of Automotive Filtration (SP-1165), SAE, Inc., Warrendale, PA.

Williams, J. C. (1996), "In-Situ Measurements of Local Efficiency for Flat Automotive Air Filter Media," M. S. Report, School of Mechanical and Aerospace Engineering, Oklahoma State University, Stillwater, Oklahoma.

Yeh, H. C. (1972), "A Fundamental Study of Aerosol Filtration by Fibrous Filters," Ph.D. Thesis, University of Minnesota, Twin Cities, Minnesota.

Yeh, Y. and Cummins H. Z. (1964), *Applied Physics Letters*, Vol. 4, pp. 176-178.

Yeh, H. C. and Liu, B. Y. H. (1974), "Aerosol Filtration by Fibrous Filters - I. Theoretical," *Aerosol Science*, Vol. 5, Pergamon Press, Great Britain, pp. 191-204.

APPENDICES

APPENDIX A

THE DSA PARAMETERS

The major parameters of the DSA parameters are defined in this appendix.

- **High Voltage.** The voltage supplied to the PMT which controls the amplification of the detected signals. It has a range of 200 to 800 volts. HV values of 370 to 400 are recommended.
- **Frequency Shift.** The frequency shift given to the Bragg cell so that the main beam is shifted in order to generate the second beam (shifted beam) for each color. The frequency shift is +40 MHz and is constant for all of the tests.
- **DC Offset.** This parameter adjusts the ground signal to a common ground level. It is adjusted so that the raw signal is just above the zero line on the oscilloscope. A value in the range of 10 to 20 mV is recommended.
- **Burst Filter.** This parameter sets the frequency band for detection of the burst signals. The burst signals falling out the specified frequency range won't be detected. The burst filter on the DSA software can be set to values of 40 MHz BP (band pass), 50 MHz LP (low pass). According to the DSA manual [1992], the 40 MHz band pass activates an acceptable range of ± 5 MHz from 40 MHz. The 10 MHz low pass

activates the frequency range of 5 to 10 MHz and the 50 MHz low pass activates the frequency range of 20 to 50 MHz. The burst filter can be set to “All Pass” so that the burst signal is not filtered. 40 MHz BP is recommended for velocities in the range of 14.2 to 14.2 m/s. For velocities outside this range, 10 MHz LP is recommended.

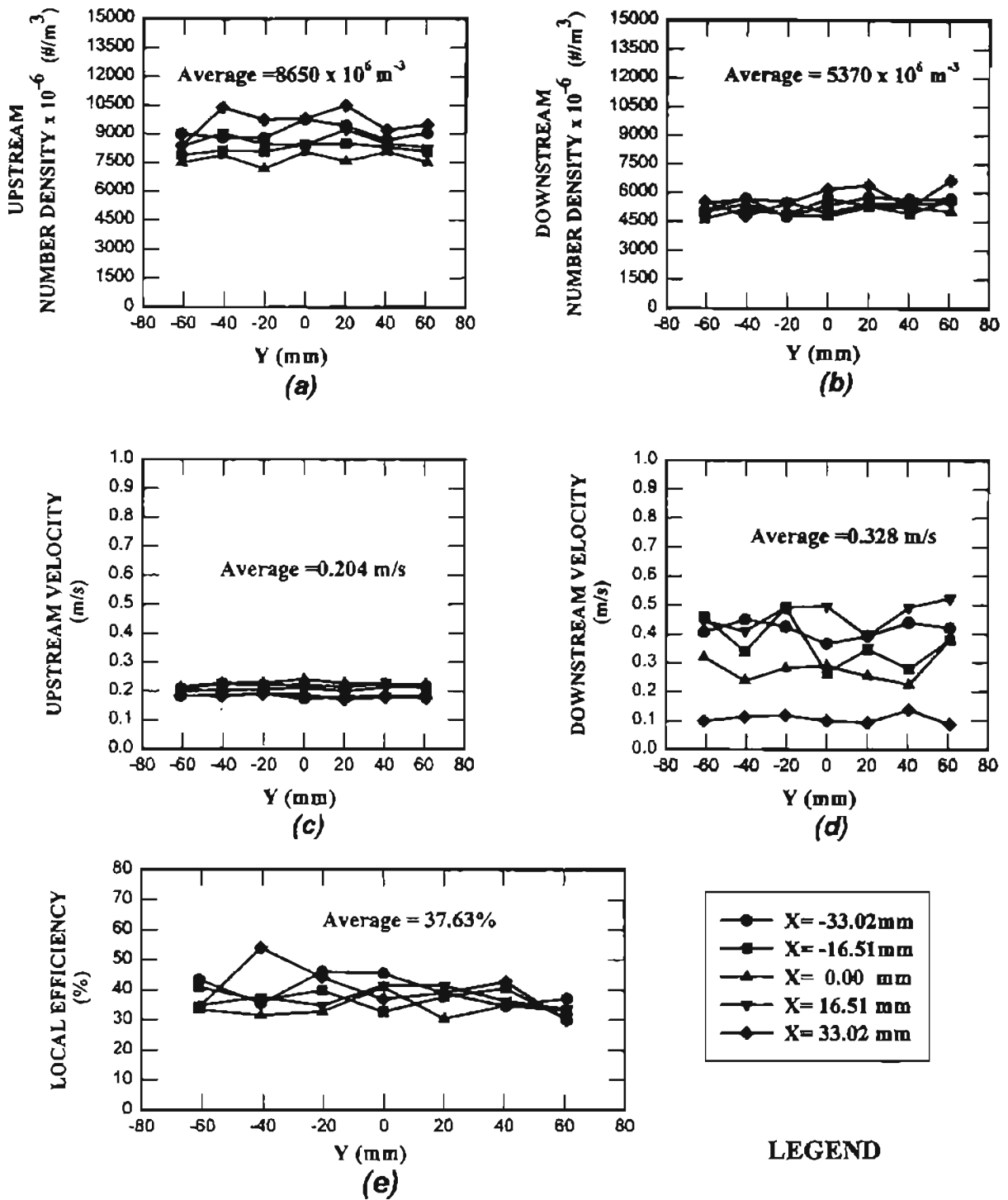
- **Threshold.** The threshold determines the minimum signal amplitude required to detect a burst. Anand [1997] has investigated the effect of threshold on the measured data. He used a value of 60 mV for his measurements. He concluded that the accuracy of the measurements is dependent on the value of the threshold and high voltage. The threshold should be set to a value so that with an optimum value of high voltage (370 to 400 V), a validity of 90 to 95% could be obtained.
- **Envelope Filter.** This parameter is used for filtration of high frequency noise. A detailed procedure for finding the optimum value of this parameter is described by Anand [1997]. The optimum value depends on the measurement conditions such as particle concentration, flow rate, etc.
- **Number of Samples and Sample Rate.** Proper values for these parameters determine the resolution of the velocity histogram. These parameters should be selected such that aliasing is avoided (appearance of two or more histograms). Anand [1997] recommended sampling rates of 5 and 2.5 MHz for low velocities (less than 0.25 m/s) and 80 MHz for higher velocities (greater than 0.5 m/s). The author used 5 MHz for tests in which the average velocity was less than 0.2 m/s and 80 MHz for flow rates with average velocities of 0.5 m/s and higher (up to 14.2 m/s). Between these two velocities, 20 MHz was chosen.

- **Signal to Noise Ratio.** These parameter provides a criteria for acceptance of the burst signal based on it's quality. A value of 0.3 as recommended by the DSA manual and Anand [1997] was used.
- **Total Number of Samples.** This is the number of detected particles in each run. It depends on the validity and the total valid samples.
- **Valid Samples.** The number of particles which are detected as a true signal (and not noise) are called valid samples. This value was set to 1000 for most of the tests. Lower numbers were used (such as 200 samples) at locations where the sample rate was relatively low and the run time exceeded 30 seconds for detection of 1000 valid samples.
- **Validity.** Validity is the ratio of the valid samples to total samples. It is dependent on other parameters, mainly high voltage and threshold (see Anand [1997]).
- **Coincidence.** When coincidence is turned on, only particles are detected as valid samples for which both their axial and transverse velocities are detected (i.e., the particles are detected as valid samples in both directions). Coincidence is useful for total velocity measurements in recirculation zones (see Section 5.6).

APPENDIX B

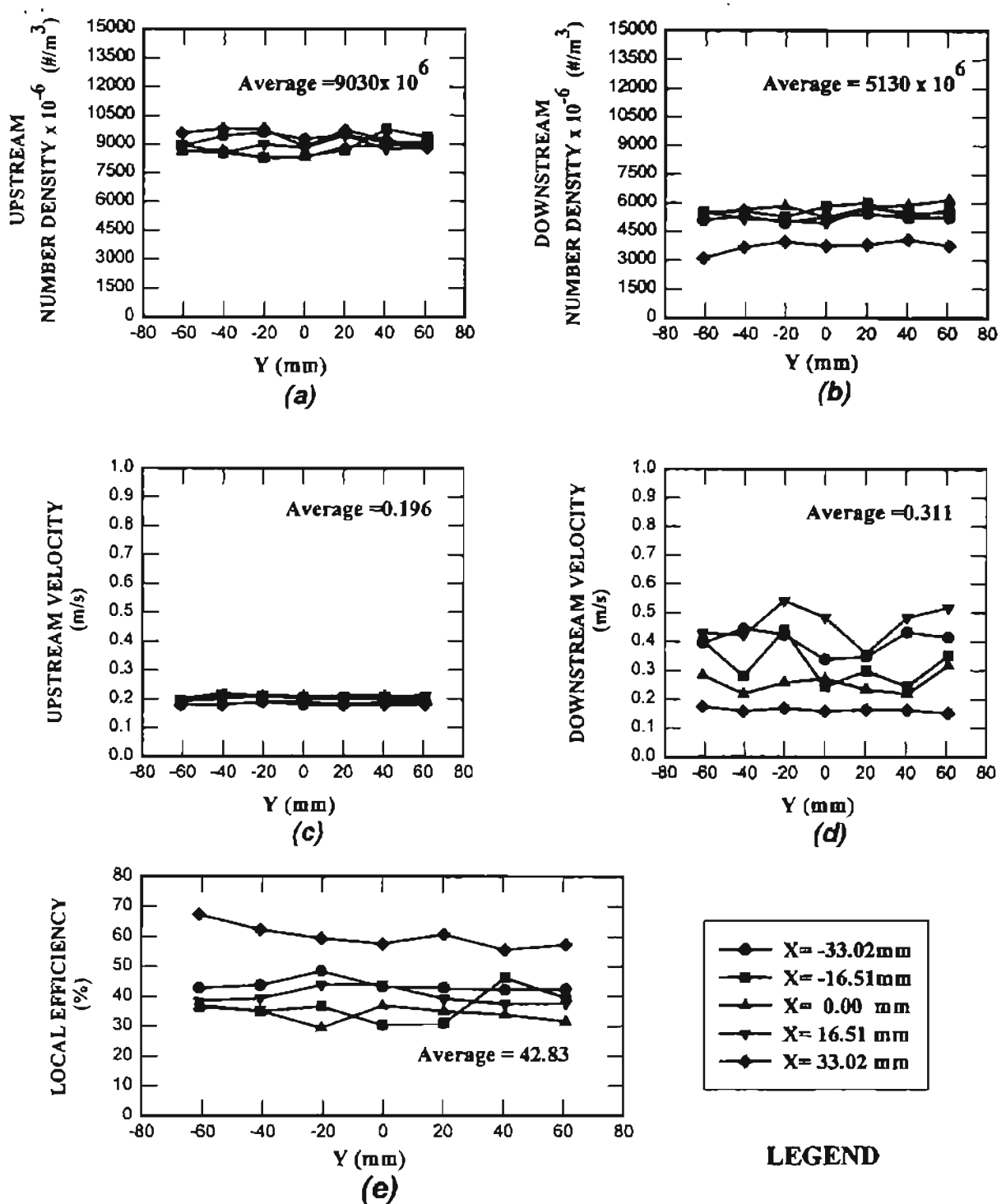
TEST RESULTS: SMALL ANGLE DIFFUSER HOUSING

The results of measurements in the small angle diffuser housing are presented in this appendix. They are presented in five curves for each test. All curves have the same legend. Figures are sorted based on the flow rates, i.e., Fig. B.1 corresponds to the plots for the lowest flow rate ($5.68 \text{ m}^3/\text{hr}$), and Fig. 5.21 presents the results of the test made at the highest flow rate ($481.8 \text{ m}^3/\text{hr}$) among all of the tests.



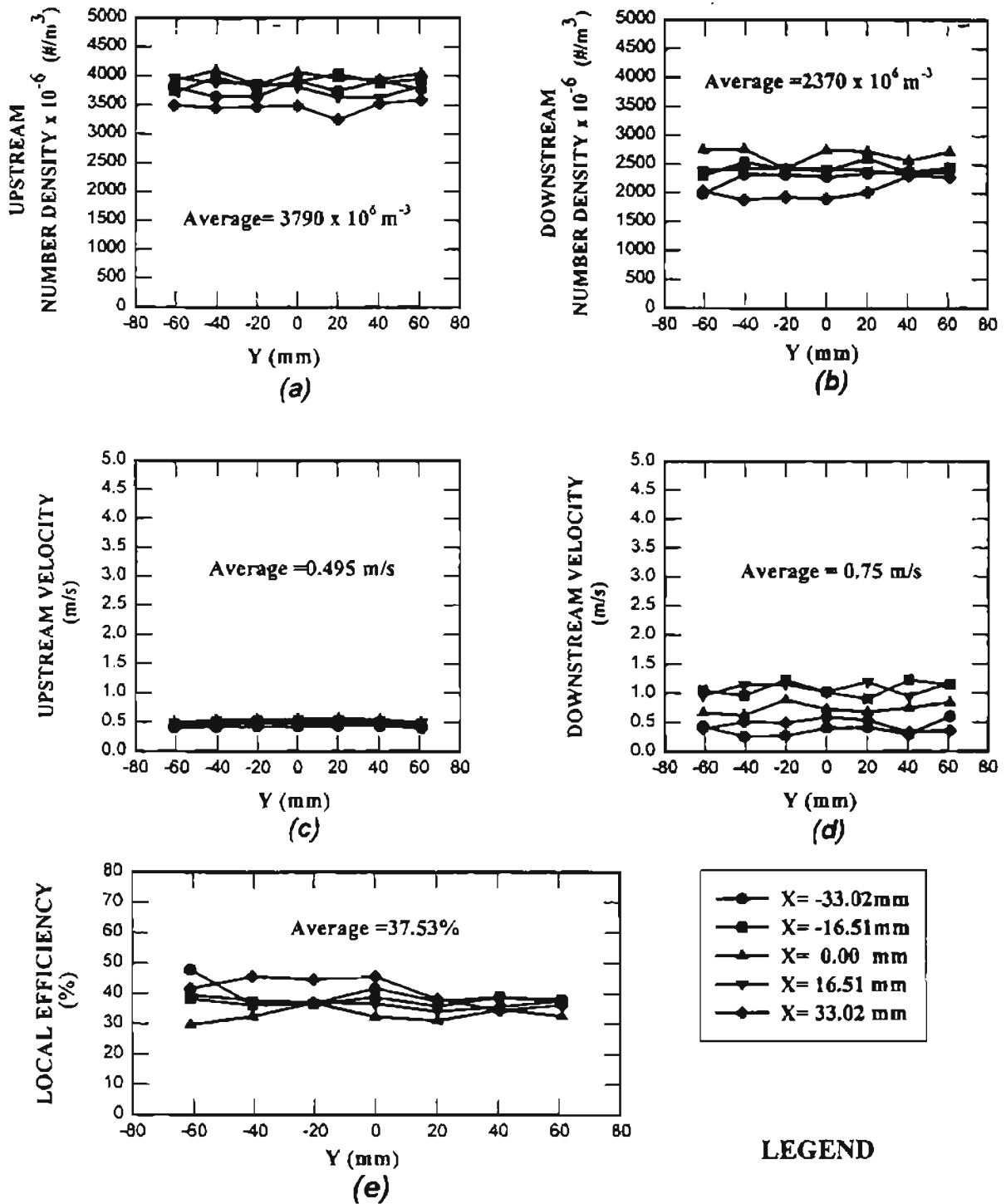
a) Upstream Number Density, b) Downstream Number Density, c) Upstream Velocity, d) Downstream Velocity, e) Local Efficiency

Figure B.1 Local Efficiency, Upstream and Downstream Number Densities and Velocity Profiles, A13192 Pleated Filter, Diffuser Housing, 0.966 Micron PSL Particles, 5.68 m³/hr Air Flow, Test # F15, 7/1/96.



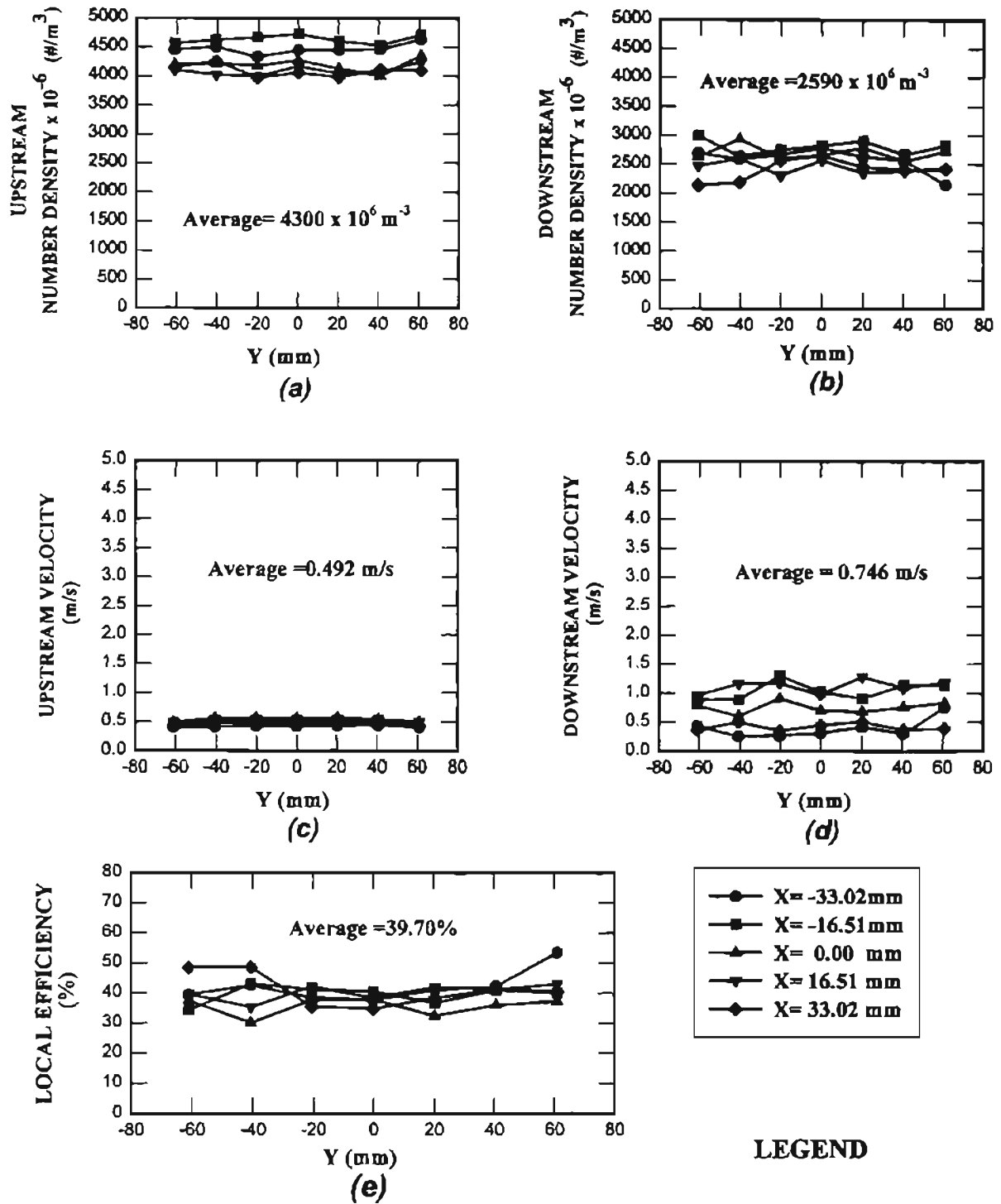
a) Upstream Number Density, b) Downstream Number Density, c) Upstream Velocity, d) Downstream Velocity, e) Local Efficiency

Figure B.2 Local Efficiency, Upstream and Downstream Number Densities and Velocity Profiles, A13192 Pleated Filter, Diffuser Housing, 0.966 Micron PSL Particles, 5.68 m³/hr Air Flow, Test # F16, 7/2/96.



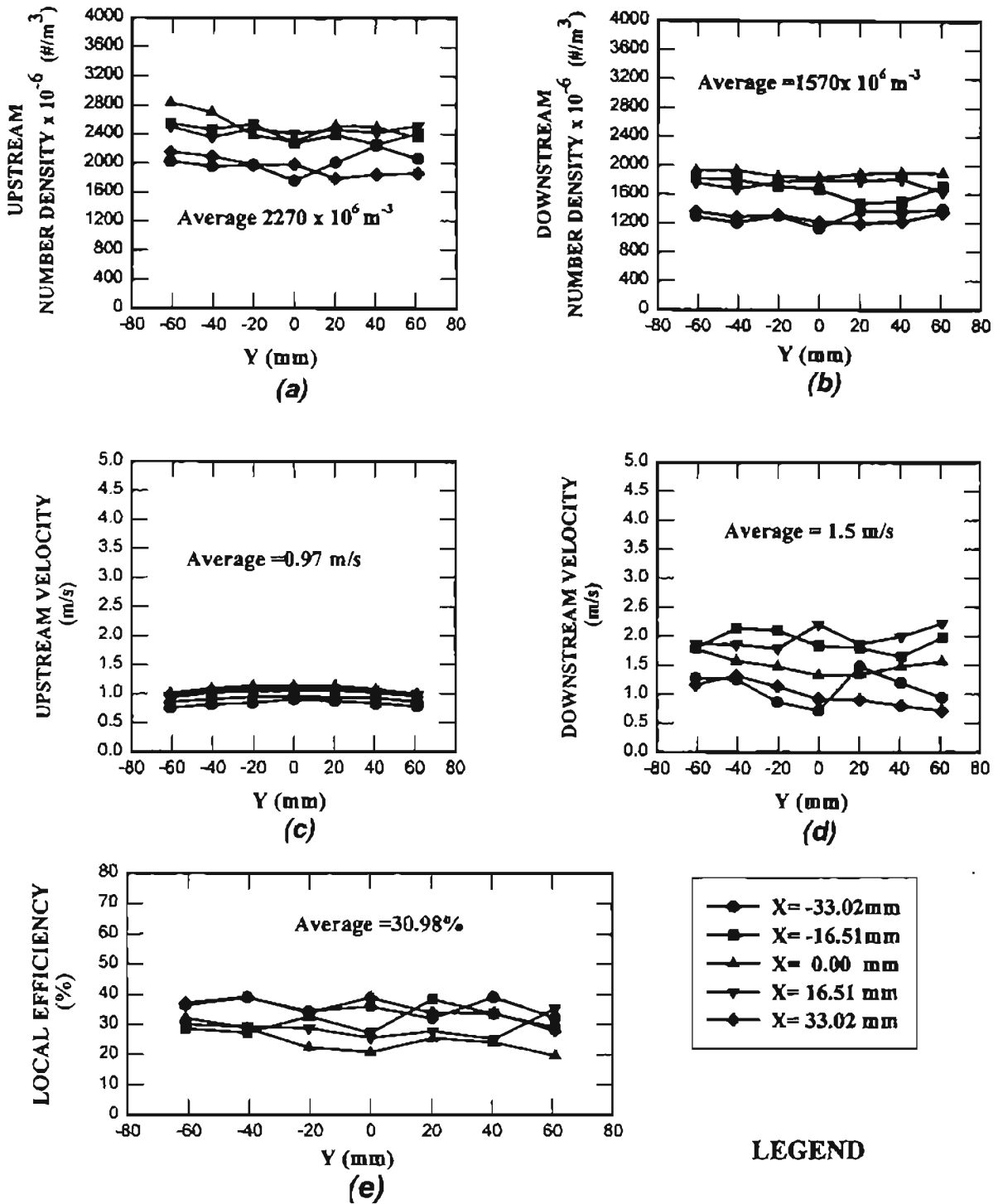
a) Upstream Number Density, b) Downstream Number Density, c) Upstream Velocity, d) Downstream Velocity, e) Local Efficiency

Figure B.3 Local Efficiency, Upstream and Downstream Number Densities and Velocity Profiles, A13192 Pleated Filter, Diffuser Housing, 0.966 Micron PSL Particles, 29.5 m³/hr Air Flow, Test # F11, 6/24/96.



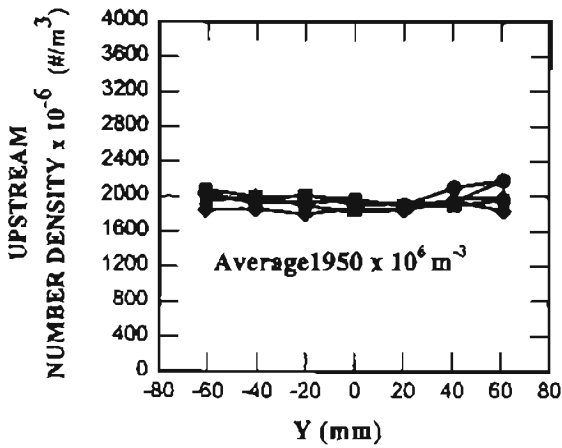
a) Upstream Number Density, b) Downstream Number Density, c) Upstream Velocity, d) Downstream Velocity, e) Local Efficiency

Figure B.4 Local Efficiency, Upstream and Downstream Number Densities and Velocity Profiles, A13192 Pleated Filter, Diffuser Housing, 0.966 Micron PSL Particles, 29.5 m³/hr Air Flow, Test # F12, 6/25/96.

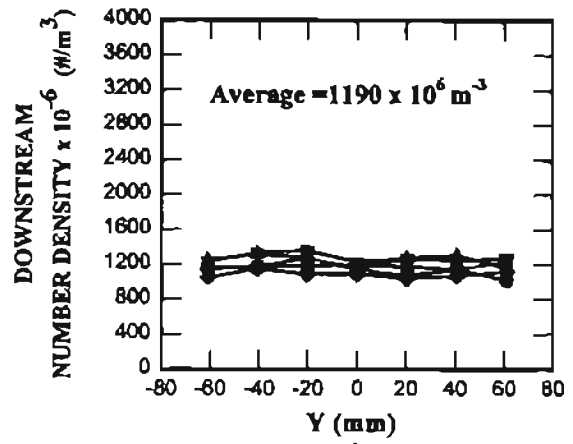


a) Upstream Number Density, b) Downstream Number Density, c) Upstream Velocity, d) Downstream Velocity, e) Local Efficiency

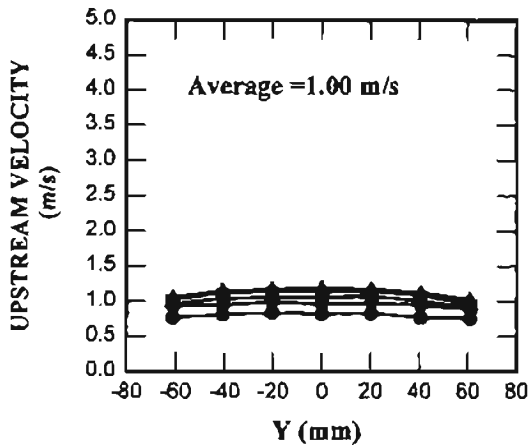
Figure B.5 Local Efficiency, Upstream and Downstream Number Densities and Velocity Profiles, A13192 Pleated Filter, Diffuser Housing, 0.966 Micron PSL Particles, 53.3 m³/hr Air Flow, Test # F23, 7/16/96.



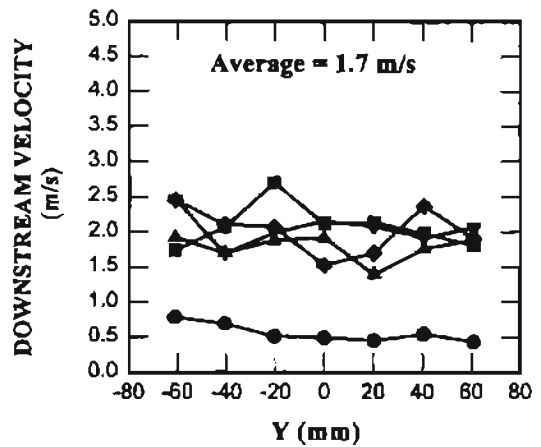
(a)



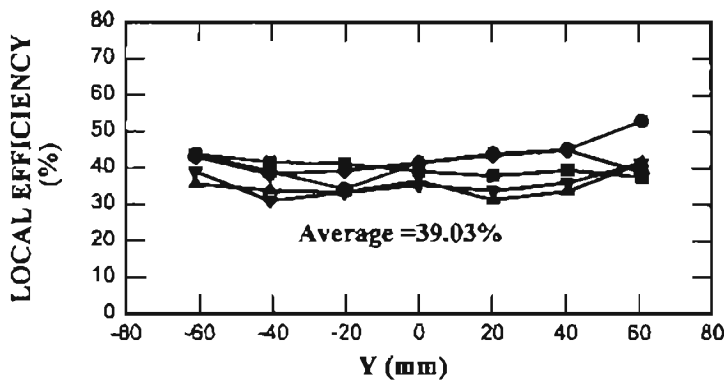
(b)



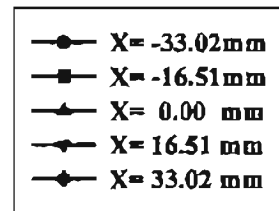
(c)



(d)



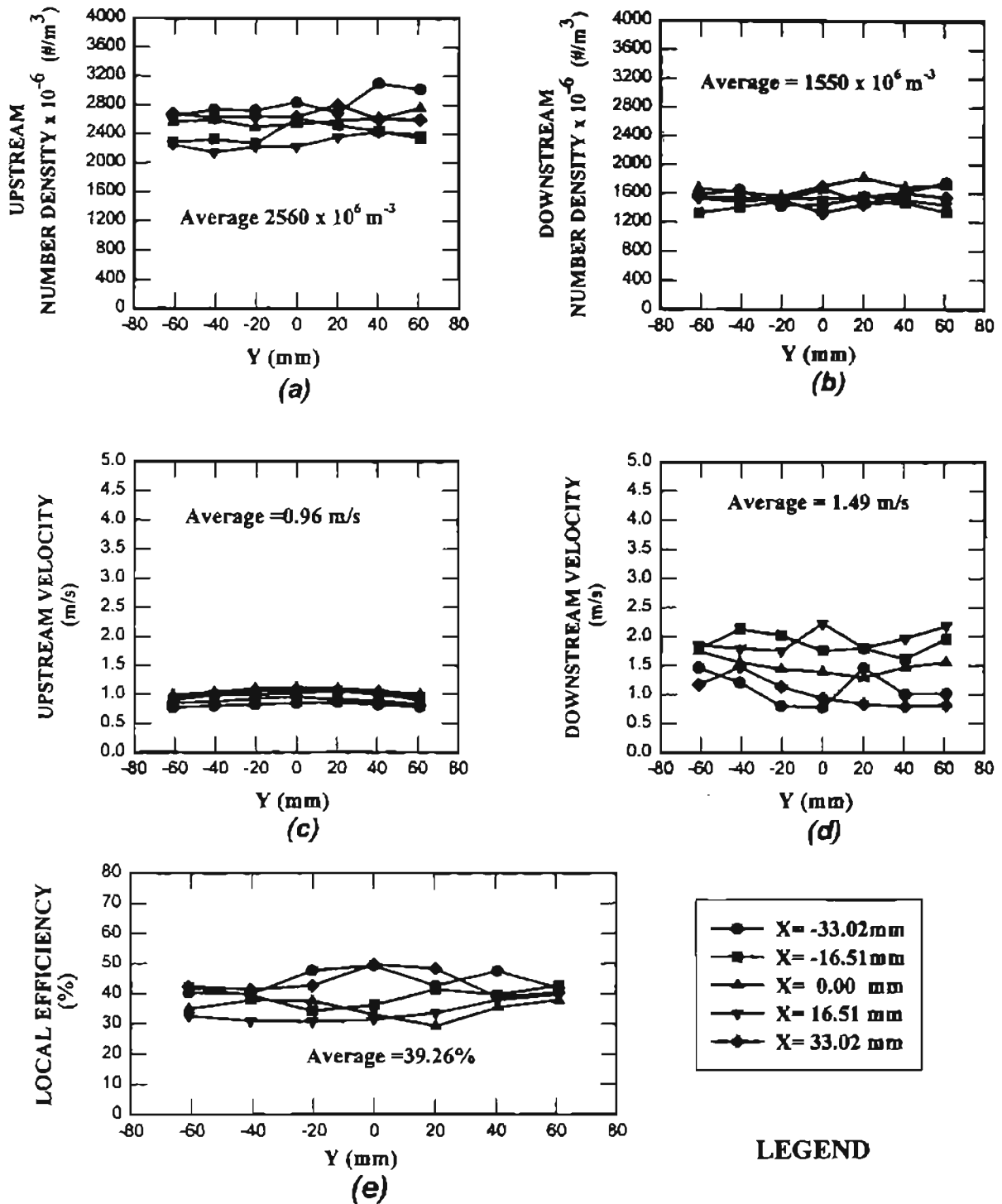
(e)



LEGEND

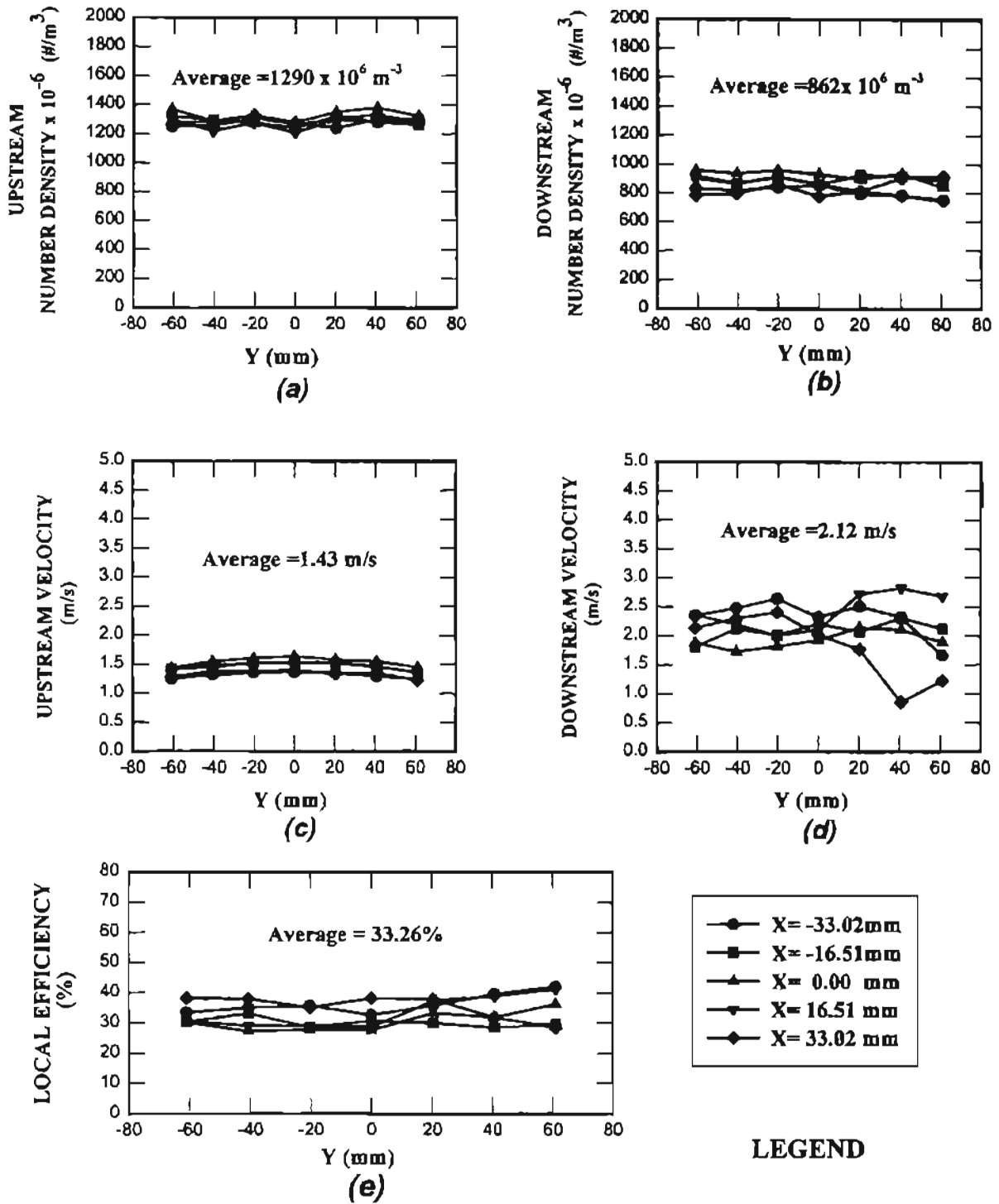
a) Upstream Number Density, b) Downstream Number Density, c) Upstream Velocity, d) Downstream Velocity, e) Local Efficiency

Figure B.6 Local Efficiency, Upstream and Downstream Number Densities and Velocity Profiles, A13192 Pleated Filter, Diffuser Housing, 0.966 Micron PSL Particles, 53.3 m³/hr Air Flow, Test # F22, 7/15/96.



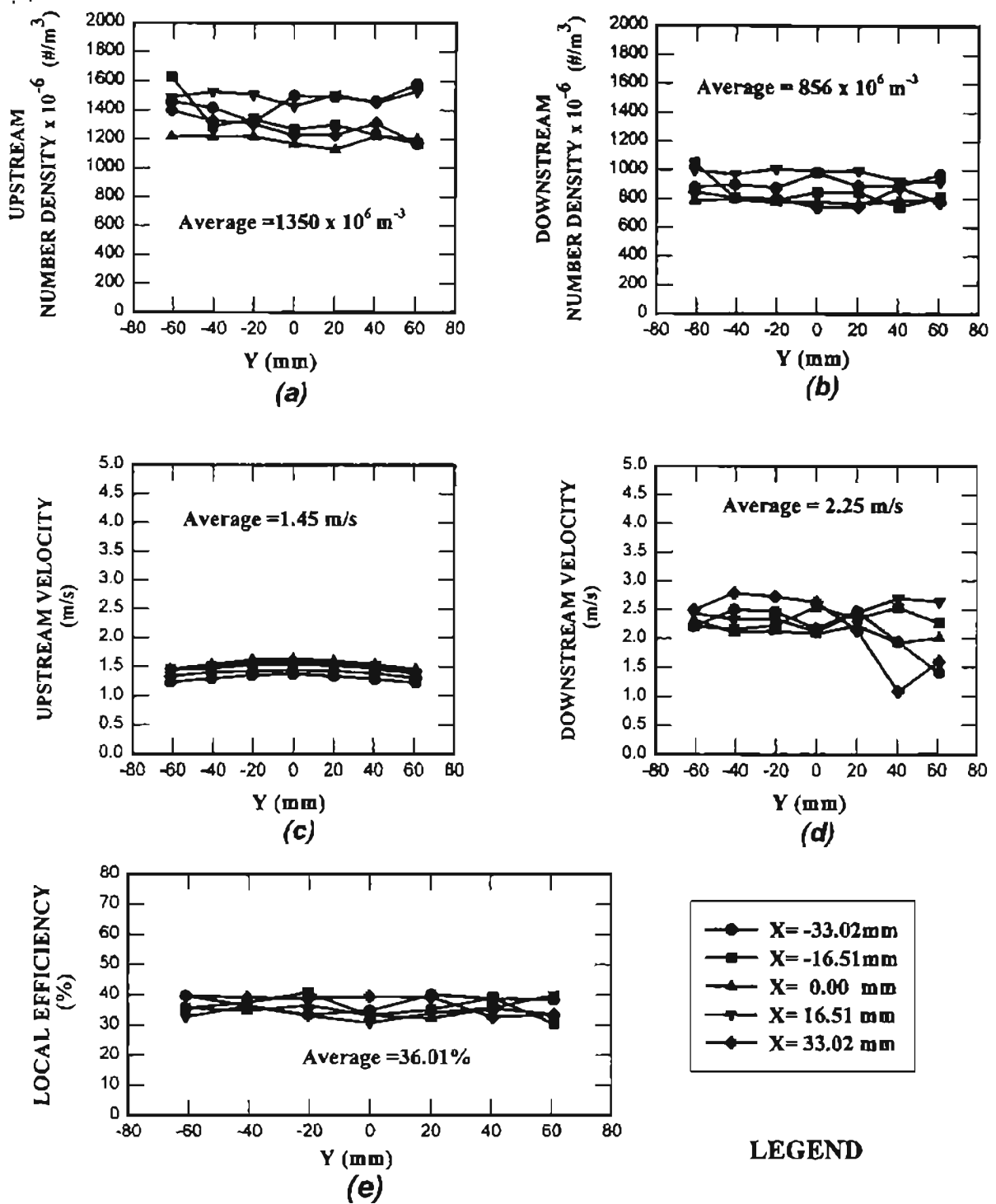
a) Upstream Number Density, b) Downstream Number Density, c) Upstream Velocity, d) Downstream Velocity, e) Local Efficiency

Figure B.7 Local Efficiency, Upstream and Downstream Number Densities and Velocity Profiles, A13192 Pleated Filter, Diffuser Housing, 0.966 Micron PSL Particles, 53.3 m³/hr Air Flow, Test # F24, 7/17/96.



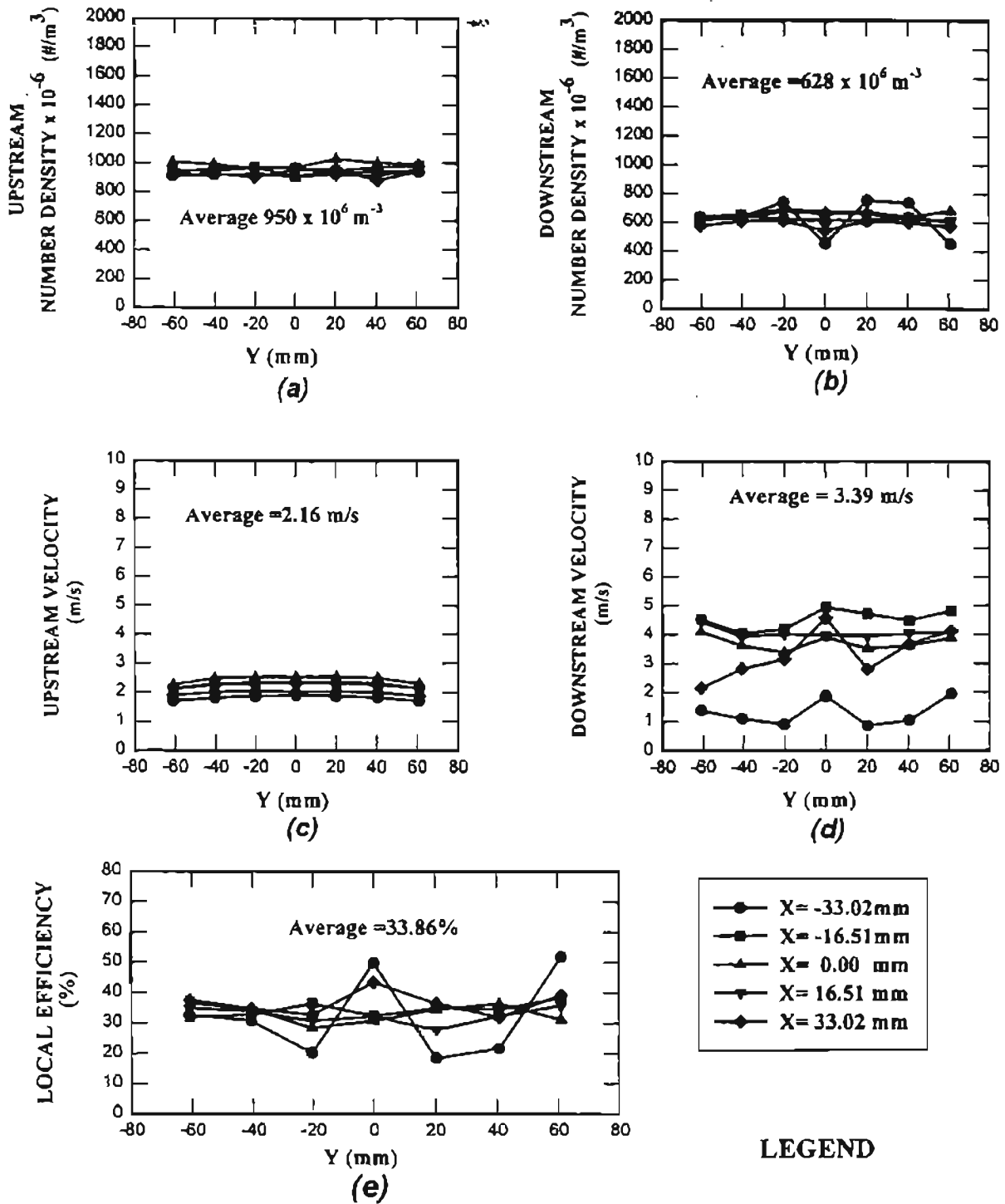
a) Upstream Number Density, b) Downstream Number Density, c) Upstream Velocity, d) Downstream Velocity, e) Local Efficiency

Figure B.8 Local Efficiency, Upstream and Downstream Number Densities and Velocity Profiles, A13192 Pleated Filter, Diffuser Housing, 0.966 Micron PSL Particles, 77.1 m³/hr Air Flow, Test # F9, 6/19/96.



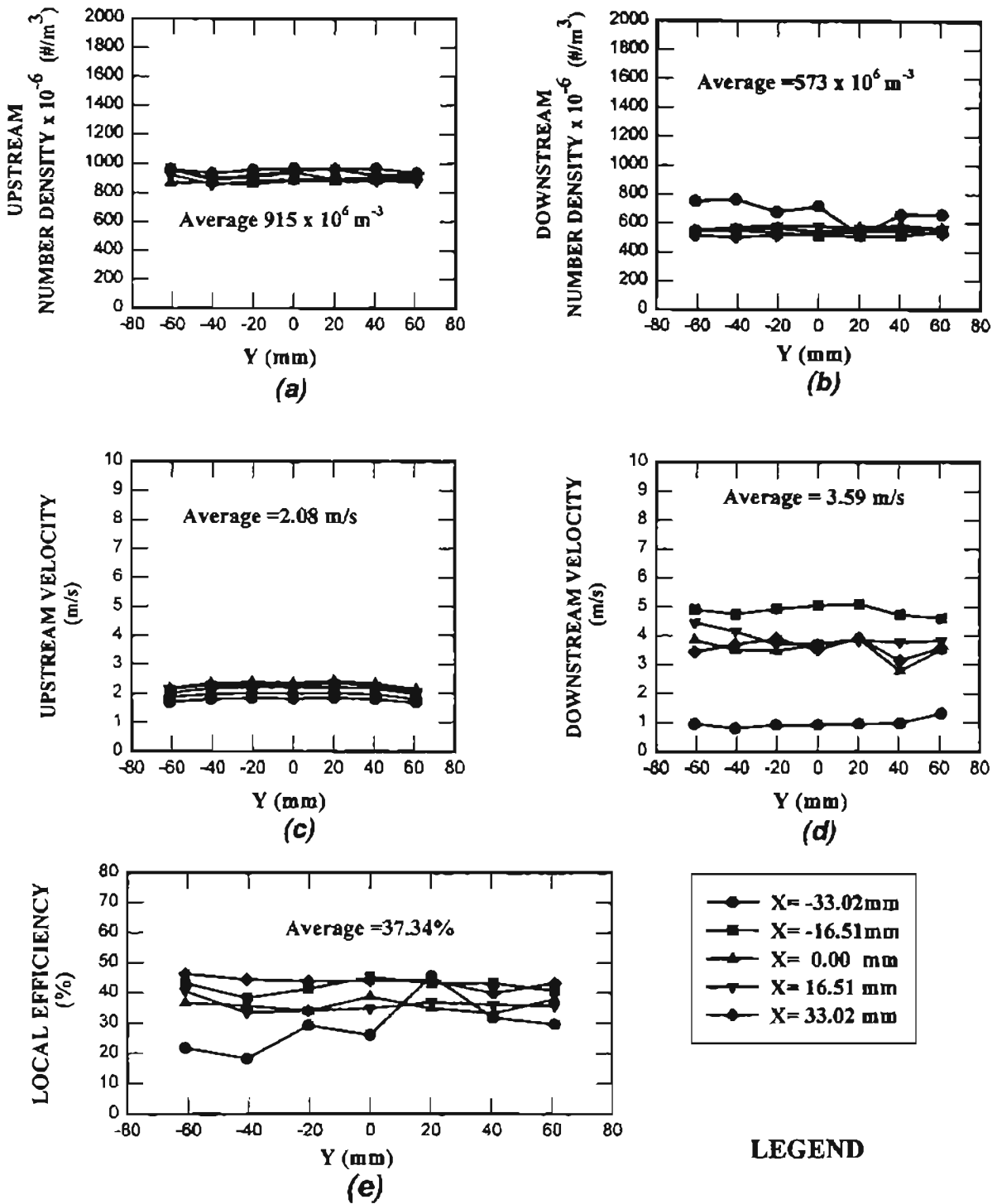
a) Upstream Number Density, b) Downstream Number Density,
c) Upstream Velocity, d) Downstream Velocity, e) Local Efficiency

Figure B.9 Local Efficiency, Upstream and Downstream Number Densities and Velocity Profiles, A13192 Pleated Filter, Diffuser Housing, 0.966 Micron PSL Particles, 77.1 m³/hr Air Flow, Test # F10, 6/20/96.



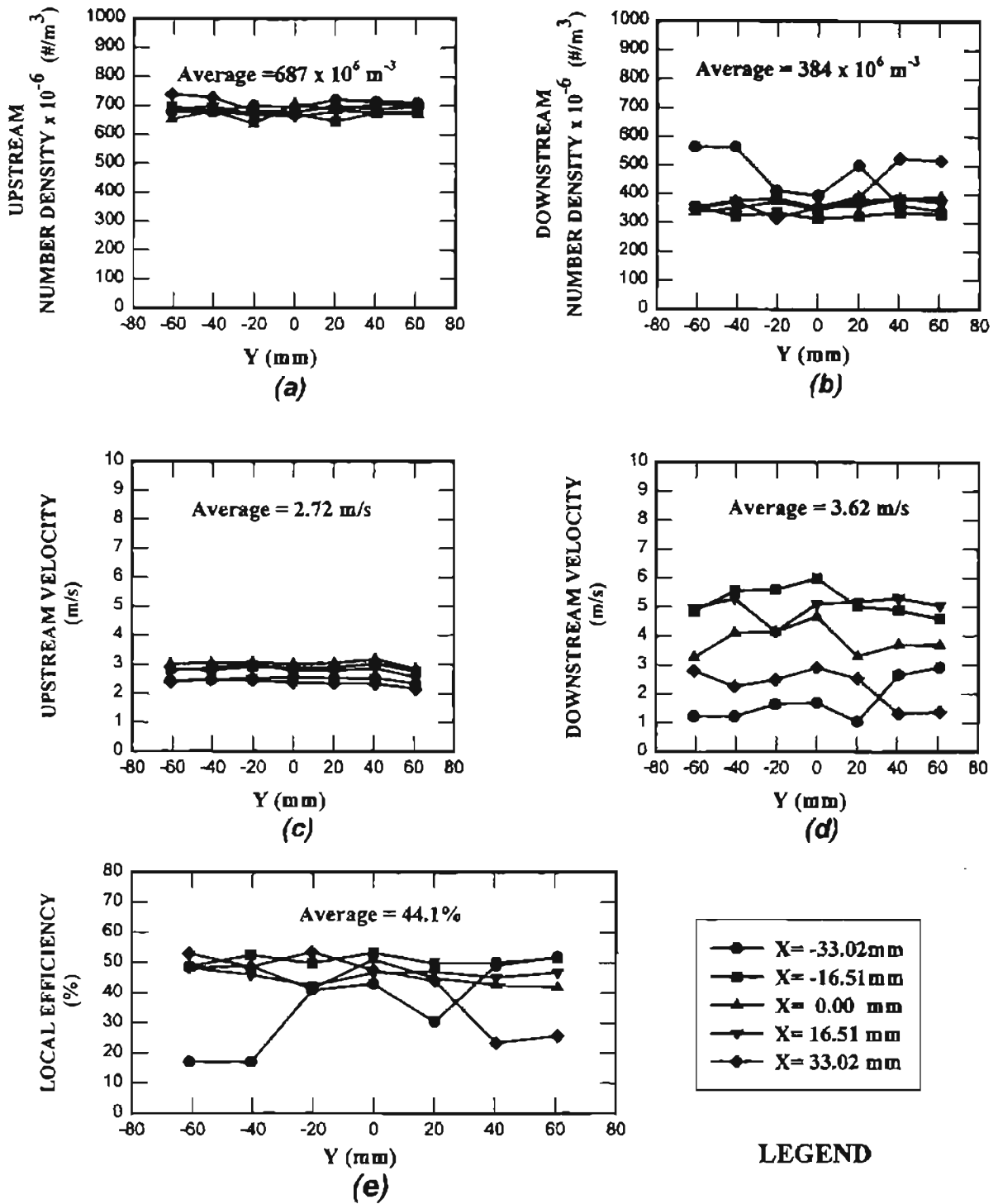
a) Upstream Number Density, b) Downstream Number Density, c) Upstream Velocity, d) Downstream Velocity, e) Local Efficiency

Figure B.10 Local Efficiency, Upstream and Downstream Number Densities and Velocity Profiles, A13192 Pleated Filter, Diffuser Housing, 0.966 Micron PSL Particles, 103.7 m³/hr Air Flow, Test # F20, 7/5/96.



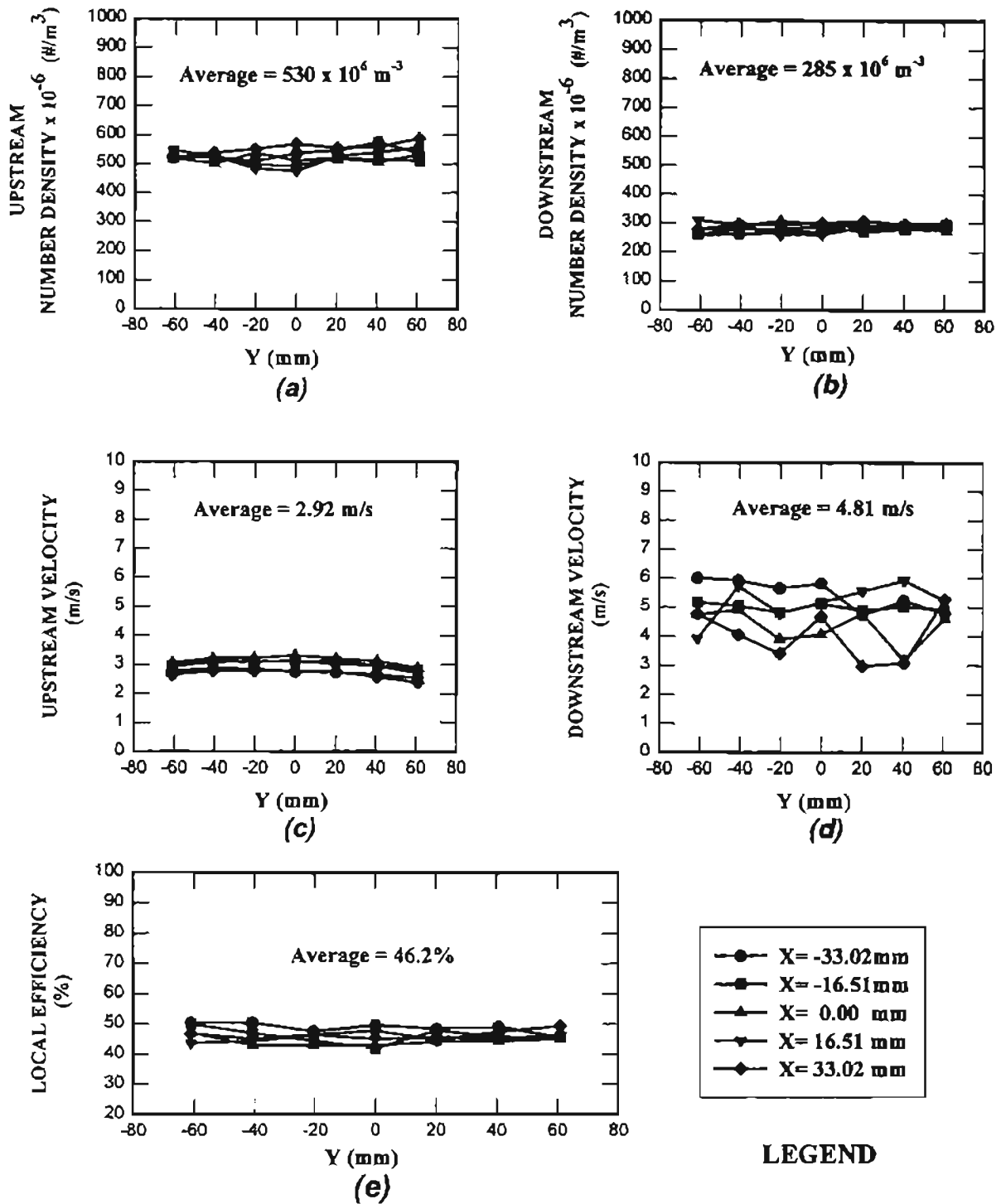
a) Upstream Number Density, b) Downstream Number Density, c) Upstream Velocity, d) Downstream Velocity, e) Local Efficiency

Figure B.11 Local Efficiency, Upstream and Downstream Number Densities and Velocity Profiles, A13192 Pleated Filter, Diffuser Housing, 0.966 Micron PSL Particles, 103.7 m³/hr Air Flow, Test # F19, 7/5/96.



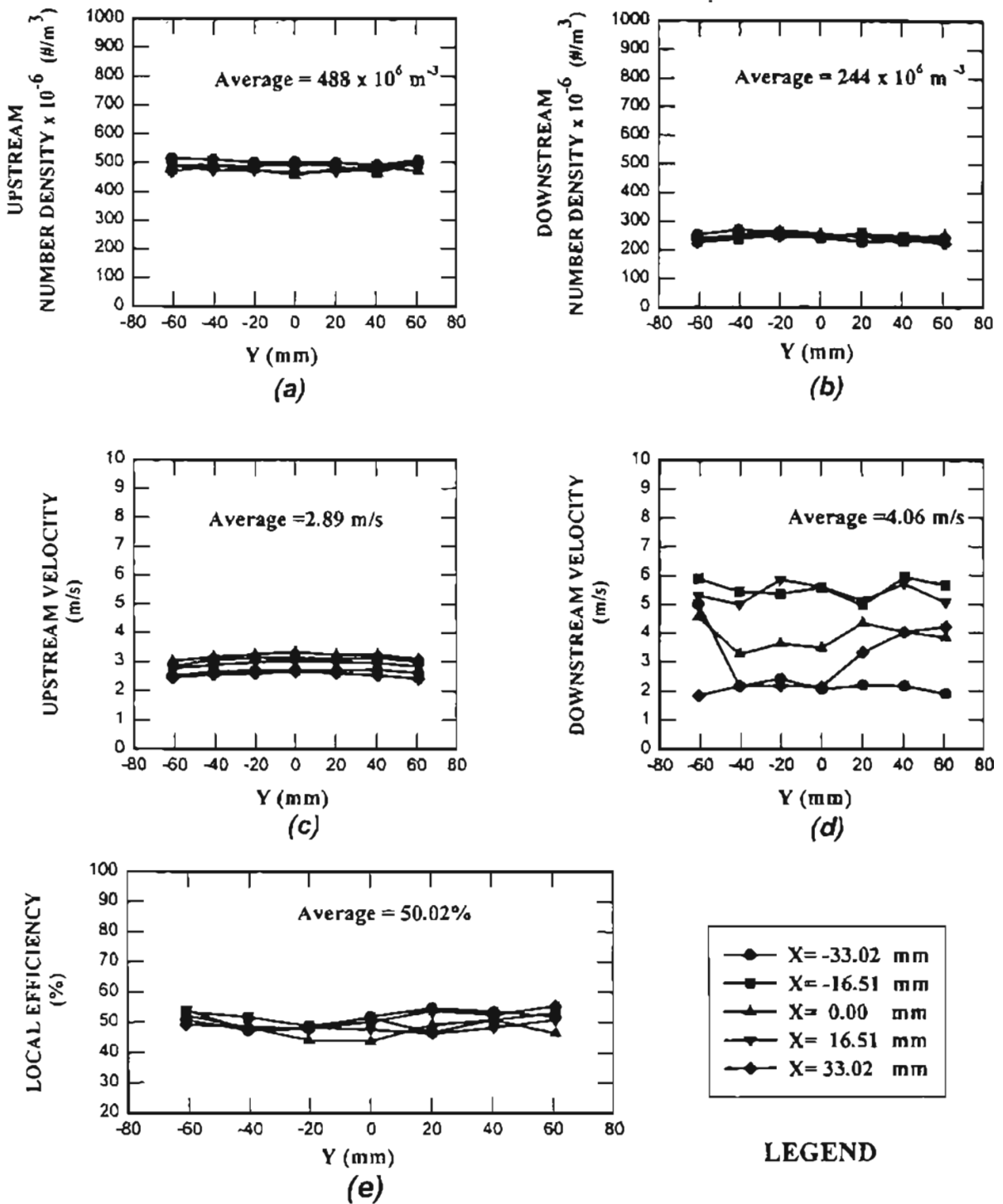
a) Upstream Number Density, b) Downstream Number Density, c) Upstream Velocity, d) Downstream Velocity, e) Local Efficiency

Figure B.12 Local Efficiency, Upstream and Downstream Number Densities and Velocity Profiles, A13192 Pleated Filter, Diffuser Housing, 0.966 Micron PSL Particles, 145.7 m³/hr Air Flow, Test # F1, 5/8/96.



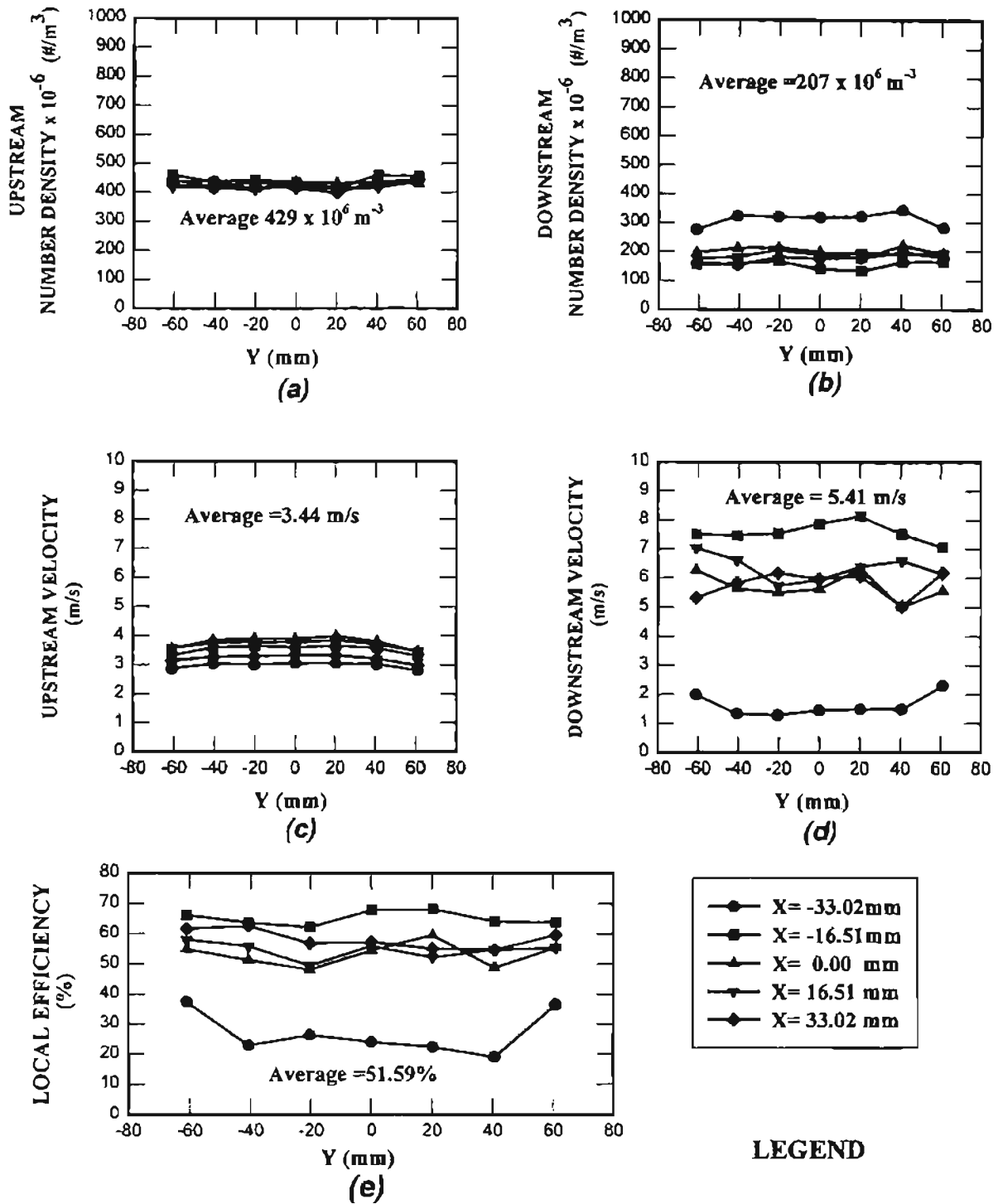
a) Upstream Number Density, b) Downstream Number Density, c) Upstream Velocity, d) Downstream Velocity, e) Local Efficiency

Figure B.13 Local Efficiency, Upstream and Downstream Number Densities and Velocity Profiles, A13192 Pleated Filter, Diffuser Housing, 0.966 Micron PSL Particles, 145.7 m³/hr Air Flow, Test # F4, 5/14/96.



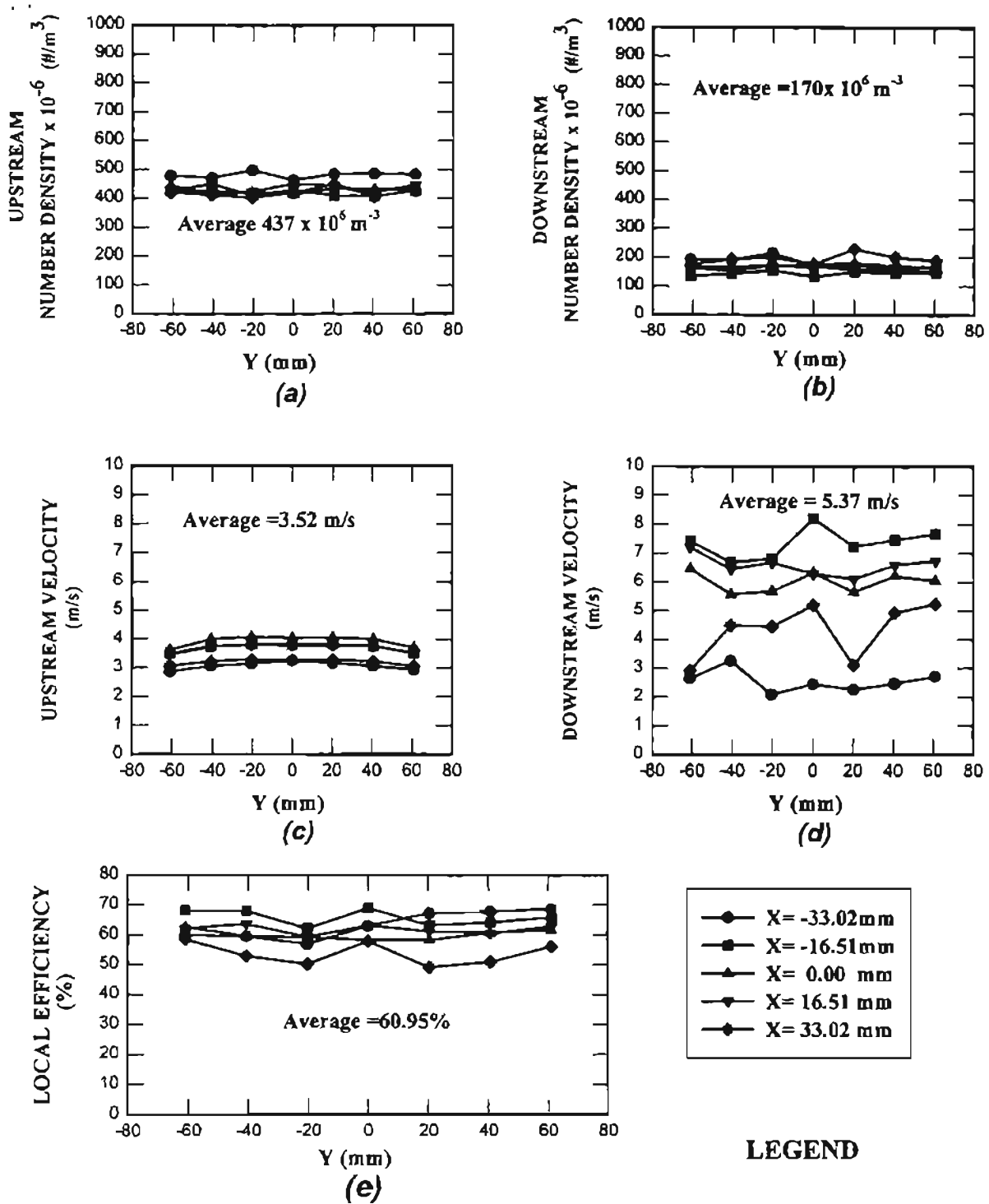
a) Upstream Number Density, b) Downstream Number Density, c) Upstream Velocity, d) Downstream Velocity, e) Local Efficiency

Figure B.14 Local Efficiency, Upstream and Downstream Number Densities and Velocity Profiles, A13192 Pleated Filter, Diffuser Housing, 0.966 Micron PSL Particles, 145.7 m³/hr Air Flow, Test # F2, 5/13/96.



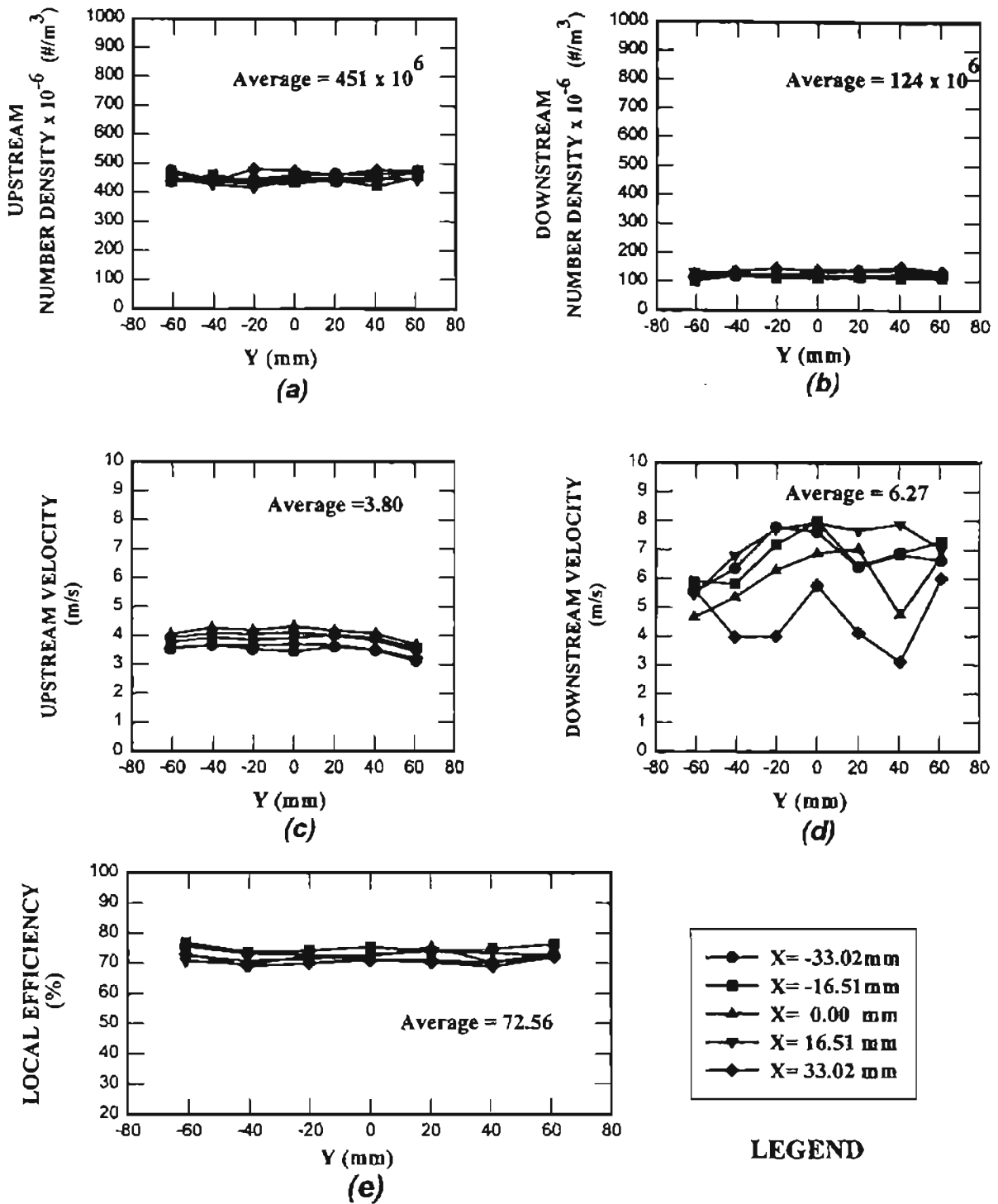
a) Upstream Number Density, b) Downstream Number Density,
c) Upstream Velocity, d) Downstream Velocity, e) Local Efficiency

Figure B.15 Local Efficiency, Upstream and Downstream Number Densities and Velocity Profiles, A13192 Pleated Filter, Diffuser Housing, 0.966 Micron PSL Particles, 187.7 m^3/hr Air Flow, Test # F18, 7/4/96.



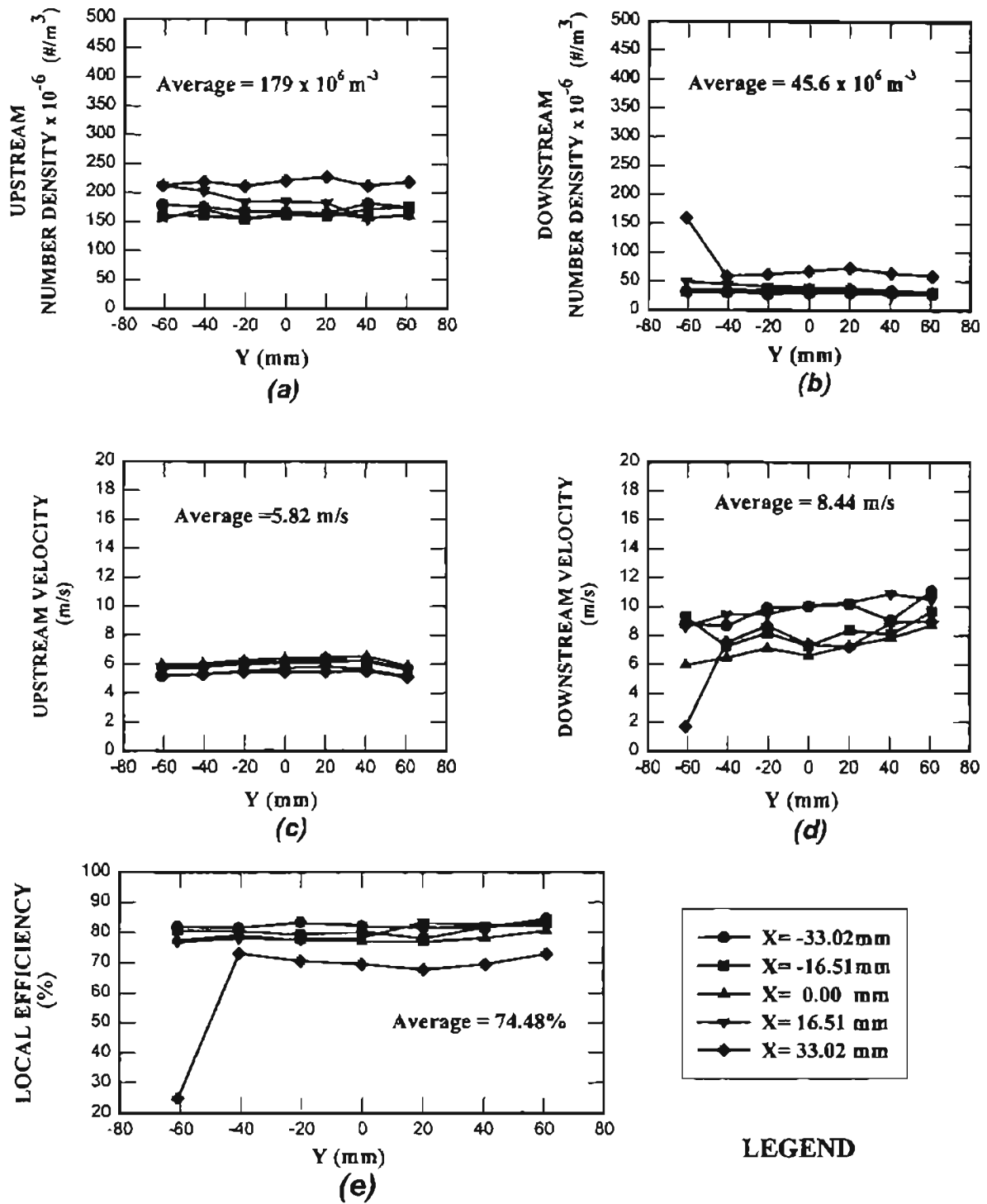
a) Upstream Number Density, b) Downstream Number Density,
c) Upstream Velocity, d) Downstream Velocity, e) Local Efficiency

Figure B.16 Local Efficiency, Upstream and Downstream Number Densities and Velocity Profiles, A13192 Pleated Filter, Diffuser Housing, 0.966 Micron PSL Particles, 187.7 m^3/hr Air Flow, Test # F21, 7/8/96.



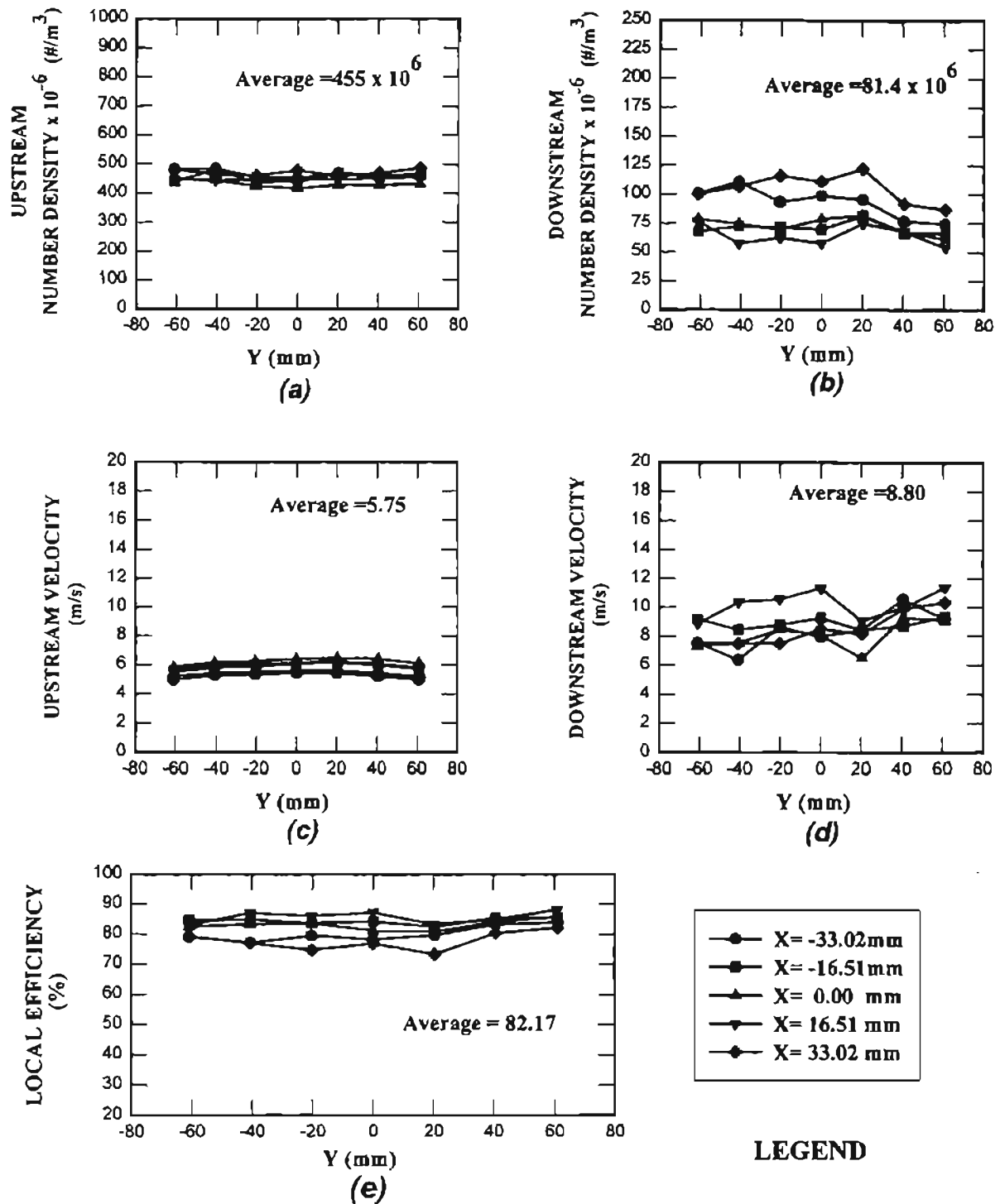
a) Upstream Number Density, b) Downstream Number Density, c) Upstream Velocity, d) Downstream Velocity, e) Local Efficiency

Figure B.17 Local Efficiency, Upstream and Downstream Number Densities and Velocity Profiles, A13192 Pleated Filter, Diffuser Housing, 0.966 Micron PSL Particles, 187.7 m³/hr Air Flow, Test # F5, 5/21/96.



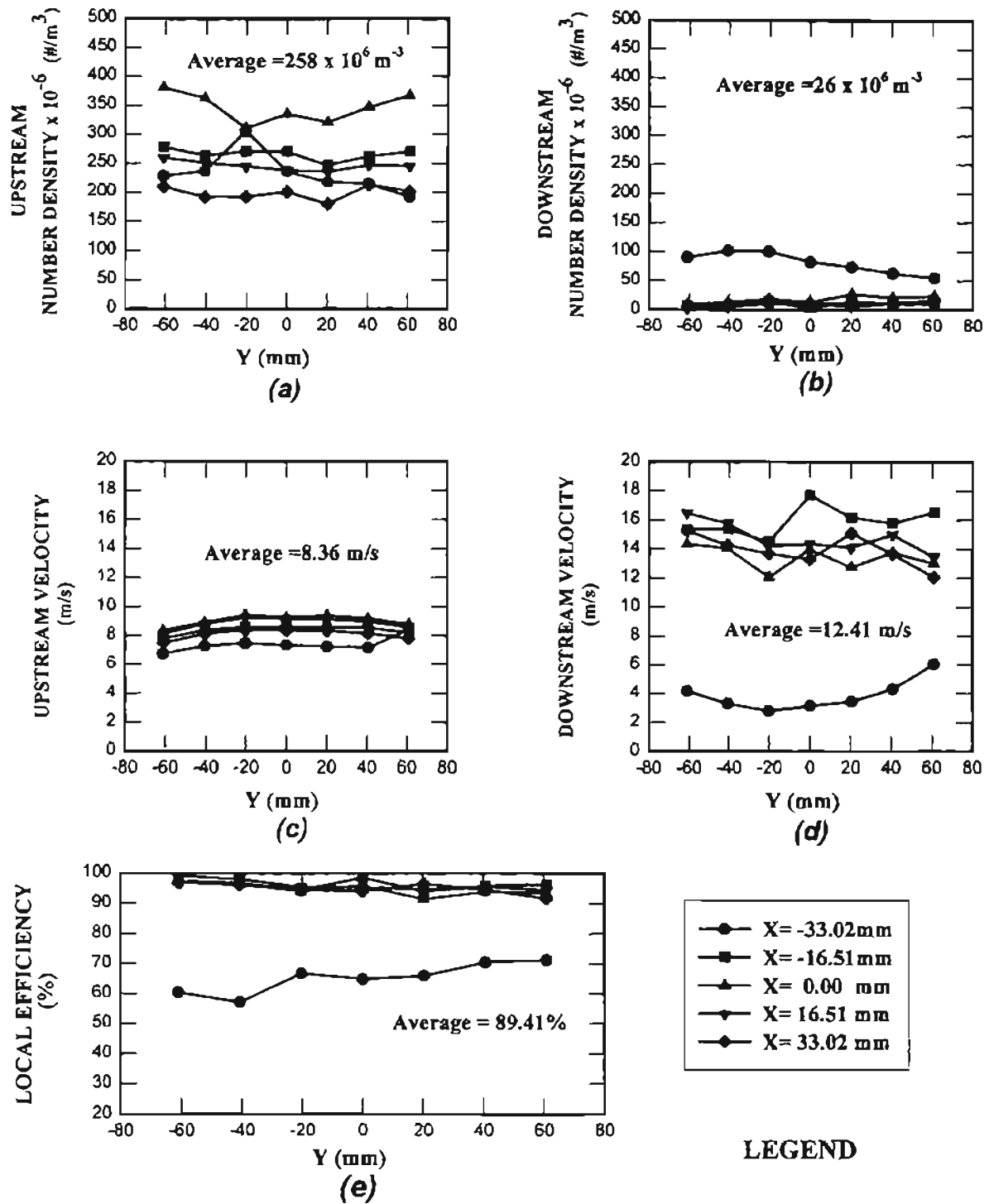
a) Upstream Number Density, b) Downstream Number Density, c) Upstream Velocity, d) Downstream Velocity, e) Local Efficiency

Figure B.18 Local Efficiency, Upstream and Downstream Number Densities and Velocity Profiles, A13192 Pleated Filter, Diffuser Housing, 0.966 Micron PSL Particles, 313.8 m³/hr Air Flow, Test # F7, 6/7/96.



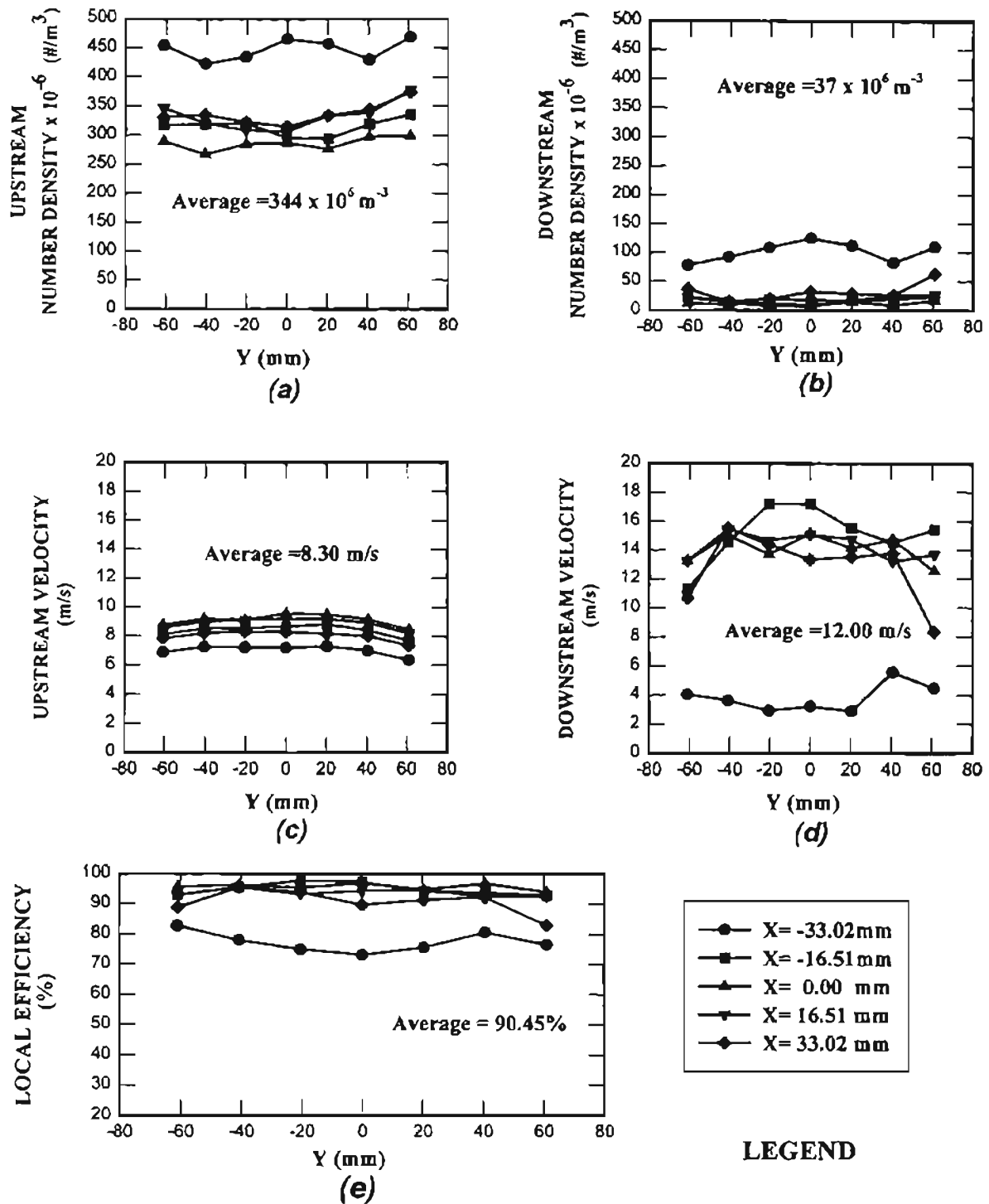
a) Upstream Number Density, b) Downstream Number Density, c) Upstream Velocity, d) Downstream Velocity, e) Local Efficiency

Figure B.19 Local Efficiency, Upstream and Downstream Number Densities and Velocity Profiles, A13192 Pleated Filter, Diffuser Housing, 0.966 Micron PSL Particles, 313.8 m³/hr Air Flow, Test # F8, 6/18/96.



a) Upstream Number Density, b) Downstream Number Density, c) Upstream Velocity, d) Downstream Velocity, e) Local Efficiency

Figure B.20 Local Efficiency, Upstream and Downstream Number Densities and Velocity Profiles, A13192 Pleated Filter, Diffuser Housing, 0.966 Micron PSL Particles, 481.8 m³/hr Air Flow, Test # F14, 6/28/96.



a) Upstream Number Density, b) Downstream Number Density, c) Upstream Velocity, d) Downstream Velocity, e) Local Efficiency

Figure B.21 Local Efficiency, Upstream and Downstream Number Densities and Velocity Profiles, A13192 Pleated Filter, Diffuser Housing, 0.966 Micron PSL Particles, 481.8 m³/hr Air Flow, Test # F17, 7/3/96.

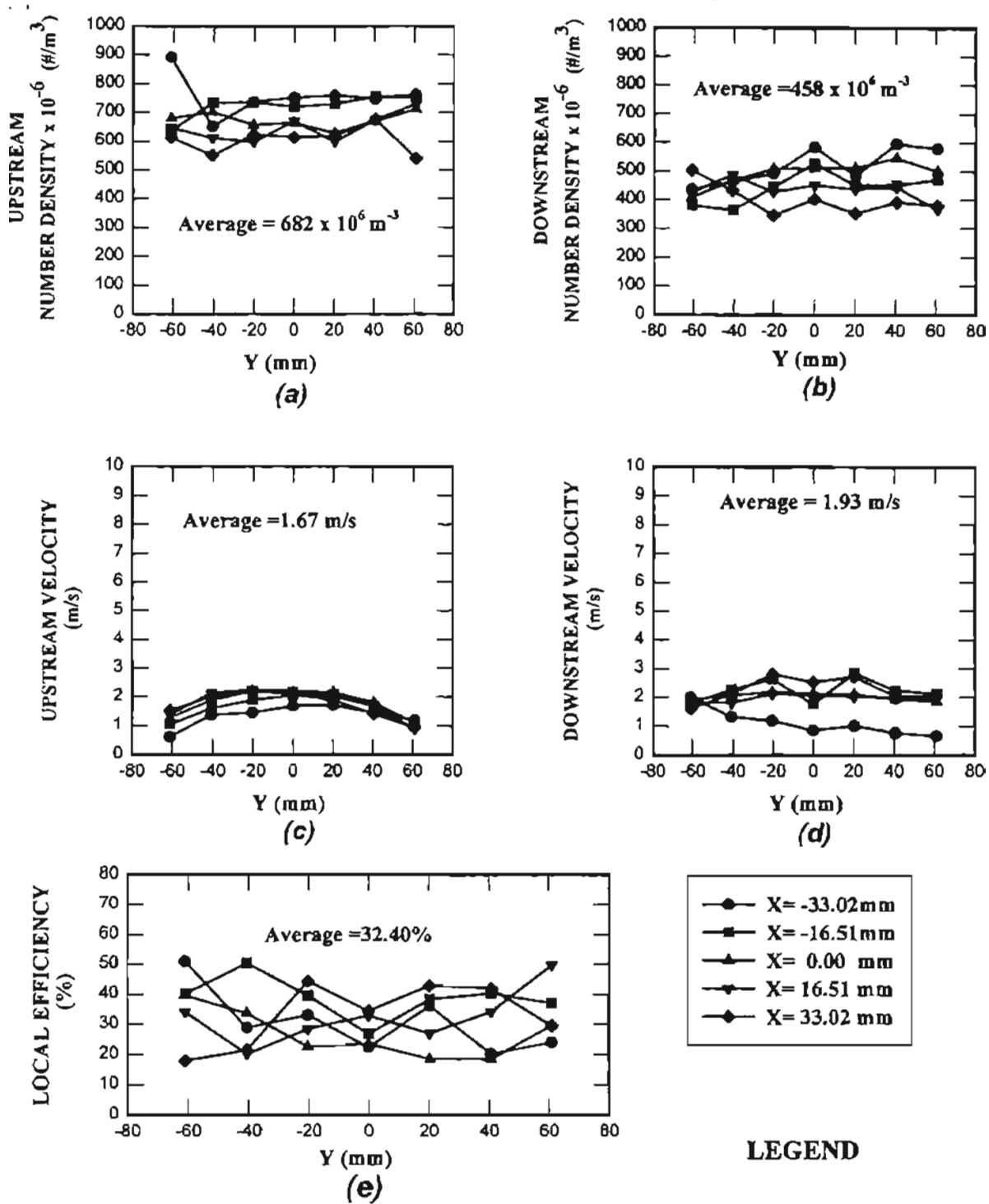
APPENDIX C

TEST RESULTS: SAE HOUSING

The results of the tests measured in the SAE housing are presented in this appendix. Summary of the SAE housing tests are listed in the following table.

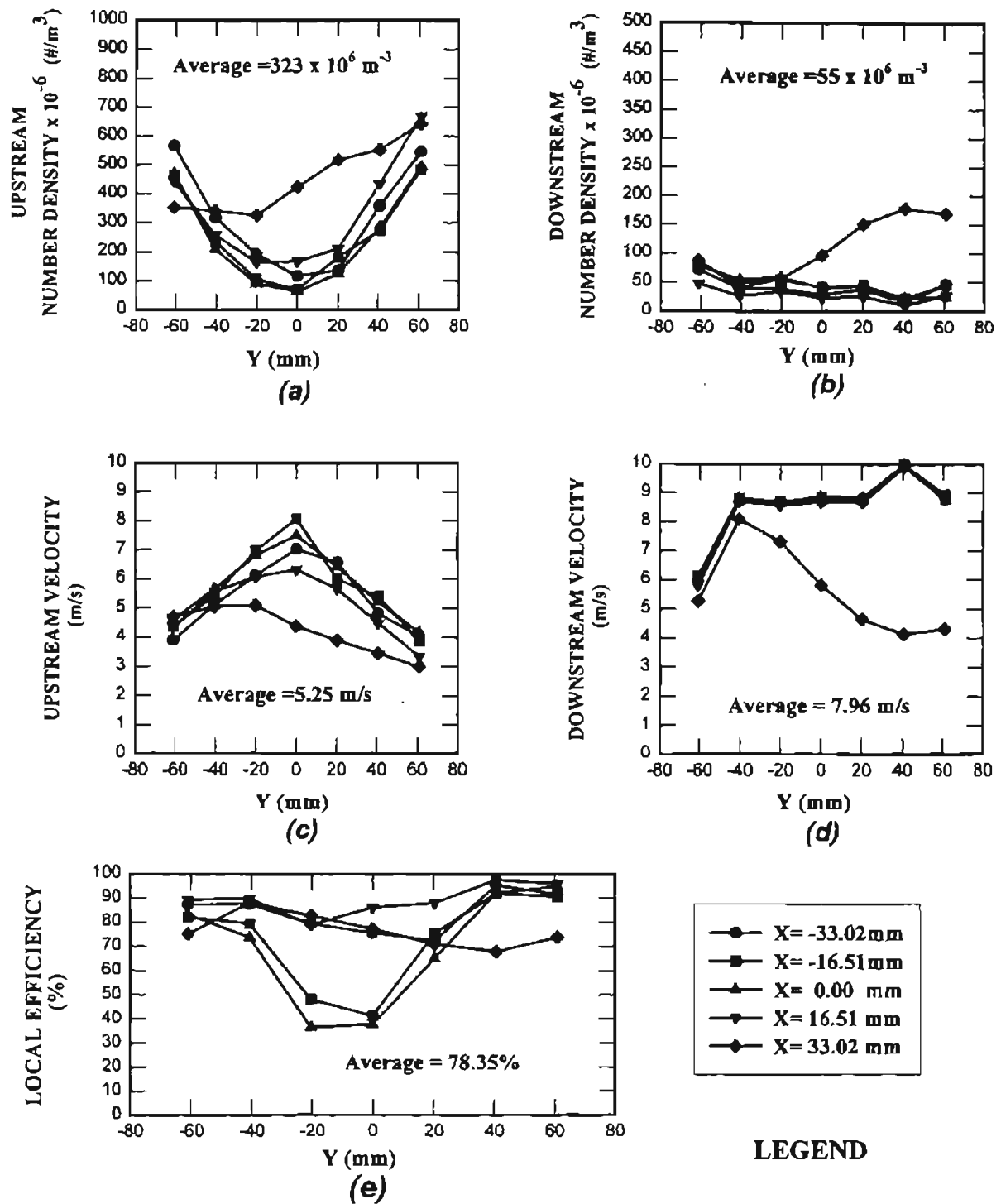
Table C.1 Summary of the SAE Housing Tests.

Flow Rate (m ³ /hr)	Efficiency (%)	Initial Pressure Drop (mm of Water)	Final Pressure Drop (mm of Water)
187.7	55.15	34.3	37.1
61.2	32.4	5.0	5.0
313.8	78.35	68.6	72.4



a) Upstream Number Density, b) Downstream Number Density, c) Upstream Velocity, d) Downstream Velocity, e) Local Efficiency

Figure C.1 Local Efficiency, Upstream and Downstream Number Densities and Velocity Profiles, SAE Housing, A13192 Pleated Filter, 0.966 Micron PSL Particles, 61.2 m³/hr Air Flow, Test # SAE3, 9/3/96.



a) Upstream Number Density, b) Downstream Number Density, c) Upstream Velocity, d) Downstream Velocity, e) Local Efficiency

Figure C.2 Local Efficiency, Upstream and Downstream Number Densities and Velocity Profiles, SAE Housing, A13192 Pleated Filter, 0.966 Micron PSL Particles, $313.8 \text{ m}^3/\text{hr}$ Air Flow, Test # SAE4, 9/4/96.

APPENDIX D

TSI FLOW METER CALIBRATION PLOTS

Anand [1997] calibrated the TSI flow meter with a one inch (25.4 mm) diameter ASME flow nozzle for flow rates less than 50 Scfm (85.5 Sm³/hr) shown in Fig. D.1. For the current measurements, the TSI flow meter was calibrated by a 3 inch (76.2 mm) ASME flow nozzle. Both calibration curves are linear but their slope is different. The curve fitting was done so that both plots show the same value at 50 scfm (85.5 Sm³/hr). The calibration curve for flow rates higher than 50 Scfm is presented in Fig. D.2.

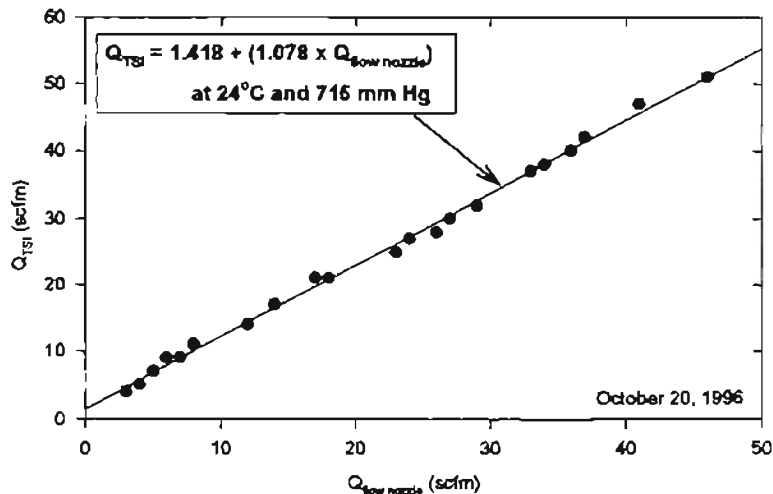


Figure D.1 Calibration Plot for TSI Flow Meter for Flow Rates Less Than 50 Scfm (85.5 Sm³/hr) [Anand, 1997].

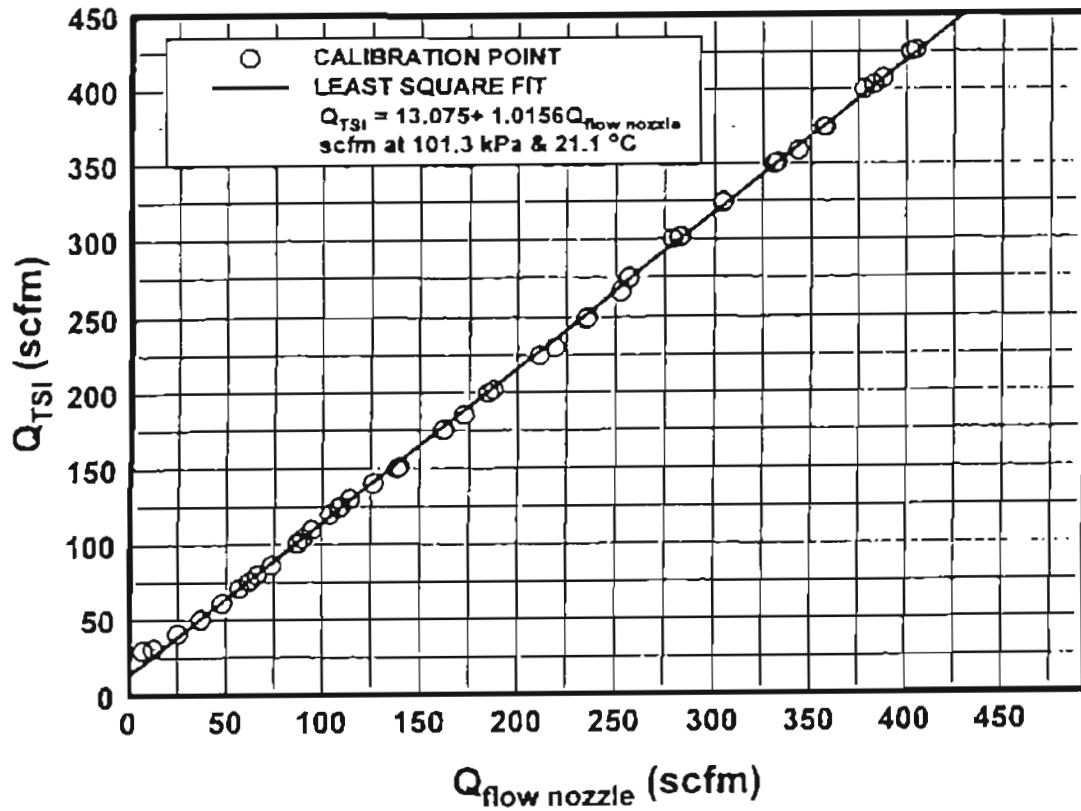


Figure D.2 Calibration Plot for TSI Flow Meter for Flow Rates More Than 50 Scfm
(85.5 Sm³/hr).

APPENDIX E

AN EXAMPLE OF THE STOKES NUMBER CALCULATION

An example of the Stokes number calculation using Eq.(2-3) is presented in this appendix. The variables in Eq. (2-3) are:

- Density of the PSL particles (ρ_p) which is within the range of 1000 to 1050 kg/m³.
- Cunningham Slip correction factor (C_m) which is considered to be one.
- Air viscosity (μ_a) which is 18.6×10^{-6} Pa-s at 30° Centigrade.
- Air velocity (U). As an example the overall average velocity upstream the filter for test F8 (flow rate of 187.7 m³/hr, Fig. 7.6) was used (3.8 m/s).
- Fiber diameter. The exact value of the average fiber diameter is not known, but a value of 38 microns was used.

From Eq. (2-3) the Stokes number is calculated as:

$$St = \frac{C_m D_p^2 \rho_p U}{18 \mu_a D_f} \quad (2-3)$$

Substituting the above listed values the Stokes number will be:

$$St = \frac{(1)[(0.966)(10^{-6})]^2 (1000)(3.8)}{18(18.6)(10^{-6})(38)(10^{-6})} = 0.278$$

APPENDIX F

LIST OF EQUIPMENT

1. 5 Watt Argon Ion laser: Coherent, Model Innova 70-A, Serial No. P/S 92K-1758
2. Remote control for the laser: Coherent, Model I-70, Serial No. 92411171
3. Fiber drive: Aerometrics, Inc., Model FBD1240, Serial No. 026
4. Bragg cell: IntraAction, Inc., Model ME-40H, Serial No. 3247
5. Photomultiplier Tubes: Aerometrics, Inc., Model RCM2200L, Serial No. 029
6. Doppler Signal Analyzer: Aerometrics, Inc., Model DSA3220, Serial No. 044
7. Computer and Monitor: Impression 3, IBM compatible 80486 DX2, 66 MHz
8. Computer for Traverse System and MS-Excel Data Acquisition Files: Gateway 2000, IBM compatible, 80486 DX2, 33 MHz
9. Laser Transceiver: Aerometrics, Inc., Model XRV1212, Serial No. 001
10. Three Stepper Motors (Sanyo Denki, Type: 103-850-11)
11. Oscilloscope: Hewlett Packard, Model 54501A
12. Plexiglas Test Housings: SAE J1669 Small Angle Diffuser Housing
13. Pleated Test Filter: Purolator, Inc., A13192 (formerly AF3192)
14. TSI Mass Flow Sensor: TSI, Model 2018, Serial No. 30644

15. Atomizer: TSI Model 9306, six-jet atomizer
16. SAE J726 Air Stand, Purolator Products, Inc.
17. Rival Compact Heater, Model T114
18. Stepper Motor Drives, Model CMD-40
19. 24 V DC - 6 A Power Supply (Acme Electronics)
20. Connector 3 for Digital Output, Model PCLD-780
21. Ultrasonic Humidifier: Pollenex, Model SH55R

APPENDIX G

COMPARISON OF EFFICIENCY CALCULATION METHODS

The Swept Volume Technique (SVT), described in Chapter five (see also Liang, 1997), was used to calculate the number densities upstream and downstream of the filter. The SVT is based on calculating the volume which is “swept” during time T_0 . In other words, the number density or the number of particles per unit volume is calculated based on measuring the number of particles in the swept volume and calculating the number of particles in a unit volume. Assuming N particles to be detected during time T_0 , having a velocity of V , the length of the swept volume is VT_0 and the total volume is VT_0A_p . The number density or the counts per unit volume will be (Fig. G.1):

$$n = \frac{N}{VT_0A_p} \quad (G-1)$$

and the efficiency can be calculated as:

$$\eta = 1 - \frac{n_2}{n_1} \quad (G-2)$$

Another approach for calculating the local efficiencies is the “Mass Flux Technique” (MFT). The mass flux technique is based on the assumption that the efficiency for each flow stream can be calculated based on the ratio of the mass flux of

particles upstream and downstream of the filter.

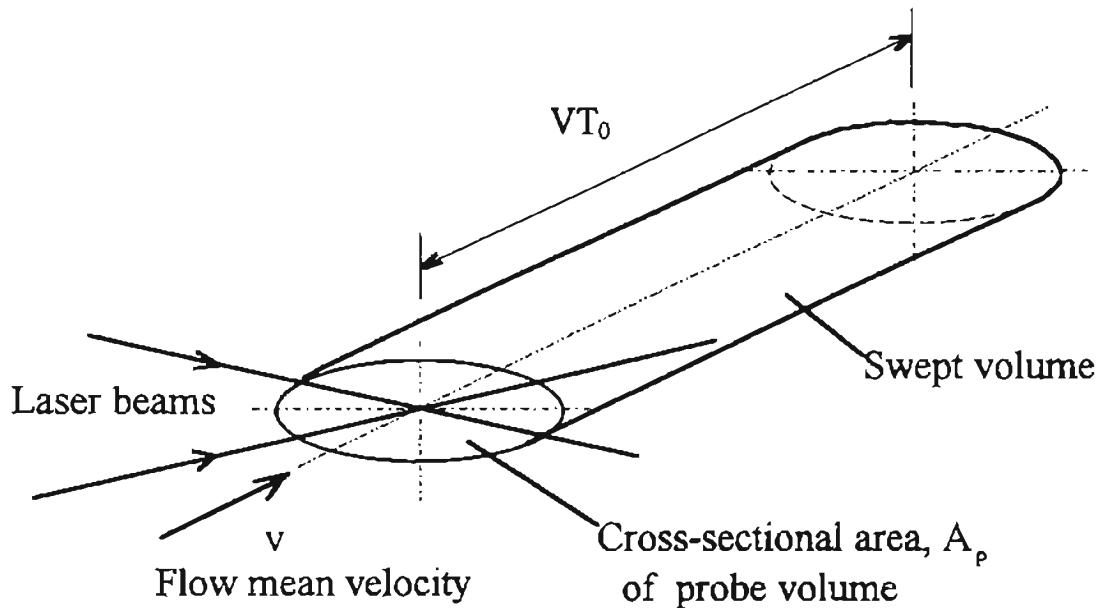


Figure G.1 The Swept Volume Technique

The mass flow rate of the air upstream of the filter (between two streamlines) has to be equal to the mass flow rate downstream of the filter (there is no flow crossing the streamlines) in order to conserve mass between two streamlines. Since the air velocity (or particle velocity) is not the same upstream and downstream of the filter, in order to conserve the mass, the cross-sectional area of the flow upstream and downstream of the filter is not the same. Current measurements show that the air velocity downstream of the filter is higher than on the upstream side. Therefore the cross-sectional area downstream of the filter has to be smaller.

The mass flux in terms of number density can be calculated as:

$$m_1 = n_1 [(4/3) \pi R_p^3 \rho_p](V_1 A_1 T_1) / (A_1 T_1) \quad (G-3)$$

$$m_2 = n_2 [(4/3) \pi R_p^3 \rho_p](V_2 A_2 T_2) / (A_2 T_2) \quad (G-4)$$

Where m_1 and m_2 are the particle mass fluxes upstream and downstream of the filter, respectively, and A_1 and A_2 are the effective areas for the flows upstream and downstream of the filter. Substituting Eqs. (G-3) and (G-4) into Eq. (G-2) and simplifying, the efficiency is calculated as:

$$\eta = 1 - \frac{m_2 V_1}{m_1 V_2} \quad (G-5)$$

Therefore in MFT as compared to SVT, instead of number densities, the ratio of mass fluxes times the inverse ratio of the velocities should be used.

APPENDIX H

COMPARISON OF THE AVERAGE EFFICIENCIES

As discussed in Chapter five, calculated efficiencies at grid locations close to the housing wall may not be as accurate as those at central region of the filter. In order to investigate the effect of the grid points close to the housing wall, the overall average efficiencies of the whole filter measurements were calculated without considering the grid points close to the wall (reducing the number of grid points used in the average from 35 to 15). These averages are compared with the previous overall averages (on the whole filter) and the three point averages as shown in Fig. H.1 (and tabulated in Table 7.1).

As can be seen from the figure, the central region averages are closer to the three point averages, supporting the idea that the calculated velocities at the grid points near the housing walls might be unreliable. As mentioned earlier, most of these velocities were calculated based on the one-dimensional SVT (due to the limited test time).

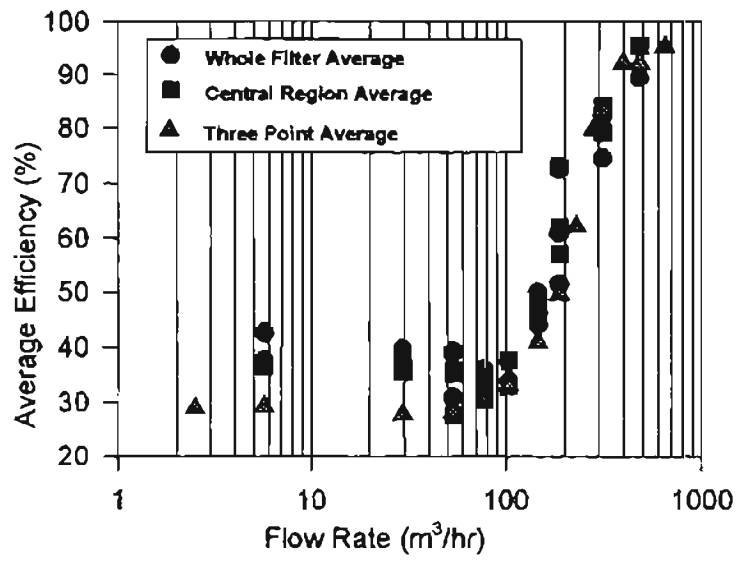


Figure H.1 Comparison of the Average Efficiencies.

VITA

Fakhroddin M. Jadbabaei

Candidate for the Degree of
Master of Science

Thesis: FILTRATION EFFICIENCY MEASUREMENTS FOR PLEATED FILTERS

Major Field: Mechanical Engineering

Biographical:

Personal Data: Born in Abadan, Iran, on October 13, 1965.

Educational: Received Bachelor of Science in Mechanical Engineering from Tehran University, Tehran, Iran in January 1988 and Master of Science in Nuclear Engineering from Sharif University of Technology, Tehran, Iran in January 1993. Completed the requirements for the Master of Science degree with a major in Mechanical Engineering at Oklahoma State University in July 1997.

Experience: Employed by Oklahoma State University as a graduate research assistant from May 1995 to October 1996 and as a graduate teaching assistant during the Spring of 1995. Worked for Sazeh Engineering Consultants, Tehran, Iran as a mechanical engineer, stress analyst and manager of the Equipment Department from 1988 to 1994.